

**Zeitschrift:** IABSE congress report = Rapport du congrès AIPC = IVBH  
Kongressbericht

**Band:** 5 (1956)

**Rubrik:** II. Slabs and various curved structures in reinforced concrete

### **Nutzungsbedingungen**

Die ETH-Bibliothek ist die Anbieterin der digitalisierten Zeitschriften auf E-Periodica. Sie besitzt keine Urheberrechte an den Zeitschriften und ist nicht verantwortlich für deren Inhalte. Die Rechte liegen in der Regel bei den Herausgebern beziehungsweise den externen Rechteinhabern. Das Veröffentlichen von Bildern in Print- und Online-Publikationen sowie auf Social Media-Kanälen oder Webseiten ist nur mit vorheriger Genehmigung der Rechteinhaber erlaubt. [Mehr erfahren](#)

### **Conditions d'utilisation**

L'ETH Library est le fournisseur des revues numérisées. Elle ne détient aucun droit d'auteur sur les revues et n'est pas responsable de leur contenu. En règle générale, les droits sont détenus par les éditeurs ou les détenteurs de droits externes. La reproduction d'images dans des publications imprimées ou en ligne ainsi que sur des canaux de médias sociaux ou des sites web n'est autorisée qu'avec l'accord préalable des détenteurs des droits. [En savoir plus](#)

### **Terms of use**

The ETH Library is the provider of the digitised journals. It does not own any copyrights to the journals and is not responsible for their content. The rights usually lie with the publishers or the external rights holders. Publishing images in print and online publications, as well as on social media channels or websites, is only permitted with the prior consent of the rights holders. [Find out more](#)

**Download PDF:** 23.02.2026

**ETH-Bibliothek Zürich, E-Periodica, <https://www.e-periodica.ch>**

## **II**

**Placas, lages e paredes delgadas**

**Voiles minces, dalles, parois minces**

**Slabs and various curved structures in  
reinforced concrete**

**Flächentragwerke**

**Relator Geral  
Rapporteur Général  
General Reporting Member  
Generalreferent**

**PROF. DR. P. LARDY  
Zurich**

## **IIa**

Cálculo geral (nos campos elástico e plástico); métodos experimentais

Calcul général (élastique et plastique); méthodes expérimentales

General calculation (in elastic and plastic fields); experimental methods

Allgemeine Berechnung (im elastischen und plastischen Bereich);  
experimentelle Methoden

## **IIb**

Adaptação dos métodos de cálculo às construções metálicas

Adaptation des méthodes de calcul aux constructions métalliques

Application of the methods of calculation to steel structures

Anwendung der Berechnungsmethoden auf Stahltragwerke

## **IIc**

Adaptação dos métodos de cálculo às construções de betão armado

Adaptation des méthodes de calcul aux constructions en béton armé

Application of the methods of calculation to reinforced concrete structures

Anwendung der Berechnungsmethoden auf Tragwerke in Eisenbeton

## **II a 1**

### **Rectangular staircases without beams**

### **Balkenlose Treppen mit rechtwinkligen Grundriss**

### **Escaliers rectangulaires sans poutres**

### **Escadas rectangulares sem vigas**

FERRY BORGES

*Research Engineer*

*Laboratório Nacional de Engenharia Civil*

Lisbon

#### **1. Introduction**

The most varied calculation methods have been adopted for the design of staircases consisting of rectangular flights and landings not supported by beams (<sup>1</sup>).

Besides the difficulties inherent in the calculations of plates, there is the further difficulty of defining the degree of support imparted to the flight and landing slabs by their intersection. The displacements of the intersection lines depend on the behaviour of the structure as prismatic.

Some results are presented of tests carried out on a plastic model and a reinforced concrete prototype. The main objective of the tests was to obtain information about the behaviour of this type of structures and so to be able to judge the calculation methods adopted.

The present case is considered to be another of the many examples demonstrating the advantages derivable from experimental studies, on both models and prototypes. In fact, the experimental methods not only supply information relative to the particular case studied, but, when suitably interpreted, furnish the necessary elements for judging the existing theories and the basis for establishing new calculation methods. This is of the greatest interest, in view of the limitations of the general theories which usually only give the solution of practical problems when supple-

---

(<sup>1</sup>) Zuchsteiner, W. — «Treppen» — Beton Kalendar, Zweiter Teil, Wilhelm Ernst und Sohn, Berlin, 1953. Krysztal, A. — «The Design of Staircases» — Concrete and Constructional Engineering, Vol. XLIX, N.° 7, London, July 1954.

mented by further hypotheses. Experiment suggests these hypotheses and allows their evaluation.

It is often verified that forecasts made before tests, even when made by experienced engineers, are as a rule invalidated by the experimental results.

These remarks apply, above all, to constructions that differ from the conventional ones because, for the latter, the experience accumulated often allows perfectly satisfactory forecasts to be made. This is only natural as for these constructions the stage for comparing the calculation methods with the actual behaviour of the structure has been passed.

## 2. *Experimental studies*

The experimental studies undertaken were made on a model and a prototype.

The model of methyl metacrylate (perspex), fig. 1, represented a staircase of the type shown schematically in fig. 2, to a scale of 1/20.

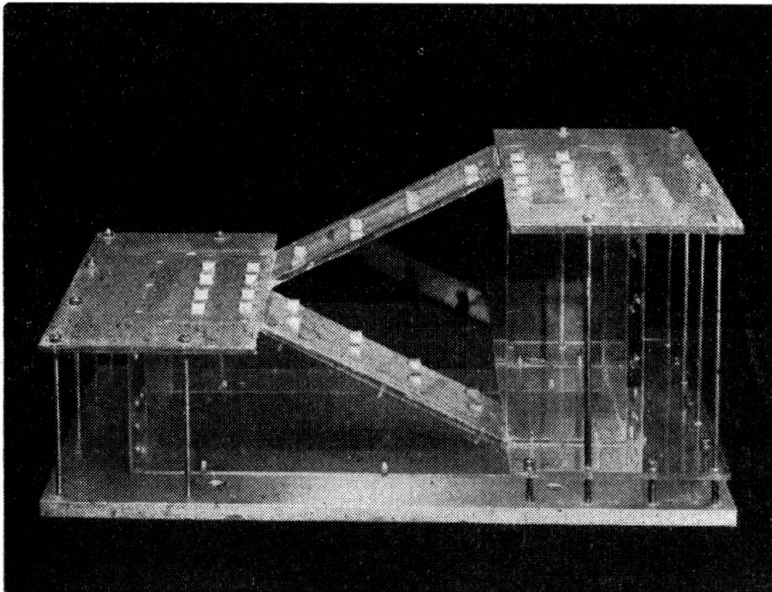


FIG. 1. Model to a scale 1/20

The numbers shown in fig. 2 indicate the dimensions of the model in centimeters. The model test consisted in the application of vertical forces and the measurements of displacements and strains at different points.

Table I gives some results obtained when applying concentrated vertical forces. Note that in spite of having sought to give a considerable horizontal rigidity to the model, this, when subject to vertical loads, underwent horizontal displacements which cannot be considered negligible.

Fig. 3 shows two of the influence surfaces of the bending moments. These surfaces were determined for 18 sections, by applying concen-

trated forces at different points and measuring the strains at the sections under study. Another test was carried out (fig. 4) in which a uniform load was applied. The deformation obtained is shown in fig. 5.

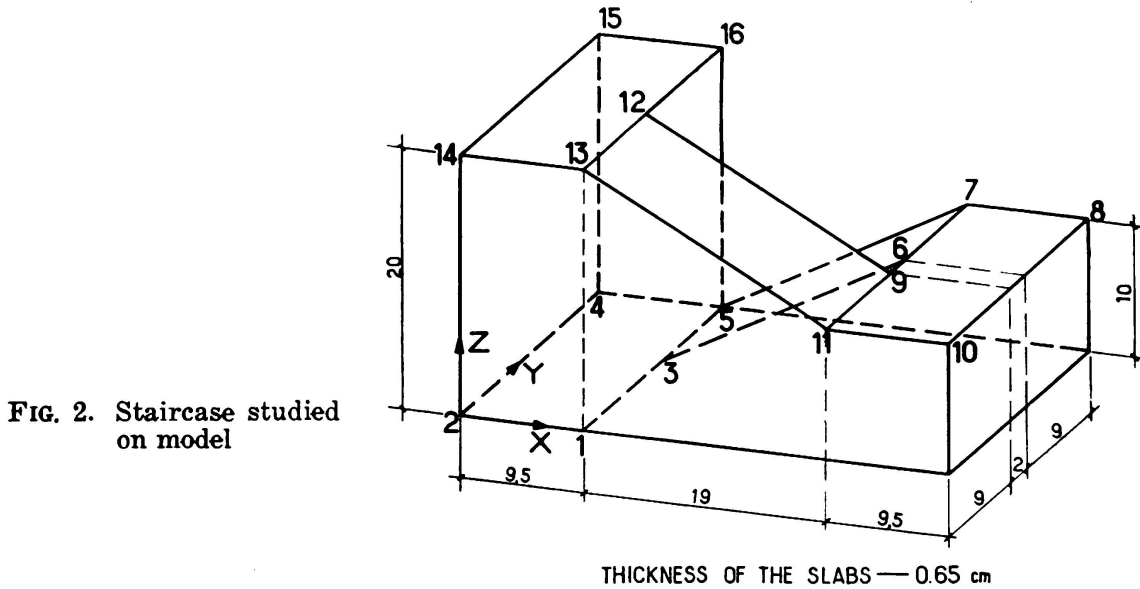


FIG. 2. Staircase studied on model

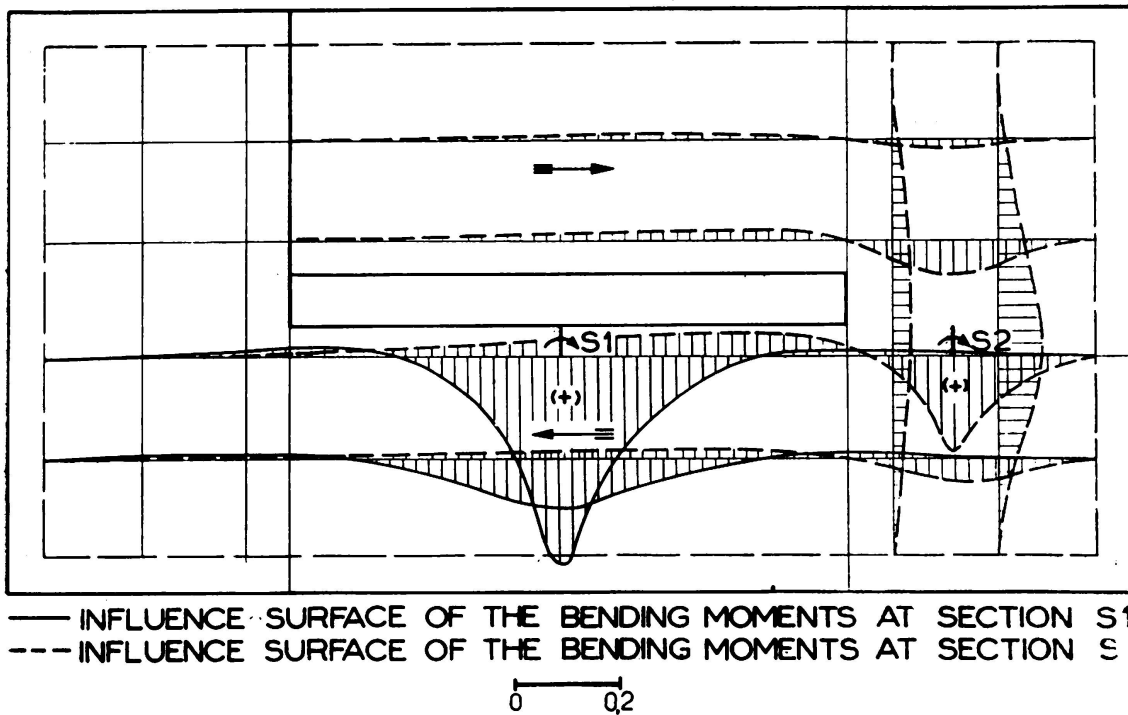


FIG. 3. Influence surfaces of the bending moments at two sections

The reinforced concrete staircase tested was of the type shown schematically in fig. 6. The landings were 20 cm thick, the flights 25 cm approximately and the rest of the dimensions are given in meters in fig. 6. As there was a guard which imparted considerable rigidity

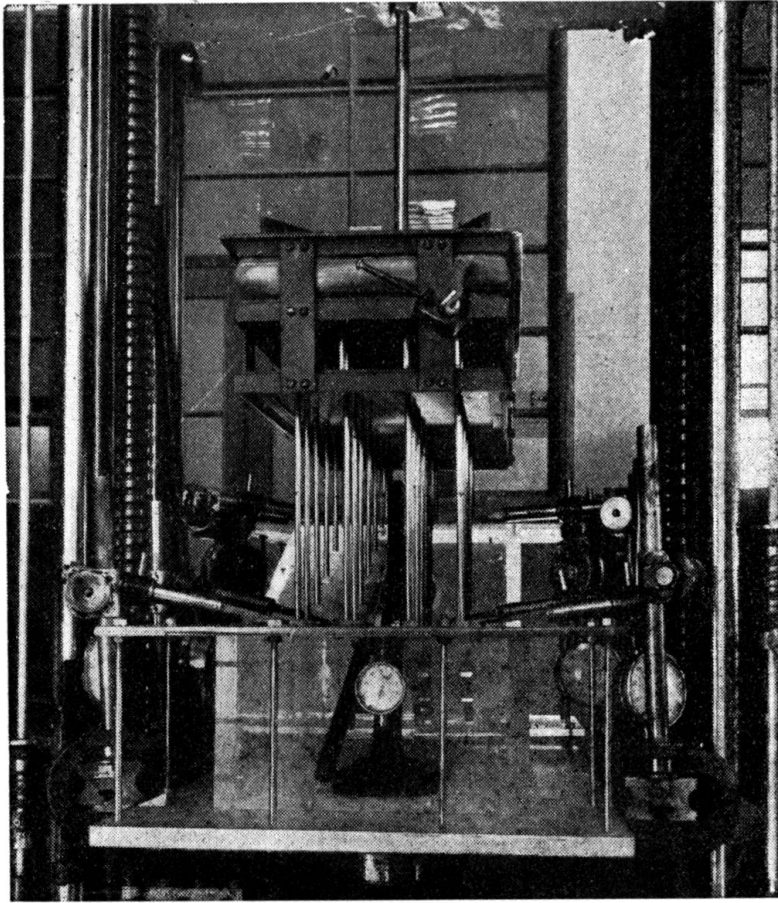


FIG. 4. Model test with uniform load

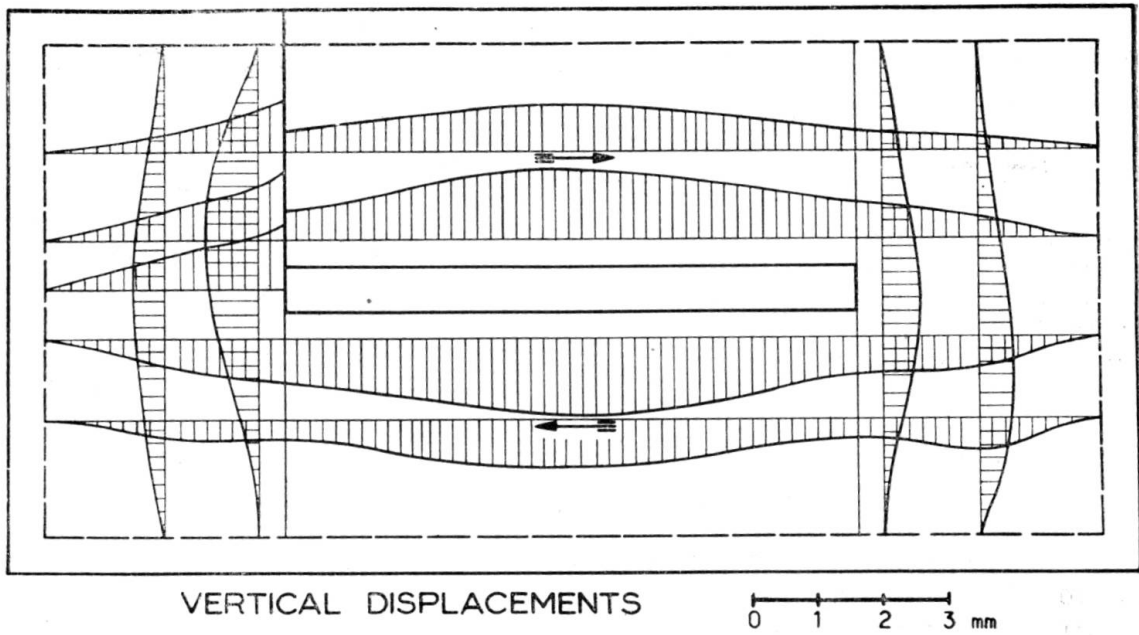


FIG. 5. Displacements due to uniform load

to the stair it was decided to make concentrated load tests before and after removal of the guard along line 17, 21 in the intermediate flight.

Fig. 7 shows the deformations obtained after removal of the guard for concentrated loads and uniform loads applied on zone (18, 19, 23, 24)

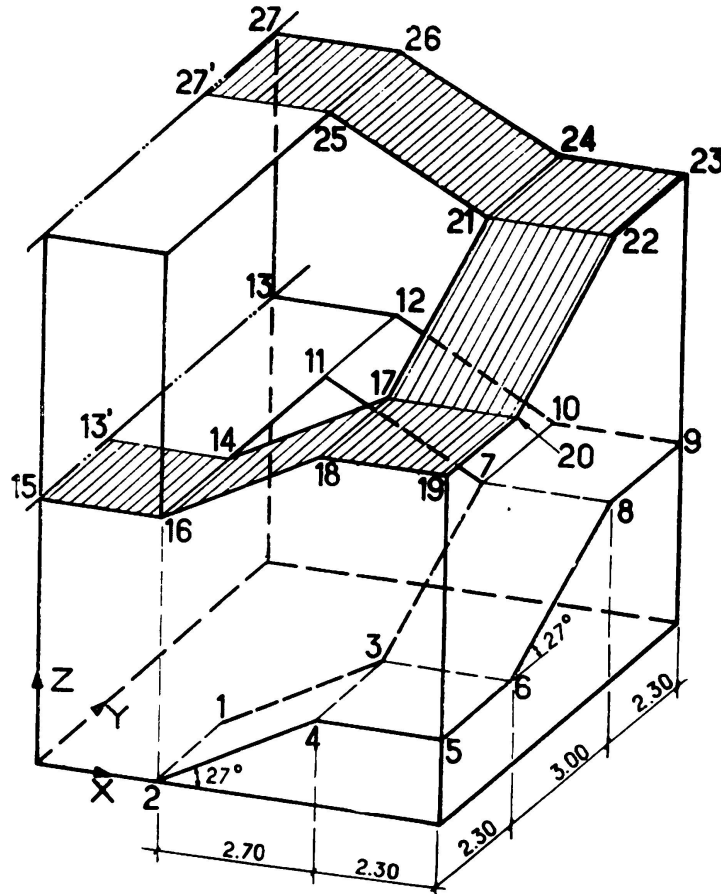


FIG. 6. Reinforced concrete staircase studied on prototype

and on the shaded zone (fig. 6). Attention is called to the considerable asymmetry of the deformations in relation to landings (17, 18, 19, 20) and (21, 22, 23, 24) which will be explained further on.

Fig. 8 gives a view of the application of the uniform load.

### 3. Calculation methods

The general theories of elastic calculation which are available cannot be applied directly to the structures concerned. The theory of plates makes it possible to study the separate behaviour of the flights or landings, but in order to be used it is necessary to know the boundary conditions which are not known, principally along the intersection lines. In fact the vertical displacements of these lines are partly impeded by

the behaviour of the structure as prismatic (forces in the plane of the plates), but, the behaviour in this way imparts considerable horizontal forces which at times cannot be absorbed.

In this case, the vertical displacement of the intersection lines can increase in relation to what they would be when calculated on the basis of the structure being prismatic and assuming that supporting points in the wall cannot move horizontally.

Considering a vertical force applied to the intersection line (fig. 9), this force will resolve itself in accordance with the planes of the plates

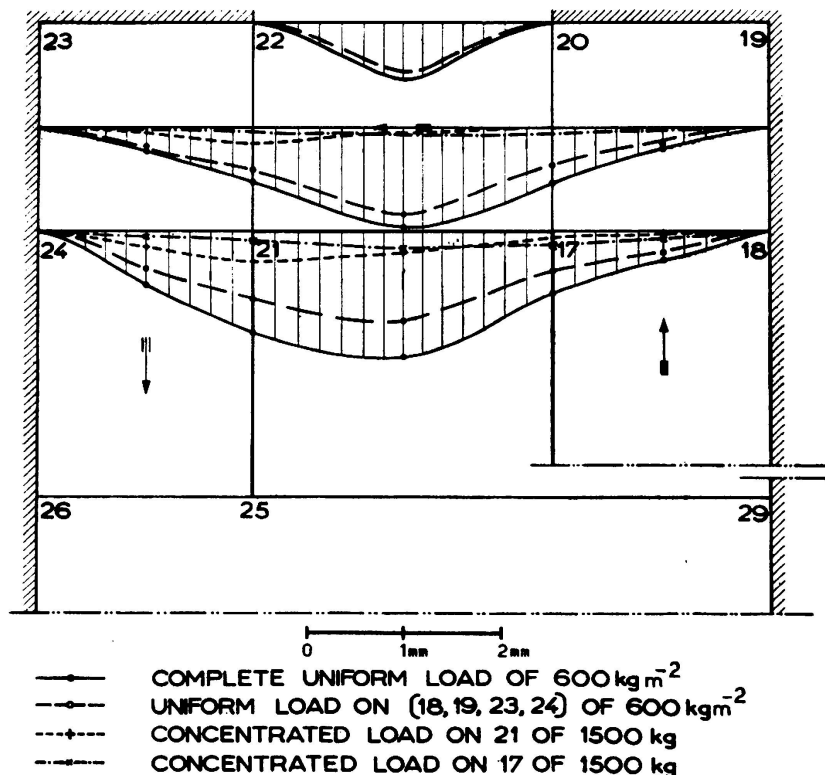


FIG. 7. Displacements measured during the test of the reinforced concrete staircase

and assuming that the points of the plates at the supports cannot undergo horizontal displacements, the vertical displacements of the intersection line can be calculated approximately from some simple hypotheses. It is considered that intersection lines remain straight and that the maximum stresses are constant along lines connecting the intersections to the supports.

Calculating, for the model of fig. 1, the displacements due to the application of a concentrated load of 10 kg at the intersection, in accordance with the above scheme, a displacement of 0.12 mm is obtained whilst the measured displacement was 0.20 mm. It is of interest to note that in the calculation the points of the other landings are assumed not to undergo deflection, which however is not borne out experimentally, as can be seen from Table I.

For the concrete staircase, the application of a concentrated load at the intersection (point 21, fig. 6), when considering the structure as prismatic, results in a calculated vertical displacement of point 21 of 0.03 mm.

The hypothesis of the structure behaving prismatically implies considerable horizontal forces, and whenever the structure cannot absorb these forces, horizontal displacements take place, which result in consi-



FIG. 8. Application of the uniform load

derable vertical displacements of the intersection lines. Thus for example in the case of the landing (21, 22, 23, 24) of the staircase of fig. 6 when applying a vertical force in 21, forces are developed having horizontal components which tend to impose horizontal displacements of the supports corresponding to a clockwise rotation of the landing slab. These horizontal displacements result in vertical displacements of the intersections. In order to calculate these last displacements the scheme given in fig. 10 can be taken and torsional rigidity and bending moments due to the connection to the wall can be ignored, only taking into consideration the bending in a vertical plane.

When the calculation is made in this way for a concentrated load of 1500 kg a vertical displacement of 0.40 mm was obtained, which is near the measured displacement of 0.31 mm, and much greater than the displacements computed when the structure is considered prismatic and joined to fixed points (0.03 mm).

The fact of the displacements of landing (17, 18, 19, 20) being much less than those of landing (21, 22, 23, 24) is explained by its rigid connection to the body of the building.

The above results show that it is very difficult to obtain a horizontal rigidity which would give vertical displacements of the intersections equal to those calculated when taking the structure as prismatic.

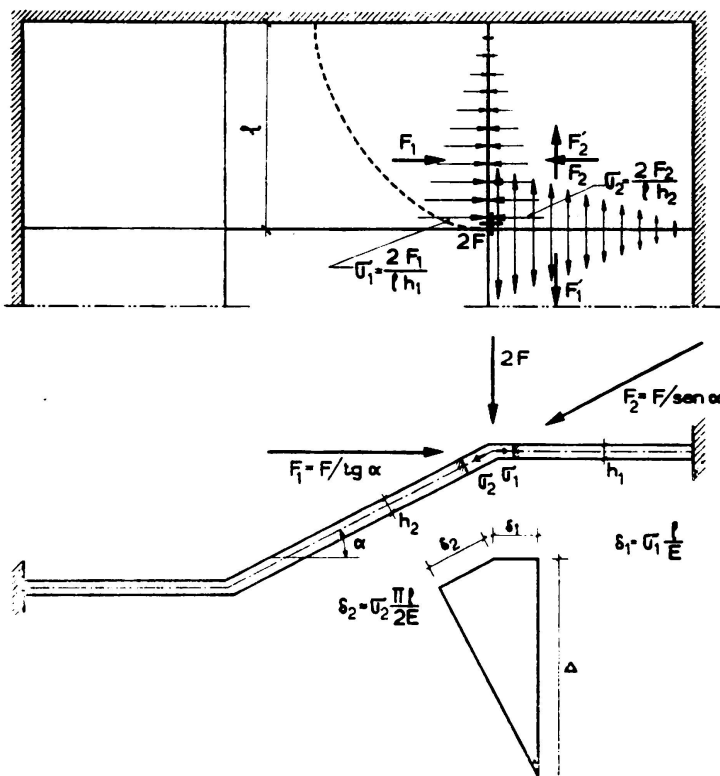


FIG. 9. Displacements of the prismatic structure

Even so, when the deformability of the staircase is small for the horizontal forces, the vertical displacements of the intersection lines between flights and landings are also small, and it would be justifiable to assume that these intersection lines function as indeformable supports in relation to the deformability of the slabs under bending. Such a hypothesis favours safety for negative bending moments at the intersections but is unfavourable for safety for positive bending moments in the middle of the flights.

When the deformability of the intersection lines is large, due to possible horizontal displacements, it becomes necessary to estimate this deformability and take it into consideration when designing the

slabs. Note, for example, that in the case of the staircase of fig. 6, in spite of the important deformability of the intersections, they contribute considerably towards reducing the positive bending moments in the flights.

4. Conclusions

The above considerations show that the difficulty of designing staircases without beams derives from the interaction of three types

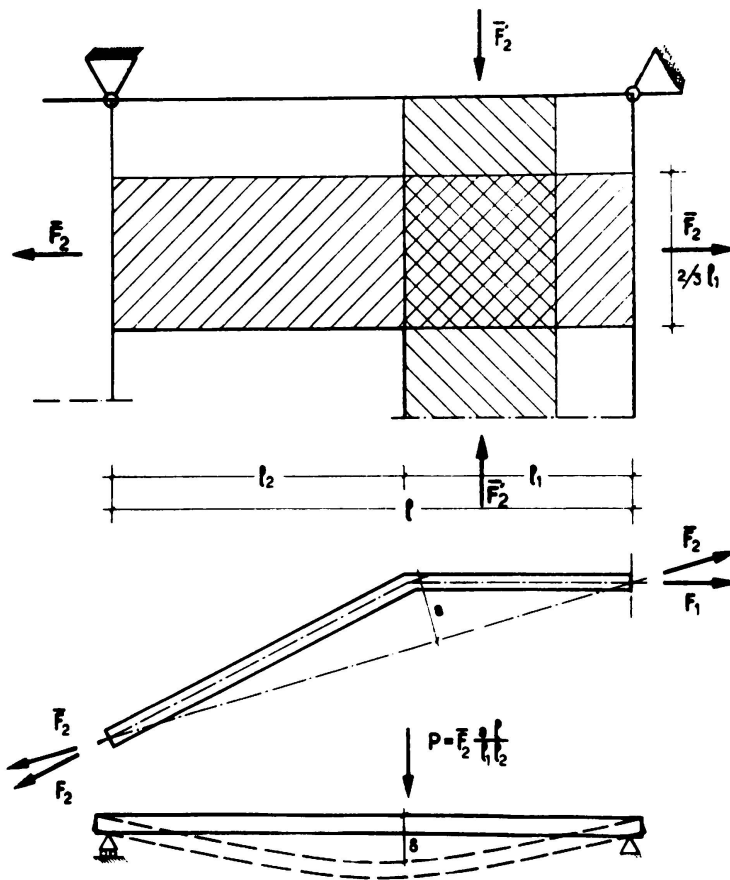


FIG. 10. Influence of horizontal displacements

of behaviour; as a plate, as a prismatic structure and in bending under the action of horizontal impulses acting on the flight and landing slabs.

In order to solve the problem it is of interest, above all, to determine the vertical deformability of the intersections, as once this is known, the problem can be solved with satisfactory approximation. This deformability depends not only on the geometry of the structure itself but also on the rigidity of the structure to which it is connected.

The considerations given are based on the criteria of elastic calculation. It is considered to be of interest also for this type of structure to develop methods of limit design.

In the case of the deformability of the intersection being small in relation to the deformability of the slabs, it should be possible to adopt a limit design for the latter assuming that the intersections behave as fixed supports. However, the value of such a method can only be proved by experiments planned for this purpose but which it has not been possible to carry out.

The author wishes to acknowledge the collaboration given by Mr. Arga e Lima in the studies related to this paper and by Mrs. Maria Emília Campos e Matos and Mr. João Madeira Costa who carried out the model and prototype tests respectively.

TABLE I

| Forces               |          | Displacements |           |          |
|----------------------|----------|---------------|-----------|----------|
| Point of application | Value kg | Point         | Direction | Value mm |
| 12                   | 10       | 12            | z z       | -0.20    |
|                      |          | 13            | x x       | +0.01    |
|                      |          | 16            | x x       | -0.03    |
|                      |          | 9             | z z       | -0.07    |
| 6 and 9              | 10       | 6 and 9       | z z       | -0.21    |
|                      |          | 13            | x x       | +0.03    |
|                      |          | 16            | x x       | -0.02    |
|                      |          | 12            | z z       | -0.09    |
|                      |          | 3             | z z       | -0.05    |
| 3                    | 10       | 3             | z z       | -0.10    |
|                      |          | 6             | z z       | -0.03    |

## SUMMARY

The results of model and prototype tests on rectangular staircases composed of slabs without beams are presented.

Design methods of this type of stairs are discussed. Such discussion is based on the interpretation of the experimental results. It is shown that to solve the problem it is especially important to determine the vertical deformability of the intersection line of the flight and landing slabs.

## ZUSAMMENFASSUNG

Die vorliegende Arbeit enthält die Ergebnisse der Modell- und Prototypversuche an Treppen rechtwinkligen Grundrisses, bestehend aus nicht von Balken getragenen Platten. Auf Grund dieser Daten werden Ver-

fahren besprochen welche zur Bemessung von Bauwerken dieser Bauart angewendet werden.

Dabei zeigt es sich, dass es besonders darauf ankommt, die lotrechte Verformung der Schnittlinien der Treppenläufe und -podeste festzustellen.

#### RESUMO

Apresentam-se os resultados de ensaios sobre modelo e sobre protótipo de escadas de planta rectangular constituídas por lages não apoiadas em vigas.

Discutem-se, a partir da interpretação dos resultados experimentais, os métodos de cálculo de estruturas deste tipo. Mostra-se que para resolver o problema interessa sobretudo determinar a deformabilidade vertical das linhas de intersecção entre as lages dos patins e dos lances.

#### RÉSUMÉ

On présente les résultats d'essais sur modèle et sur prototype d'escaliers, rectangulaires en plan, constitués par des dalles non appuyées sur des poutres.

Les méthodes de calcul de ce type d'escalier sont discutées en se fondant sur l'interprétation des résultats expérimentaux. On montre que, pour résoudre le problème, il importe surtout de déterminer la déformabilité verticale des lignes d'intersection des dalles des paliers avec celles des volées.

Leere Seite  
Blank page  
Page vide

## **II a 2**

**Design of shells based on the experimental determination  
of funicular surfaces**

**Schalenbemessung durch experimentelle Darstellung  
der Seilflächen**

**Dimensionamento das cúpulas a partir do traçado experimental  
das superfícies funiculares**

**Dimensionnement des coupôles minces d'après le tracé  
experimental des surfaces funiculaires**

J. F. LOBO FIALHO

Lisbon

### **1 - Introduction**

In the structural theory of shells, membrane equilibrium is defined as an abstraction of the static equilibrium of a shell obtained exclusively by means of forces contained on a plane tangent in every point to its middle surface, that is, by means of normal forces (compressive and tensile) and shear forces.

Let  $\lambda$  and  $\mu$  denote two parameters by means of which the position of a point  $P$  on the surface of a membrane can be defined so that the equations  $\lambda = \text{const.}$  and  $\mu = \text{const.}$  are two families of lines on the surface (Gauss).

The square of the line element is expressed by

$$ds^2 = \alpha^2 d\lambda^2 + \beta^2 d\mu^2 = ds_1^2 + ds_2^2 \quad (1)$$

where  $\alpha = \alpha(\lambda, \mu)$  and  $\beta = \beta(\lambda, \mu)$ .

The equations of equilibrium of a surface element of sides  $ds_1, ds_2, ds_3, ds_4$ , are obtained by making equal to zero the forces and moments acting on the element considered.

It is established in the Differential Geometry <sup>(1)</sup> that:

$$\begin{aligned} ds_1 &= \beta \, d\mu \\ ds_2 &= \alpha \, d\lambda \\ ds_3 &= \left( \beta + \frac{\partial \beta}{\partial \lambda} d\lambda \right) d\mu \\ ds_4 &= \left( \alpha + \frac{\partial \alpha}{\partial \mu} d\mu \right) d\lambda \end{aligned} \quad (2)$$

Hence angles  $\theta$  and  $\varphi$  (fig. 1) are:

$$\begin{aligned} \theta &= \frac{ds_2 - ds_4}{ds_1} = -\frac{1}{\beta} \frac{\partial \alpha}{\partial \mu} d\lambda \\ \varphi &= \frac{ds_3 - ds_4}{ds_2} = \frac{1}{\alpha} \frac{\partial \beta}{\partial \lambda} d\mu \end{aligned} \quad (3)$$

With the same stress notations as in the theory of plates <sup>(2)</sup> the internal forces on the edges of the element  $N_\lambda$ ,  $N_\mu$  and  $N_{\lambda\mu}$  are in equilibrium with the external forces of components  $P_x$ ,  $P_y$  and  $P_z$  per unit of area. Resolution of the forces in the directions of the line element  $ds_2$  yields:

$$\begin{aligned} & -N_\lambda \beta \, d\mu + N_\lambda \beta \, d\mu + \frac{\partial (N_\lambda \beta)}{\partial \lambda} d\lambda \, d\mu - N_{\lambda\mu} \alpha \, d\lambda + N_{\lambda\mu} \alpha \, d\lambda \\ & + \frac{\partial (N_{\lambda\mu} \alpha)}{\partial \mu} d\lambda \, d\mu - N_{\lambda\mu} \theta \beta \, d\mu - N_\mu \varphi \alpha \, d\lambda + P_x \alpha \beta \, d\lambda \, d\mu = 0 \end{aligned}$$

since the area of the element can be taken to be  $\alpha \beta \, d\lambda \, d\mu$ .

A similar equation is obtained for the equilibrium of forces in the direction of the line element  $ds_1$ . Elimination of  $\theta$  and  $\varphi$  by means of equations (3) and simplification of results, yields the equations for shear forces:

$$\begin{cases} \beta \frac{\partial N_\lambda}{\partial \lambda} + \alpha \frac{\partial N_{\lambda\mu}}{\partial \mu} + N_\lambda \frac{\partial \beta}{\partial \lambda} + 2 N_{\lambda\mu} \frac{\partial \alpha}{\partial \mu} - N_\mu \frac{\partial \beta}{\partial \lambda} + \alpha \beta P_x = 0 \\ \beta \frac{\partial N_{\lambda\mu}}{\partial \lambda} + \alpha \frac{\partial N_\mu}{\partial \mu} - N_\lambda \frac{\partial \alpha}{\partial \mu} + 2 N_{\lambda\mu} \frac{\partial \beta}{\partial \lambda} + N_\mu \frac{\partial \alpha}{\partial \mu} + \alpha \beta P_y = 0 \end{cases} \quad (4)$$

<sup>(1)</sup> W. C. Graustein — «Differential Geometry» — The Macmillan Company, New York, NY 1935.  
<sup>(2)</sup> Timoshenko — Theory of Plates and Shells — Mc Graw-Hill Book Company, Inc. New York, 1940.

Let  $R_I$  and  $R_{II}$  be the principal radii of curvature of the surface and OXYZ a rectangular system of co-ordinates connected to each point of the membrane so that OZ has the direction of the normal to the lines of principal curvature  $\lambda_0, \mu_0$ , Fig. 2.

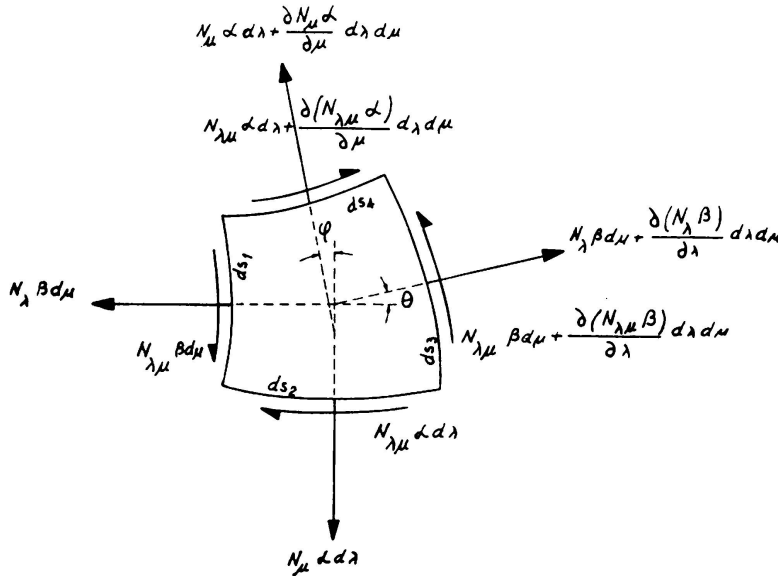


FIG. 1. Membrane equilibrium

The equilibrium equation in the direction of the normal to the surface at the point takes the following well-known form:

$$\frac{N_{\lambda_0}}{R_I} + \frac{N_{\mu_0}}{R_{II}} = P_z \tag{5}$$

These 3 equations (4) and (5) allow to evaluate the state of stress of a thin shell whatever, under a given field of forces, as they contain but three unknowns,  $N_\lambda$ ,  $N_\mu$  and  $N_{\lambda\mu}$  (tensile forces).

**2 - Funicular surfaces**

It is easy to demonstrate that any structural surface can be in membrane equilibrium under a given field of forces but, as a rule this equilibrium is not funicular, i. e. the shell will be subject to compressive and tensile normal forces that will vary from point to point so as to achieve a static equilibrium between the internal shell forces and the external acting forces. In other words, this means that middle surfaces can be chosen for the shell such that under the acting field of forces, all the internal stresses will be of the same sign-all compressive or all tensile stresses. Such surfaces, called funiculars of the field of forces given, have important structural properties and are of great interest for Building Engineering.

Indeed if the middle surface of a very thin plain or slightly reinforced concrete shell is shaped as an anti-funicular surface of the acting

forces a structure is obtained taking the maximum advantage of the strength of this building material. If, on the contrary, the material is steel the structural surface should receive the form of the funicular surface of the acting forces, if steel properties are to be used to the fullest.

In truth, all the builders have had this purpose intuitively in view with a more or less perfect degree of theoretical approximation,

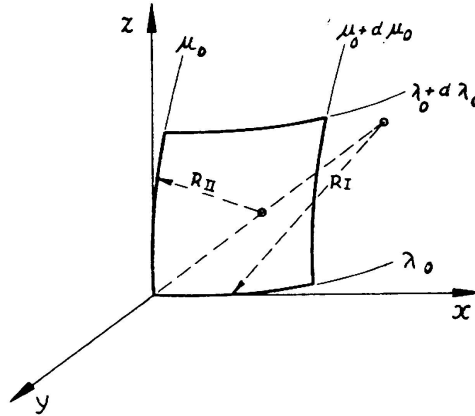


FIG. 2. Lines of curvature of a surface

what is seen in the predominant structural forms in use in all times.

Choosing at a point P a co-ordinate system  $\lambda_0, \mu_0, z_0$ , whose  $z_0$  — axis is normal to the shell surface and assuming the membrane to be uniformly stretched in all directions and  $N_{\lambda_0} = N_{\mu_0} = \text{const.}$ , the differential equation of the funicular surface may be written:

$$\left\{ \begin{array}{l} \frac{1}{R_I} + \frac{1}{R_{II}} = - \frac{p z_0}{\sigma d} \end{array} \right. \quad (6a)$$

$$\left\{ \begin{array}{l} \sigma \frac{\partial d}{\partial \lambda} + \alpha p_{\lambda_0} = 0 \end{array} \right. \quad (6b)$$

$$\left\{ \begin{array}{l} \sigma \frac{\partial d}{\partial \mu} + \beta p_{\mu_0} = 0 \end{array} \right. \quad (6c)$$

in which  $p_{\lambda_0}, p_{\mu_0}, p_{z_0}$  are the components of the uniformly distributed load along the  $\lambda_0, \mu_0$  and  $z_0$  axes,  $d$  the shell thickness at the point in reference and  $\sigma$  the constant stress in the funicular surface (tensile stresses).

$$\sigma \times d = N = \text{const.}$$

The load being uniform and hydrostatic, equations 6b and 6c disappear and taking as approximate values of the membrane curvature the second

order derivatives of the deflections  $\xi_0$  of the funicular surface in relation to the OXY plane, the following equations are obtained:

$$\begin{cases} \frac{1}{R_1} = -\frac{\partial^2 \xi}{\partial x^2} \\ \frac{1}{R_{II}} = -\frac{\partial^2 \xi}{\partial y^2} \end{cases}$$

which substituted in (6a) yield:

$$\frac{\partial^2 \xi}{\partial x^2} + \frac{\partial^2 \xi}{\partial y^2} = -\frac{p}{N} \quad (7)$$

It is thus seen that even in this particular case the determination of a funicular surface calls for the integration of Poisson's equation

$$\nabla^2 \xi = F(x, y) \quad (8)$$

Funicular surfaces have properties in respect to plates similar to those of the funicular curves in relation to beams.

Thus expressions like  $\frac{d^4 \xi}{dx^4} = -\frac{p}{EI}$ ;  $\frac{d^2 \xi}{dx^2} = -\frac{M}{EI}$  and  $\frac{d^2 M}{dx^2} = -p$

are equivalent to  $\nabla^4 \xi = -\frac{p}{EI_p}$ ;  $\nabla^2 \xi = -\frac{M}{EI_p}$  and  $\nabla^2 M = p$  for plates,

provided that in the latter  $I_p = \frac{e^3}{12(1-\nu^2)}$  and  $M = \frac{m_x + m_y}{1+\nu}$ .

Thus, it is seen, that as in the case of beams and arches, laws could be obtained for plates and shells connecting the shape of the funicular surface with the bending and twisting moments acting on the shell.

### 3 - Search for a funicular surface by experimental means

Scholars have always found that the search for the most adequate constant strength structural forms for certain types of acting forces is an exciting subject. Among other valuable works, mention should be made of a thesis presented at the Yugoslav Academy of Sciences in 1908 by Milankovic «Über Schalen gleicher Festigkeit». In this paper — which originated many others by other authors — Pöschl, Flugge, Forchheimer<sup>(3)</sup>, etc. — it was sought to determine by analytical means the shape of some constant strength shells under acting forces with radial symmetry.

<sup>(3)</sup> Pöschl, Th.: Bauing. 8 (1927) S. 624.

Flügge, W.: Statik und Dynamik der Schalen. Berlin 1934, S. 32.

Forchheimer, Ph.: Die Berechnung ebener und gekrümmter Behälterböden. 3 Auflage. Berlin 1931, S. 23.

The differential equation of the constant strength funicular surface can be integrated in this case and the constant strength forms of radially symmetric shells and reservoirs can be obtained by analytical or graphical means.

When no radial symmetry exists for the loads or their distribution is irregular, the mathematical tool has so far been unable to solve the

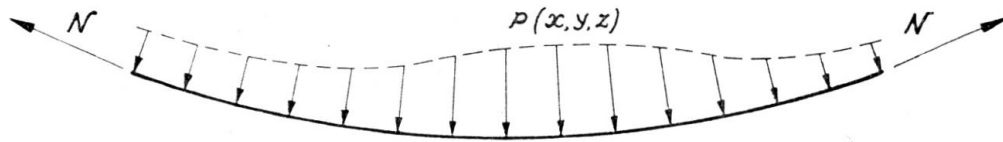


FIG. 3. Funicular equilibrium for  $p(x,y,z)$

problem. The method we have developed half-experimental, half-analytic allows to make good this deficiency of the mathematical tools.

Consider a membrane thin and flexible enough, in tensile equilibrium under a given field of forces, fig. 3.

Obviously the shape it takes, assumed without wrinkles or folds, represents a materialization of one of the funicular surfaces of the field of forces in reference. We say one of the funicular surfaces since there is a double infinity of surfaces enjoying this property, each of them corresponding to a well-defined state of membrane equilibrium.

By a suitable variation of the membrane thickness a funicular surface of constant strength can be obtained. It suffices that the stress field in the membrane be hydrostatic and constant.

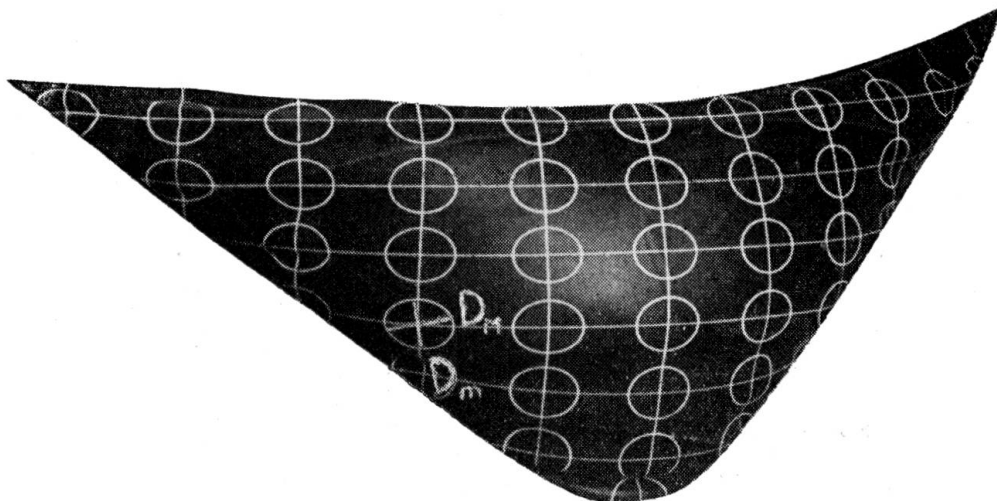


FIG. 4.

From the dimension analysis it is possible to deduce the similitude relationships between the state of stress in the elastic membrane and the state of stress in a shell whose middle surface is homologous to the model.

*It is thus seen that the present method besides allowing to determine the constant strength shape of the shell surface for a given force, immediately yields the state of stress of the corresponding membrane.*

4 - Experimental technique

A rubber membrane is satisfactory from this standpoint, allowing one funicular surface for a given system of forces to be very quickly obtained.

Let us suppose that on the rubber membrane that is going to be used, circumferences are drawn with diameters  $D_0$  and center at different points. Assuming the membrane to be continuous and isotropic the circumferences of small diameter  $D_0$  will change into ellipses, the diameters of which  $D_m$  and  $D_M$ , fig. 4 and 5, will be variable from point to point both in magnitude and direction, allowing the state of stress of the membrane to be calculated. In fact let  $E$  and  $\nu$  be the longitudinal modulus of elasticity and the Poisson's ratio of the membrane. Instead of defining the mean finite strains in the usual

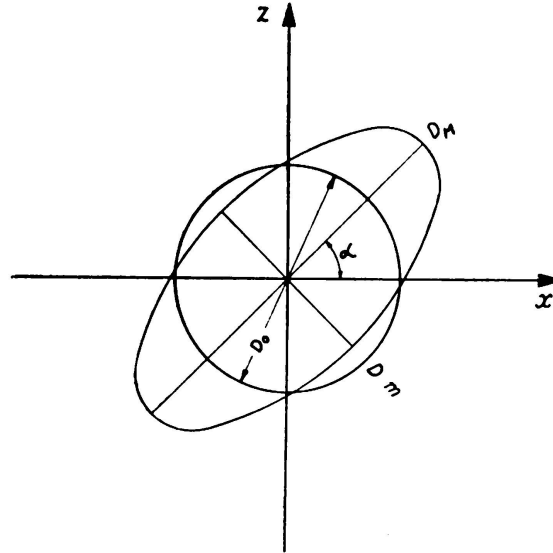


FIG. 5. Homogeneous deformation of a circle

way  $\epsilon = \frac{D_m - D_0}{D_0}$ , the summation of the infinitesimal strains may be used according to Hencky and Chilton (\*).

$$\begin{aligned} \epsilon_M &= \int \frac{D_M}{D_0} d\epsilon = \int \frac{D_M}{D_0} \frac{dx}{x} = \text{Log} \frac{D_M}{D_0} \\ \epsilon_m &= \int \frac{D_m}{D_0} d\epsilon = \int \frac{D_m}{D_0} \frac{dx}{x} = \text{Log} \frac{D_m}{D_0} \end{aligned} \tag{9}$$

For strains of this magnitude and taking the deformed cross-sections of the rubber as the effective sections, Hooke's law is approximately obeyed, provided that  $\epsilon_m \leq 0.1$ .

The corresponding principal stresses may be expressed by means of Hooke's law:

$$\begin{cases} \sigma_M = \frac{E}{1 - \nu^2} (\epsilon_M + \nu \epsilon_m) = \frac{E}{1 - \nu^2} \left( \text{Log} \frac{D_M}{D_0} + \nu \text{Log} \frac{D_m}{D_0} \right) \\ \sigma_m = \frac{E}{1 - \nu^2} (\epsilon_m + \nu \epsilon_M) = \frac{E}{1 - \nu^2} \left( \text{Log} \frac{D_m}{D_0} + \nu \text{Log} \frac{D_M}{D_0} \right) \end{cases} \tag{10}$$

(\*) E. G. Chilton — Graduation Thesis at Stanford University.

These expressions hold for rubber as a first approximation, provided a certain value  $\epsilon$  is not exceeded. However the deformation which rubber and similar substances undergo is much too large to be covered by the classical theory of small strains. An entirely new approach is required for any adequate theory of elasticity of rubber (<sup>5</sup>).

The two families of isostatics on the membrane form two orthogonal funicular nets on the surface. The stress tensor  $N$  on the membrane has at each point of the surface a maximum component given by  $N_M = \sigma_M d$ , in which  $d$  represents the thickness of the deformed membrane at that point.

Once obtained the tensorial field of a funicular surface as defined by the values of  $N_M$  and  $N_m$  at any point and the two isostatics families, the state of stress of a shell with that shape can be calculated in a first approximation. Indeed, the shell having a thickness  $d_b$  and its middle surface coinciding with the funicular surface for the applied forces to a given scale  $\frac{1}{\rho}$ , the following expression is obtained for each point and direction:

$$\sigma = \frac{N \rho^2}{d_b} \quad (11)$$

$N$  being the membrane stresses in the same point and direction.

It is clear that this is but an approximate value, as deformations are set up in the shell which alter its state of stress, when the field of

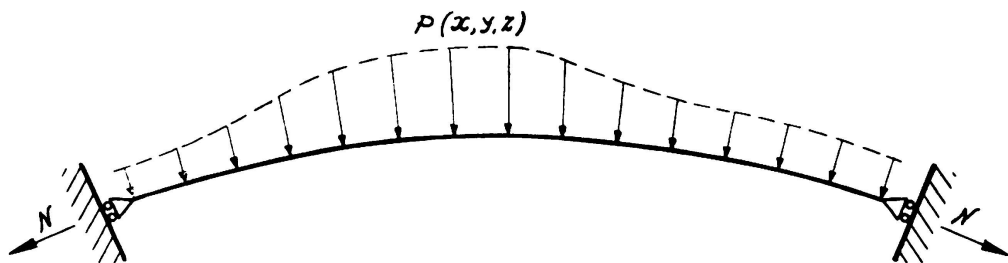


FIG. 6. Membrane condition at the edge

forces is applied. This increase of stress may be safeguarded against, by designing the shell in such a way that the membrane stresses are not much altered. The major factor disturbing the state of stress of the membrane comes from the edge conditions. For this disturbing factor to be lessened, a joint should be built allowing frictionless displacements of the edge of the shell only along a normal to the middle surface, i. e., reproducing the boundary conditions of the membrane, fig. 6. The execution of such a joint presents no technical difficulty whatsoever, improving moreover the structural behaviour of the shell and supplying more space to volumetric changes (temperature, shrinkage, etc).

(<sup>5</sup>) M. Mooney — A Theory of large elastic deformation — Journal of applied physics — Vol. 11, No. 9.

It may still be feared that this method leads to shells so thin as to make probable phenomena of buckling. The theory of the buckling of shells is still in the beginning but approximate formulas are available which give satisfactory results and connect  $\sigma_I$  and  $\sigma_{II}$ , the principal stresses, with the thickness of the shell, the modulus of elasticity and the Poisson's ratio of the material, and the two principal radii of curvature at each point.

5 - Application of the method to the design of dams

The method described in 3 was developed by the author for the study of the shape of a dam to be built in a given valley.

Indeed, dams being built in plain concrete for economic reasons, the middle surface of the structural shape adopted, should coincide with

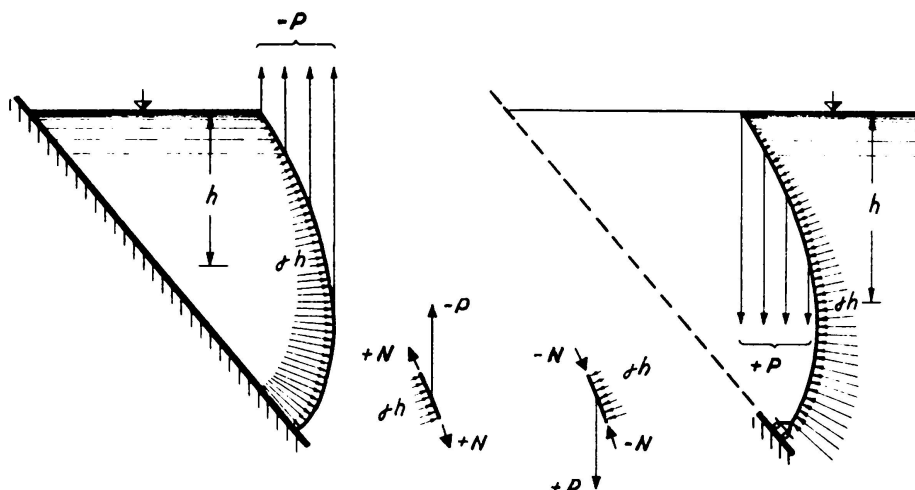


FIG. 7. Membrane equilibrium of a dam

one of the antifunicular surfaces for the forces applied. For dams, however, there are almost exclusively two important static loads: deadweight and water pressure.

Let us consider then a rubber membrane inserted in a boundary geometrically similar to the line of contour of the valley in which the dam is to be placed. This line must be selected according to the shape and geology of the site. Be  $\frac{1}{\rho}$  the scale to which this contour is reproduced. Let us take this line as the contour of a vessel for a liquid of specific gravity  $\gamma$ , held by a rubber membrane, fig. 7. Let us assume, additionally, that the upper contour of the membrane has no rigid connections, remaining on the free level of the fluid. Now we apply at

each point of the rubber membrane a vertical load  $P$ , directed upwards,  $P$  being equal to the weight, to the scale  $\frac{1}{\rho}$ , of each volume element of a shell having the same middle surface but built in concrete, that is:

$$P = -2,4 \gamma \frac{1}{\rho} S \quad (12)$$

$S$  being the area of the surface of the membrane in the center of gravity of which  $P$  acts, and  $d$  the estimated average thickness of the shell in that point.

If the shape of equilibrium displays no folds or wrinkles at any point of its surface, we may say it materializes a funicular surface for the hydrostatic pressure caused by the liquid of specific gravity  $\gamma$  and for the deadweight of a shell, having a middle surface with that shape, so that in each point we have:

$$\frac{N_I}{R_I} + \frac{N_{II}}{R_{II}} = \gamma z + p_n \quad (13)$$

$N_I$  and  $N_{II}$  being the principal membrane forces,  $R_I$  and  $R_{II}$  the two principal radii of curvature, and  $p_n$  the normal component of the deadweight. The field of membrane forces  $N$  can be evaluated by the method described in the foregoing paragraph, so that the state of stress of a dam having as middle surface the shape of the membrane under the action of the deadweight and hydrostatic pressure would be:

$$\sigma = \frac{N \rho^2}{d \gamma} \quad (14)$$

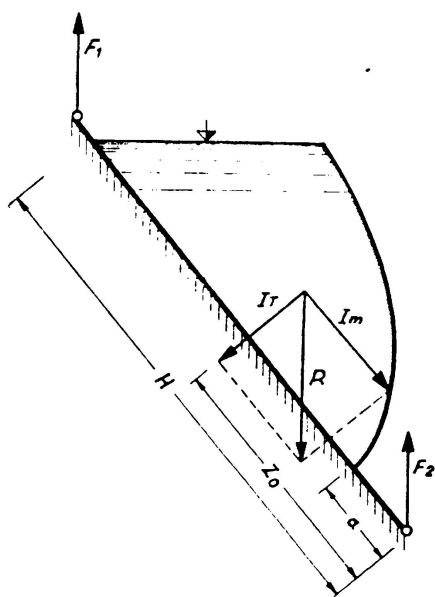


FIG. 8. Resulting vectorial equilibrium

As said above this expression holds only as a first approximation.

The following procedure, for instance, may be followed to design the dam so that the maximum stresses, as calculated by means of expression (14), do not exceed 50 kg. cm<sup>-2</sup>, the increase of these stresses being checked by means of a more accurate method, e. g. three dimensional models <sup>(8)</sup> <sup>(9)</sup>.

Likewise, the total hydrostatic pressure on the dam, can be evaluated by experimental means, the analytical determination being a difficult problem, owing to the shape of the upstream face.

<sup>(8)</sup> G. Oberti — *La Ricerche Sperimentale su modelli como contributo al progetto delle grandi costruzioni* — *Tecnica Italiana* — N.° 2, 1951.

<sup>(9)</sup> M. Rocha — *General review of the present status of the experimental method of structural design*. Sep. da Publicação Preliminar do 3.º Congresso da Association Internationale des Ponts et Charpentes, Cambridge e Londres, 1952.

The hydrostatic force on the membrane is given by the following vector difference, fig. 8:

$$\vec{I}_m = \vec{R} - \vec{I}_t \tag{15}$$

R being the total weight of the container held by the membrane, which is easy to measure.

$$\vec{R} = \vec{F}_1 + \vec{F}_2 \tag{16}$$

The value  $I_t$ , resultant of the hydrostatic pressure on the plate is also easy to compute, provided the contour of the membrane has an easy analytical expression.

$$I_t = \int_a^H \gamma z (H - z) dz \tag{17}$$

The resultant  $I_t$  acts in a direction normal to the plate, at a point at a distance  $Z_o$  from the center of application of  $F_2$ ,

$$Z_o = \frac{\int_a^H (H - z) z dz}{\int_a^H (H - z) dz} \tag{18}$$

Thus by means of a simple graphical construction  $I_m$  can be determined, hence the total hydrostatic pressure on the dam is:

$$\vec{I} = - I_m \vec{e}^3 \tag{19}$$

**6 - Illustrative example**

In order to design a dam by the foregoing method the author devised an adequate apparatus, fig. 9. This, essentially, is made up of a plate of insertion for the membrane (1), a graduated plane to which the rubber membranes are connected by means of a hoop that materializes the insertion line. All the setup hangs from a dynamometric system (3).

A tridimensional co-ordinometer was used to measure the deformed membrane and to determine its co-ordinates referred to the system of axes OXYZ. It consists of three bars representing the three axes of the co-ordinate system, its movement being controlled by one button only (7). Before starting the test, the apparatus is set up. The plate is given the desired inclination and the position of the axes relatively to the plate is recorded by means of various adjusting screws of the co-ordinometer.

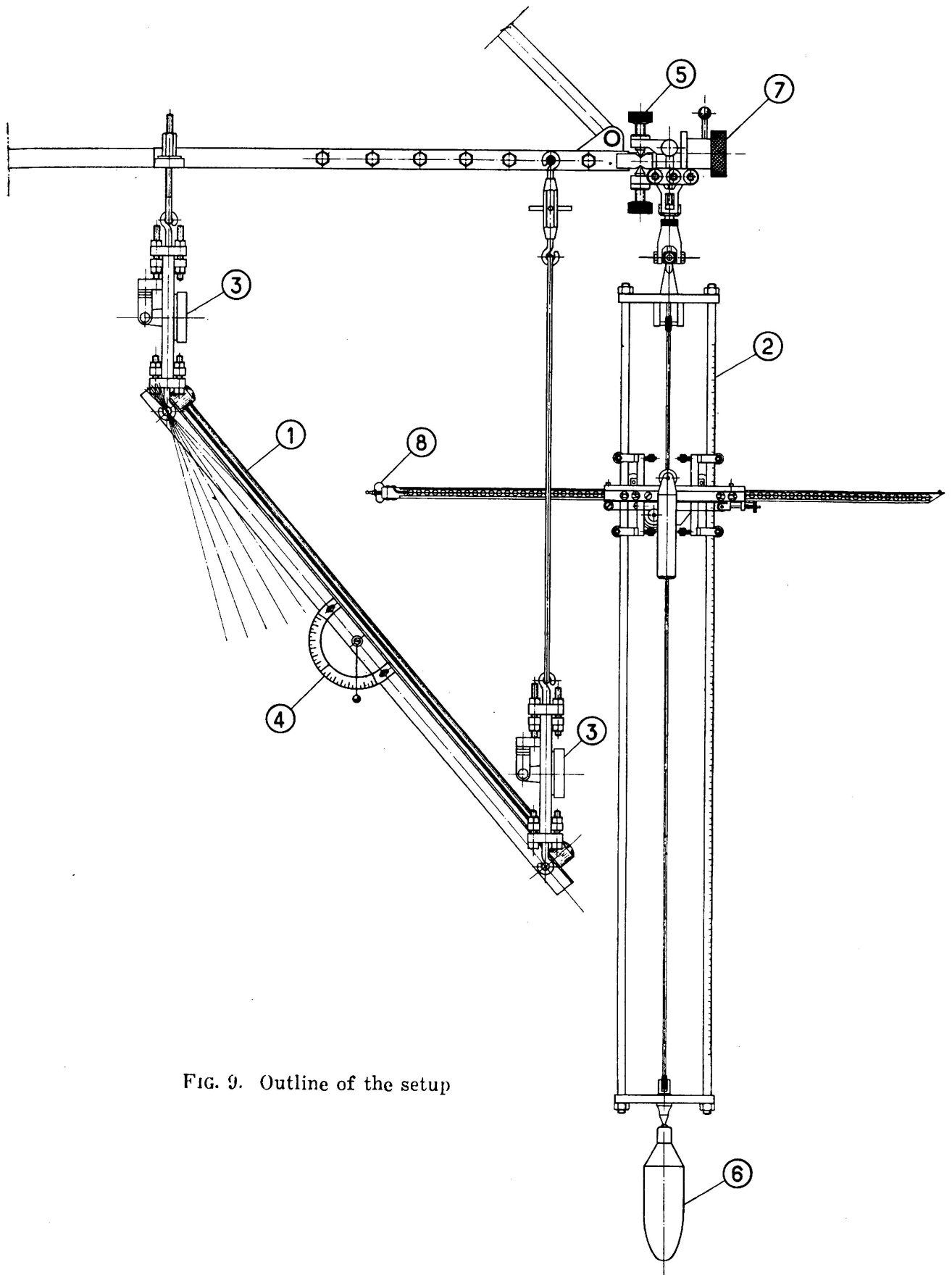


FIG. 9. Outline of the setup

The method of design, based on this experimental technique was applied to an actual case in order to check the shape and volume of a dam planned by this means <sup>(10)</sup>.

The valley selected possessed an exceptional symmetry on the site of the dam, so that a symmetrical contour of simple analytical expression could be adopted.

Fig. 10 shows in full line the insertion contour adopted and in dotted line the topographic section obtained by cutting the valley by a plane.

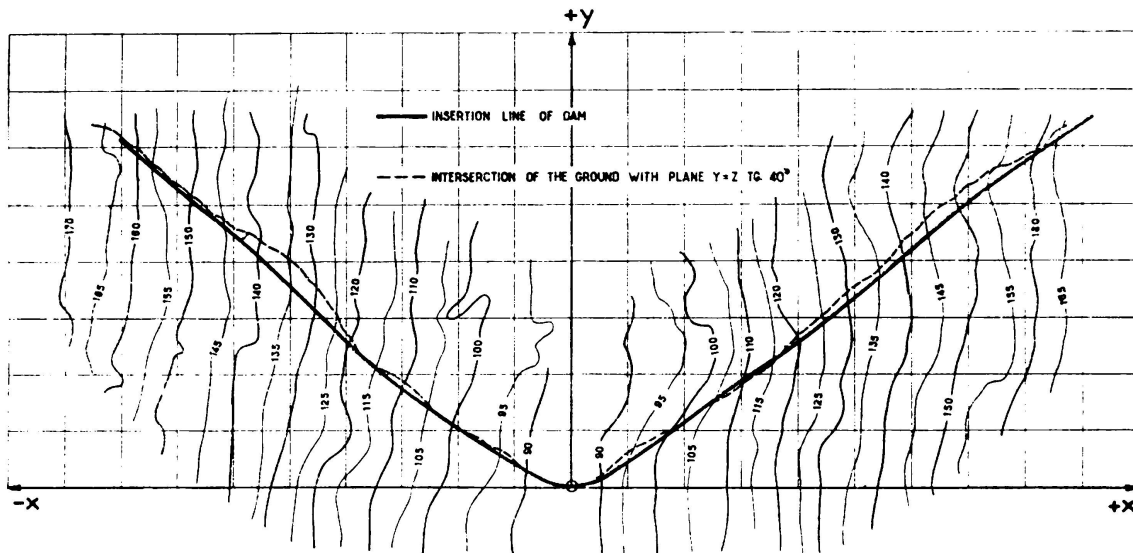


FIG. 10. Insertion lines

Relatively to the co-ordinate system OXYZ shown in the figure, in which OZ is vertical, the chosen contour is represented by the equation:

$$\begin{cases} x = \pm \sqrt{\frac{y(y + 22.886)}{0,595}} \\ y = z \operatorname{tg} 40^\circ \end{cases} \quad (20)$$

This is a branch of hyperbola resting on a plane making a 50° angle with the horizontal plane.

Pure vulcanized rubber was used to manufacture the membrane; it was calendered in both directions, in order to ensure a more perfect isotropy. The elastic properties were evaluated up to values  $\epsilon \cong 0,1$ , fig. 11.

Furthermore it was sought to give such thicknesses to the membrane as to obtain surfaces of equilibrium not very different from the most recent shapes of arch dams in order to prevent constructional objections.

<sup>(10)</sup> The study of this dam was carried out in collaboration with Mr. Peres Rodrigues.

After some trials the shape of equilibrium shown in fig. 12 was selected. It corresponds to a distribution of thickness allowing the stress in the membrane not to exceed  $50 \text{ kg.cm}^{-2}$  as we can see in table I and fig. 13 in which the magnitudes and directions of the principal stresses were evaluated.

Afterwards the membrane was measured by means of the pendulum, and the co-ordinates in various points of the same vertical profile were determined, table II. In fig. 14 we show the horizontal curves of the deflected membrane.

The analytical definition of the dam was based on the following geometric procedure: The upstream and downstream faces were obtained

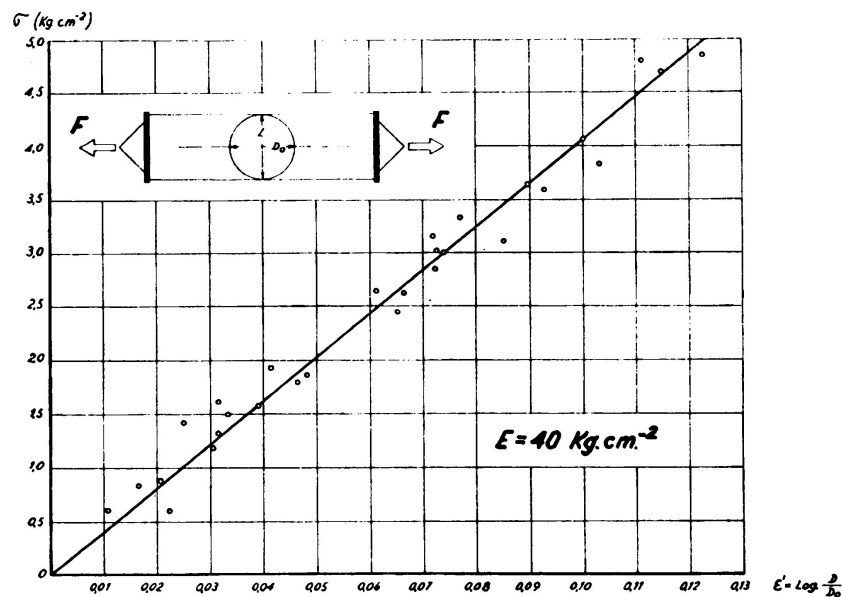


FIG. 11. Stress-strain relationship for rubber

from a middle surface, approaching as much as possible the surface of the membrane to the scale of the dam, by marking along the normal for both sides half the thickness calculated for each point.

The solid — dam — is therefore totally defined, once the equation of the middle surface and the law of the variation of thickness are settled.

The analytical definition of a middle surface as near as possible to the surface of the membrane and at the same time simple, was obtained in the following manner:

The horizontal curves are conic sections having 5 directrices (also conics) intersecting at point  $(0, 0, 0)$ . Thus the analytically defined geometric surface has no less than 17 points of contact with the surface obtained experimentally, fig. 15.

The general equation for the horizontal curves is therefore:

$$y = c - \sqrt{b - ax^2}$$

The parameters a, b, c are obtained by the condition of contact with the following directrices:

*Directrix d<sub>c</sub>* — Corresponding to the branch of hyperbola, defining the insertion line of the dam

$$\begin{cases} x_e = \pm \frac{y_e (y_e + 22,886)}{0,595} \\ y_e = z \operatorname{tg} 40^\circ \end{cases}$$

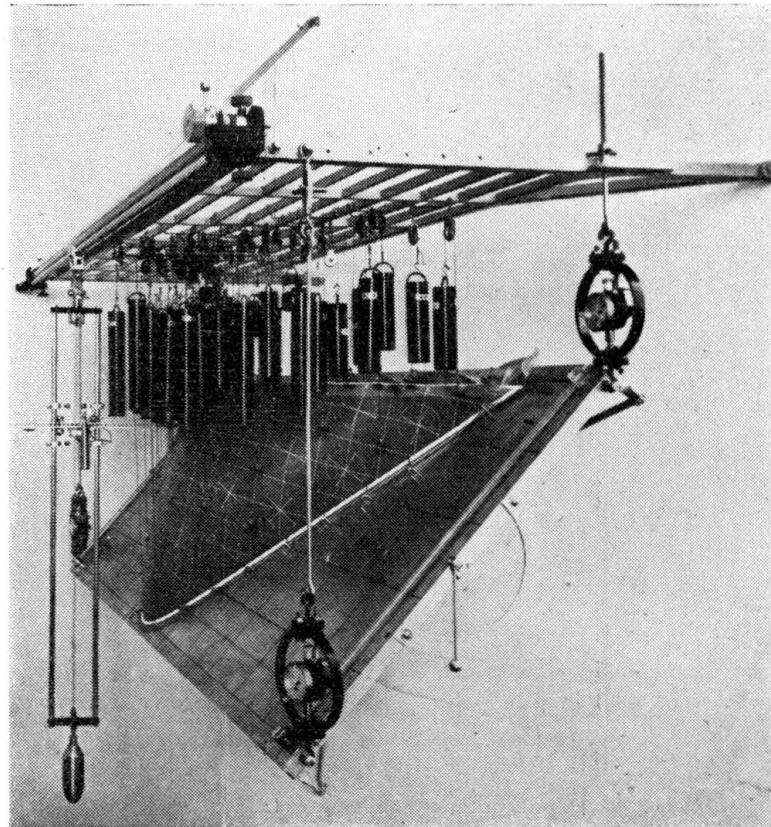


FIG. 12.

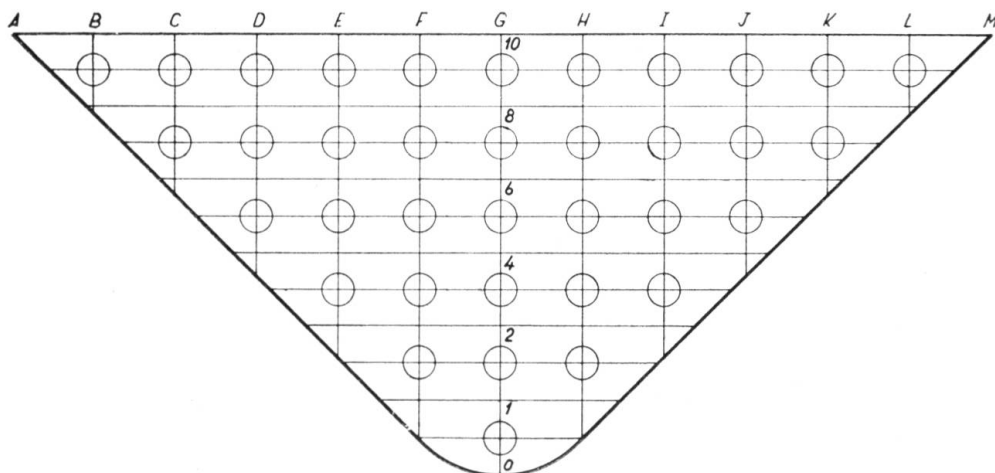


FIG. 13. Points at which the stress was measured

*Directrix*  $d_0$  — Vertical profile through point (0, 0, 0)

$$\begin{cases} y_0^2 - (0,579 Z + 24,240) y_0 + (0,225 Z^2 - 5,7087 Z) = 0 \\ x_0 = 0 \end{cases}$$

*Directrices*  $d_m$  — Two branches of a conic section given by the expressions

$$\begin{cases} x_m^2 - (3,094 y_m + 2,511) x_m + (5,587 y_m^2 + 0,920 y_m) = 0 \\ y_m = \frac{Z}{2} \end{cases}$$

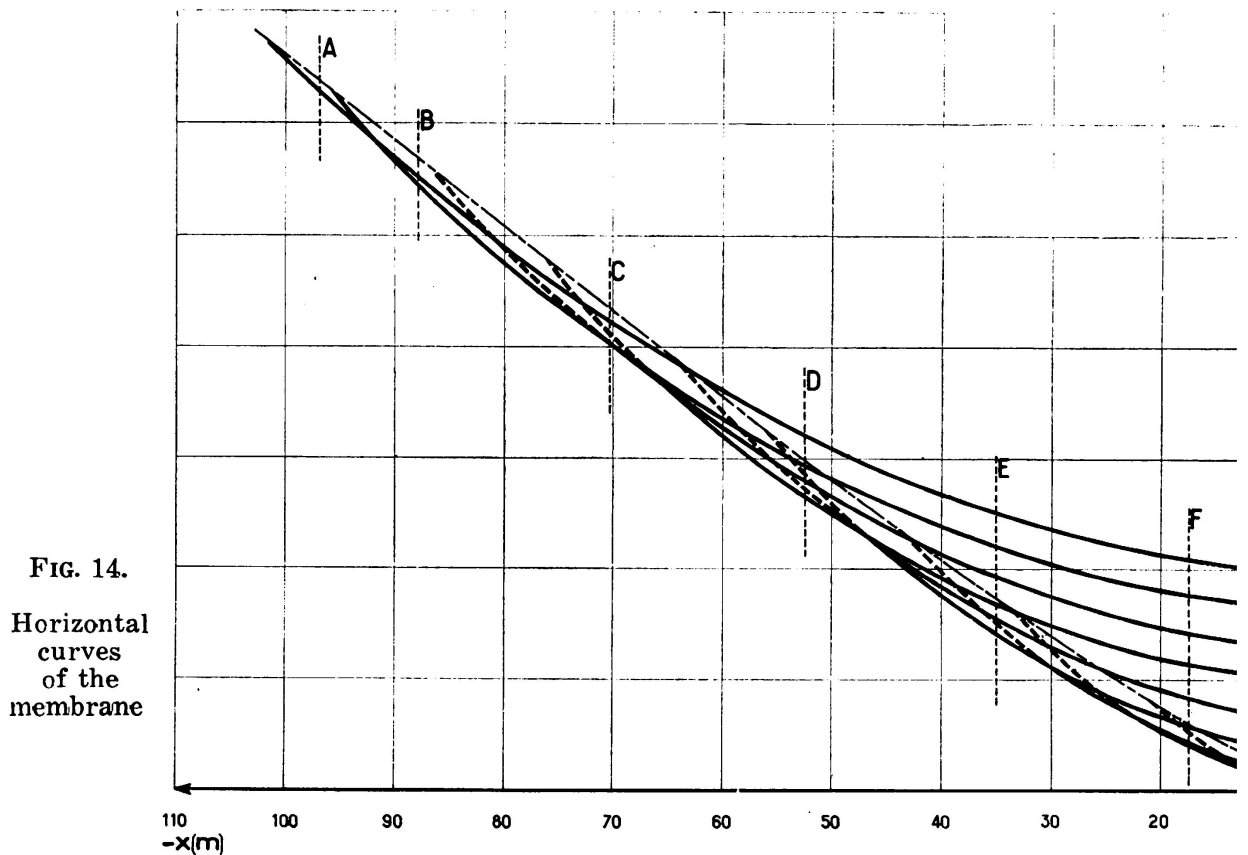


FIG. 14.  
Horizontal  
curves  
of the  
membrane

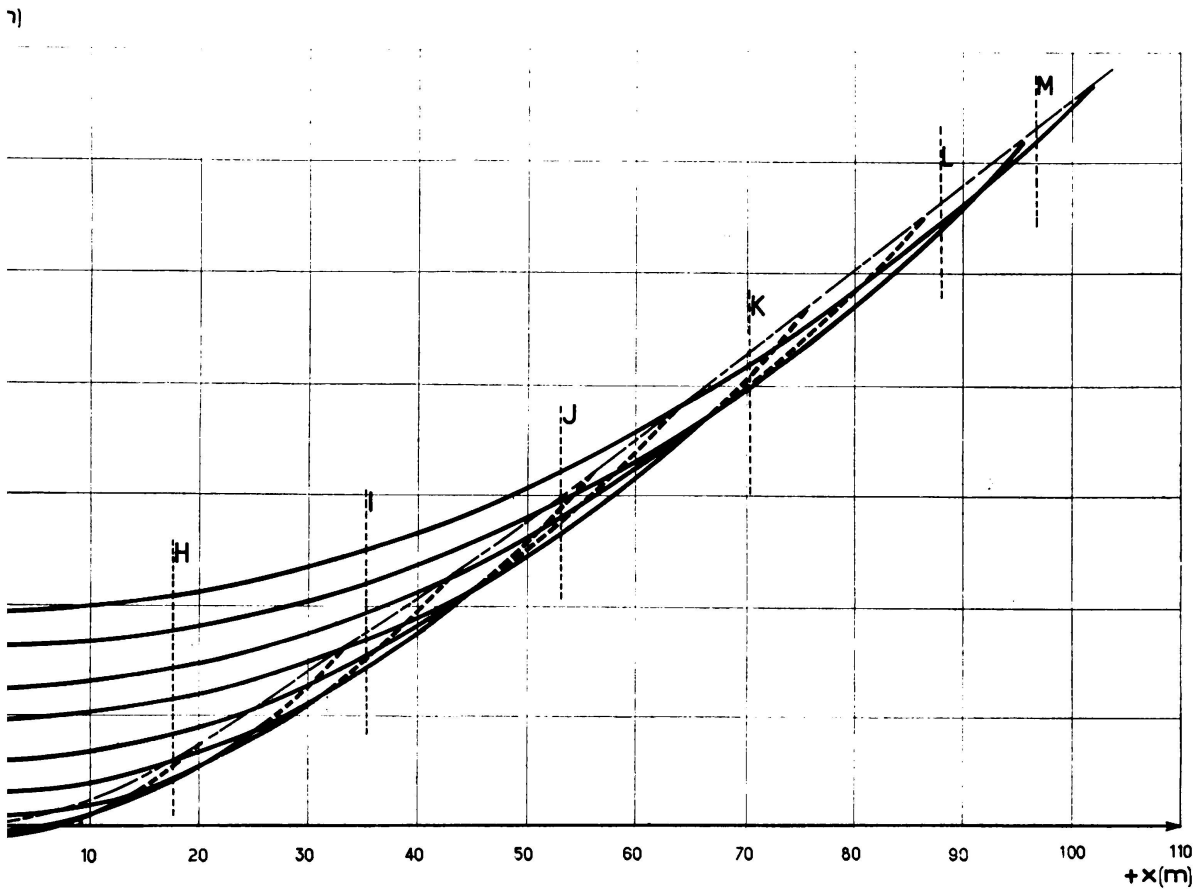
In fig. 16 are indicated the vertical profiles of the surface, as analytically defined, and the points obtained experimentally from the co-ordinate measurements on the stretched membrane. The maximum differences do not exceed 3 mm to a scale of 1/200, that is to say they are less than 60 cm in the prototype.

The variation of the thickness of the dam was chosen in such a way, as to correspond to the loads fixed for the deadweight and, within the limits imposed by this condition, to bring about the best possible distribution of stresses inside the dam.

Thus two laws of variation for the thickness were selected according to the boundary conditions, fig. 17.

1<sup>st</sup> Case — *Built-in contour* — The thickness along the normal varies only, with respect to the elevation i. e. it does not change along a horizontal curve.

2<sup>nd</sup> Case — *Shell with a perimetric contour joint* — This joint should be made in such a way as not to disturb to a large extent the membrane conditions of the contour.



Along one horizontal curve of elevation  $z$  the thickness measured along the normal, changes according to the expression:

$$e_x = e_0 - \frac{e_0 - e_n}{d^2} x^2$$

where  $e_0$  is the thickness of the middle cross-section as defined by the law concerning the built-in case and  $e_n$  represents the thickness

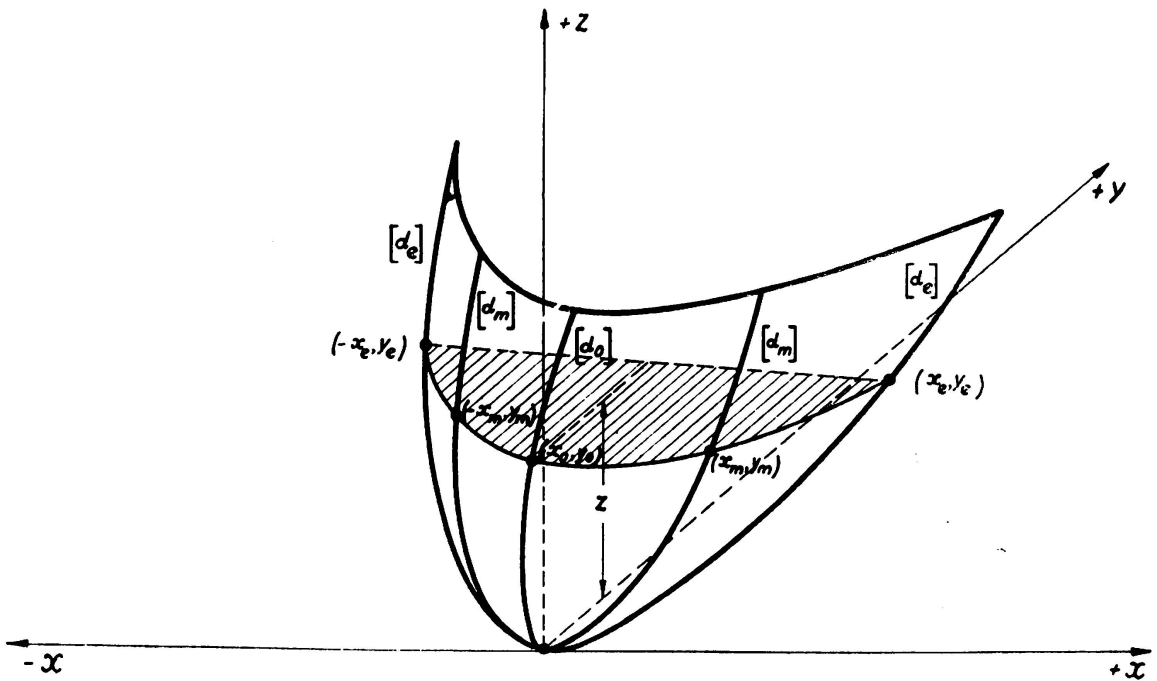


FIG. 15. Analytic expression of the middle surface

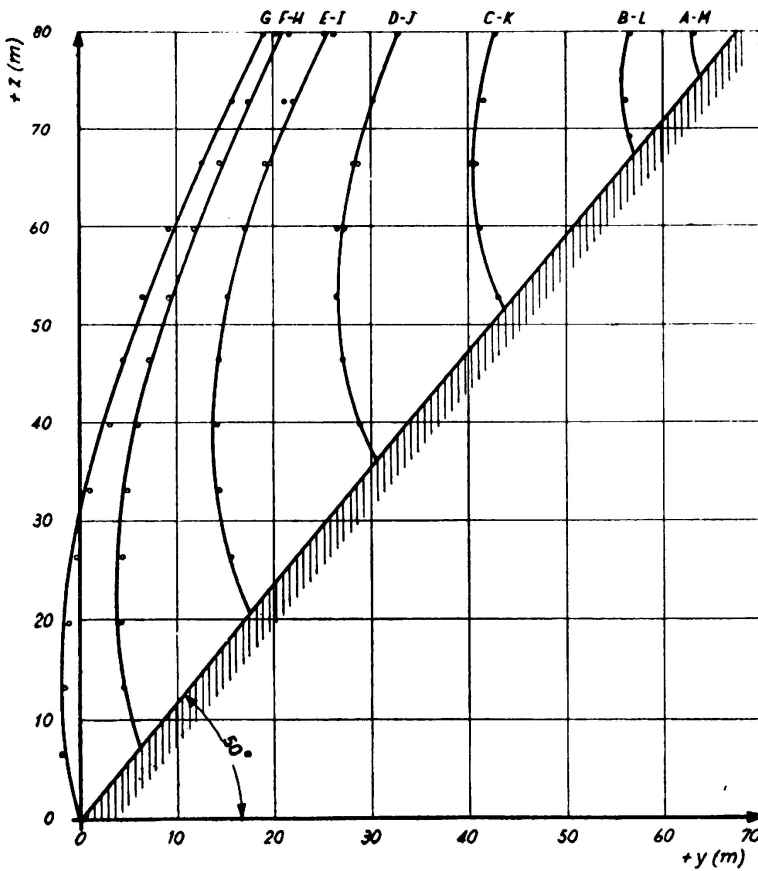


FIG. 16. Computed and experimental profiles

in the insertion contour:

$$e_n = -0,00146 z^2 + 0,0567 z + 6$$

d being the half-chord of the horizontal curves at that level;

$$d = \frac{z(z + 27,274)}{0,845}$$

That is, in this case the thickness can be somewhat smaller along the contour as the perimetral joint diminishes the moments due to the differences between the funicular surface and the middle surface, when deflected under load.

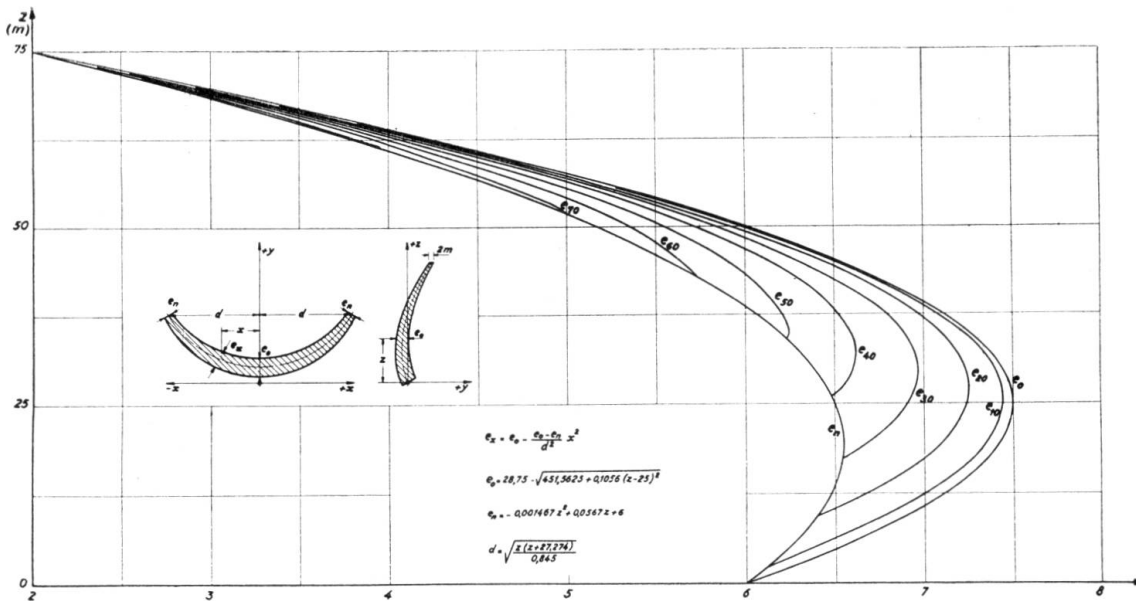


FIG. 17. Law of variation of the thickness

From these data the dam was designed with the following characteristics, fig. 18.

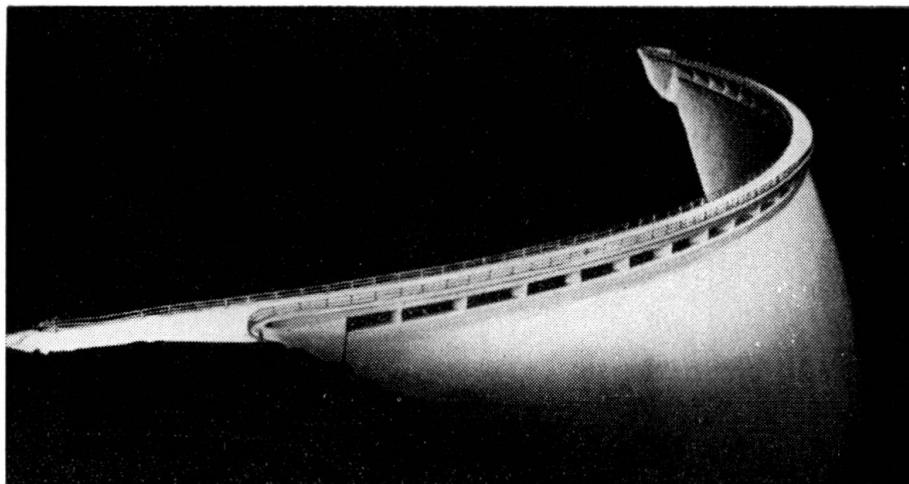


FIG. 18

|   |     |                                     |
|---|-----|-------------------------------------|
| Height  | ... | H = 77 m                            |
| Semi-axes of the ellipse of crest                               | ... | { a = 434,9 m                       |
|   |     | { b = 207,7 m                       |
| Angular width between the normals to the ellipse in the contour | ... | $\varphi = 92^\circ$                |
| Maximum thickness of the dam                                    | ... | $e_m = 7,5$ m                       |
| Volume of concrete  | ... | V = $54 \times 10^3$ m <sup>3</sup> |
| Maximum length chord  | ... | C = 198 m                           |
| Maximum membrane stress (compressive)                           | ... | = 46 kg. cm <sup>-2</sup>           |

TABLE I

| Point     | Model     |                                  |                                  |                                |                                |                           |                           | Prototype    |   |  |
|-----------|-----------|----------------------------------|----------------------------------|--------------------------------|--------------------------------|---------------------------|---------------------------|--------------|---|--|
|           | d<br>(mm) | $\varepsilon_M$<br>( $10^{-2}$ ) | $\varepsilon_m$<br>( $10^{-2}$ ) | $\sigma_M$<br>(Kg cm $^{-2}$ ) | $\sigma_m$<br>(Kg cm $^{-2}$ ) | $N_M$<br>(Kg cm $^{-1}$ ) | $N_m$<br>(Kg cm $^{-1}$ ) | $d_b$<br>(m) | $\sigma_b^I = N_M \frac{\rho^2}{d_b}$<br>(Kg cm $^{-2}$ ) | $\sigma_b^{II} = N_m \frac{\rho^2}{d_b}$<br>(Kg cm $^{-2}$ ) |
| 10B - 10L | 0,65      | 3,1                              | -                                | 1,3                            | 0                              | 0,08                      | 0                         | 2,00         | 20  | 0  |
| 10C - 10K | 0,65      | 4,2                              | -                                | 1,7                            | 0                              | 0,11                      | 0                         | 2,00         | 26  | 0  |
| 10D - 10J | 0,65      | 5,6                              | -                                | 2,3                            | 0                              | 0,15                      | 0                         | 2,00         | 35  | 0  |
| 10E - 10I | 0,65      | 6,3                              | -                                | 2,5                            | 0                              | 0,16                      | 0                         | 2,00         | 40  | 0  |
| 10F - 10H | 0,65      | 6,3                              | -                                | 2,5                            | 0                              | 0,16                      | 0                         | 2,00         | 40  | 0  |
| 10G       | 0,65      | 7,2                              | -                                | 2,9                            | 0                              | 0,19                      | 0                         | 2,00         | 46  | 0  |
| 8C - 8K   | 1,10      | 6,4                              | 1,3                              | 2,6                            | 0,3                            | 0,29                      | 0,03                      | 4,10         | 34  | 4  |
| 8D - 8J   | 1,10      | 6,4                              | 1,3                              | 2,6                            | 0,3                            | 0,29                      | 0,03                      | 4,10         | 34  | 4  |
| 8E - 8I   | 1,10      | 7,8                              | 1,2                              | 3,3                            | 0,5                            | 0,36                      | 0,05                      | 4,10         | 42  | 6  |
| 8F - 8H   | 1,10      | 8,0                              | 1,0                              | 3,4                            | 0,6                            | 0,37                      | 0,07                      | 4,10         | 44  | 8  |
| 8G        | 1,10      | 8,6                              | 1,0                              | 3,7                            | 0,7                            | 0,40                      | 0,08                      | 4,10         | 46  | 9  |
| 6D - 6J   | 1,10      | 9,3                              | 0                                | 4,1                            | 1,2                            | 0,45                      | 0,14                      | 5,80         | 38  | 11   |
| 6E - 6I   | 1,10      | 9,4                              | 1,0                              | 4,0                            | 0,9                            | 0,44                      | 0,09                      | 5,80         | 37  | 8  |
| 6F - 6H   | 1,10      | 9,6                              | 1,2                              | 4,1                            | 0,7                            | 0,45                      | 0,08                      | 5,80         | 37  | 7  |
| 6G        | 1,10      | 9,9                              | 1,4                              | 4,2                            | 0,6                            | 0,46                      | 0,07                      | 5,80         | 38  | 6  |
| 4E - 4I   | 1,65      | 9,0                              | 2,4                              | 3,6                            | 1,1                            | 0,60                      | 0,19                      | 7,00         | 41  | 13   |
| 4F - 4H   | 1,65      | 9,0                              | 2,4                              | 3,6                            | 1,1                            | 0,60                      | 0,19                      | 7,00         | 41  | 13   |
| 4G        | 1,65      | 9,1                              | 0                                | 4,0                            | 1,2                            | 0,66                      | 0,20                      | 7,00         | 46  | 14   |
| 2F - 2H   | 1,65      | 8,0                              | 2,0                              | 3,2                            | 1,2                            | 0,54                      | 0,20                      | 7,00         | 37  | 14   |
| 1G        | 1,7       | 4,7                              | 0,4                              | 2,0                            | 0,4                            | 0,34                      | 0,08                      | 6,40         | 26  | 10   |

TABLE II

| Profiles | $y = f(x,z)$ (mm) |       |       |       |       |       |     |
|----------|-------------------|-------|-------|-------|-------|-------|-----|
|          | A — M             | B — L | C — K | D — J | E — I | F — H | G   |
| 0        |                   |       |       |       |       |       | 40  |
| 2        |                   |       |       |       |       | 62    | 35  |
| 4        |                   |       |       | 172   | 106   | 69    | 55  |
| 6        |                   |       | 172   | 160   | 110   | 80    | 70  |
| 8        |                   |       | 225   | 167   | 128   | 105   | 97  |
| 10       | 334               | 300   | 238   | 192   | 159   | 140   | 134 |

## SUMMARY

The author begins by presenting the advantages of putting to avail the three dimensionality in the structural behaviour of a shell, by giving it a double curved shape, so as to obtain an almost exclusively compressive state of stress. He then introduces the notion of funicular surface, a generalization of the funicular curve to the three dimensions.

A mathematical basis is given for an analytical approach to the problem but owing to its complexity, it is only sketched.

It is shown that the problem is very easy to solve by experimental means, the state of stress of the funicular surface being likewise calculated by a quick method, whatever the shape obtained.

The method expounded is then applied to the design of an 80 m high dam.

## ZUSAMMENFASSUNG

Der Verfasser weist in erster Linie auf die Zweckmässigkeit der Ausnützung dreier Dimensionen beim Entwurf einer Schale hin. Es soll dieser eine doppelte Krümmung gegeben werden, so dass die Eigenspannungen fast ausschliesslich und in allen Richtungen Druckspannungen sind. Dann wird der Begriff «Seilfläche», eine Erweiterung der Seilkurven auf drei Dimensionen, dargelegt.

Der Verfasser erörtert eine mathematische Grundlage zur analytischen Betrachtung dieser Frage, die aber wegen ihrer Komplexität nur leicht skizziert wird.

Es wird die Möglichkeit gezeigt, wie man das Problem experimentell leicht lösen kann, wobei auch der Spannungszustand in der Seilfläche ungeachtet der gefundenen Form rasch festzustellen ist.

Die beschriebene Methode wird dann angewendet zur Berechnung einer 80 m hohen Staumauer.

#### RESUMO

O autor começa por apresentar a vantagem de se tirar partido das três dimensões no comportamento estrutural duma cúpula dando-lhe dupla curvatura por forma que o estado de tensão seja quase exclusivamente de compressão em todas as direcções. Introduce em seguida a noção de superfície funicular, generalização a 3 dimensões das linhas funiculares.

Apresenta uma base matemática para o tratamento analítico deste problema mas, dada a sua complexidade fica apenas esboçada.

Seguidamente mostra a possibilidade de resolver aquele problema com grande simplicidade por via experimental podendo também calcular-se o estado de tensão na superfície funicular por meio dum método rápido, qualquer que seja a forma obtida.

O método é aplicado a título de exemplo no dimensionamento duma barragem de 80 m de altura.

#### RÉSUMÉ

L'auteur présente d'abord les avantages que l'on peut avoir à tirer parti des trois dimensions dans le comportement structural d'une coupole, en lui donnant une forme à double courbure de façon à obtenir presque exclusivement des contraintes de compression. Il introduit ensuite la notion de surface funiculaire, généralisation des courbes funiculaires aux trois dimensions.

Il présente une base mathématique permettant de traiter analytiquement le problème, mais, étant donné sa complexité, cette méthode n'est qu' ébauchée.

Il montre ensuite la possibilité de résoudre ce problème très aisément par voie expérimentale, la contrainte à la surface funiculaire pouvant être également calculée au moyen d'une méthode rapide, quelle que soit la forme obtenue.

À titre d'exemple la méthode présentée est appliquée au calcul d'un barrage de 80 m de hauteur.

## **II a 3**

### **Statischen Behandlung von schiefen Platten**

#### **Ensaaios estáticos de placas oblíquas**

#### **Essais statiques de plaques obliques**

#### **Statical tests of skew plates**

DR. ING H. VOGT

Eckernförde

Der heutige Verkehr erfordert eine gerade Führung der Verkehrswege auch bei Unter- und Überführungen. Die meisten Brücken, insbesondere fast alle kleineren, müssen daher als schiefe Brücken erstellt werden. Bei vielen dieser Brücken wird das Tragsystem durch eine schiefe Platte über ein Feld oder über mehrere Felder durchlaufend gebildet. Die Frage nach dem Tragverhalten schiefer Platten ist daher für den Brückenbau von grösster Wichtigkeit.

In der letzten Zeit hatte ich Gelegenheit, mehrere schiefe Plattenbrücken zu bearbeiten. Die auftretenden Momente wurden mit Hilfe von Modellversuchen und zwar durch Krümmungsmessungen an Modellen aus Kunststoffplatten [1] bestimmt. Diese Methode der modellmässigen Ermittlung der Momente hat sich bei dieser Bauwerksart bewährt. Durch vergleichende Betrachtungen der einzelnen Untersuchungen in Verbindung mit den vorliegenden theoretischen Untersuchungen konnten wertvolle Erkenntnisse zusammengestellt werden. An dieser Stelle kann ich natürlich die Frage nicht erschöpfend behandeln, sondern kann nur ein ganz kleines Bild von dem umfangreichen Material bringen. Im übrigen weise ich auf die in Kürze erscheinenden Abhandlungen hin.

Es zeigt sich, dass es möglich ist, die Momente, die Momentenrichtungen, die Form der Momentenflächen, sowie die Auflagerkräfte einer schiefen Einfeldplatte mit der für die Praxis erforderlichen Genauigkeit abzuschätzen. Modellversuche für normale, d. h. nicht gleichzeitig gekrümmte schiefe Einfeldplatten sind daher nicht mehr erforderlich.

Die Momente einer schiefen Einfeldplatte können nach den Momenten einer entsprechenden rechtwinkligen Vergleichsplatte berechnet werden. In Bild 1 sind als Beispiel einige Beziehungen dargestellt. Die Beiwerte  $\beta$  und  $\gamma$  sind von dem Verhältnis  $b/l$  und der Schiefe  $\varphi$  abhängig

und sind bereits in einer Abhandlung in der Zeitschrift Beton- und Stahlbetonbau 1955 [2] veröffentlicht. Die Richtung der Hauptmomente einer schiefen Platte kann für den Bereich der Plattenmitte in erster Annäherung in einer mittleren Richtung zwischen der Richtung des freien Randes und einer Senkrechten auf das Widerlager angenommen werden.

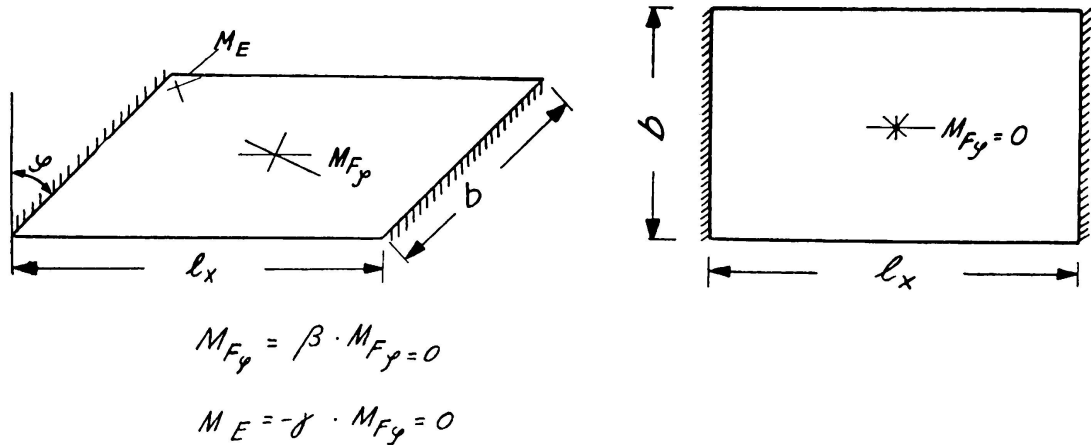


BILD. 1

Aber nicht nur die Momente, sondern auch die Gestalt der Momentenfläche einer schiefen Platte ändert sich gegenüber derjenigen einer rechtwinkligen. Es tritt eine Verschiebung des maximalen Momentenpunktes zur stumpfen Ecke hin auf. Bild 2 und Bild 3 zeigen diese Verschiebung. Der Beiwert «u» ist nur von der Schiefe abhängig. Die

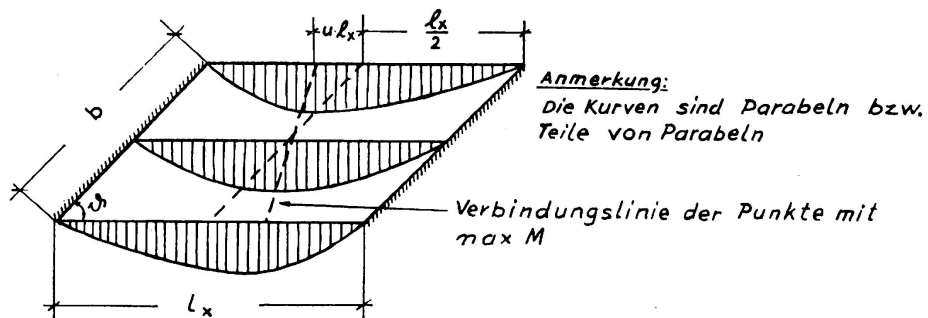


BILD. 2. Momente in Tragrichtung durch ständige Last

grössten Abweichungen gegenüber den Momenten einer rechtwinkligen Platte treten jedoch auf für die Momente quer zur Tragrichtung. Die typischen Formen der Momentenlinien gehen aus Bild 4 hervor. Die Grösse und das Vorzeichen der Momente für den Schnitt c-c ist von der Schiefe und dem Verhältnis  $b/l_1$  abhängig. Bei breiten Platten können die Momente positiv werden. Schon bei verhältnismässig geringer Schiefe kann das negative Moment in der stumpfen Ecke grösser als das maximale Feldmoment werden.

Was die Berechnung der Auflagerkräfte anbelangt, so lassen sich auch hier einfache Beziehungen ableiten, so dass sie für eine schiefe Einfeldbrücke leicht ermittelt werden können.

BILD. 3. Momente in Tragrichtung durch Verkehrslast

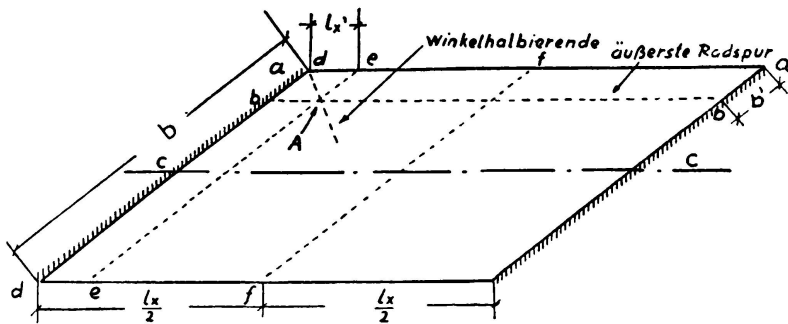
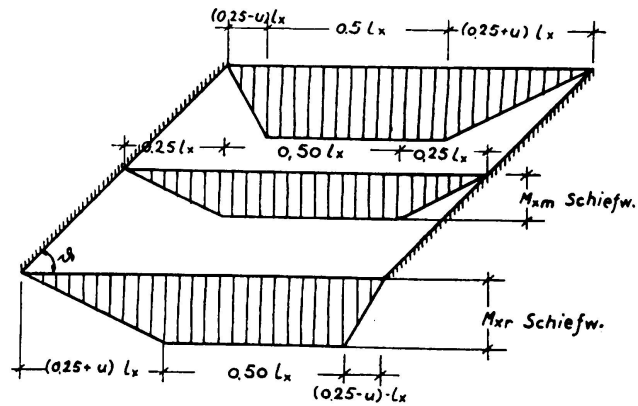
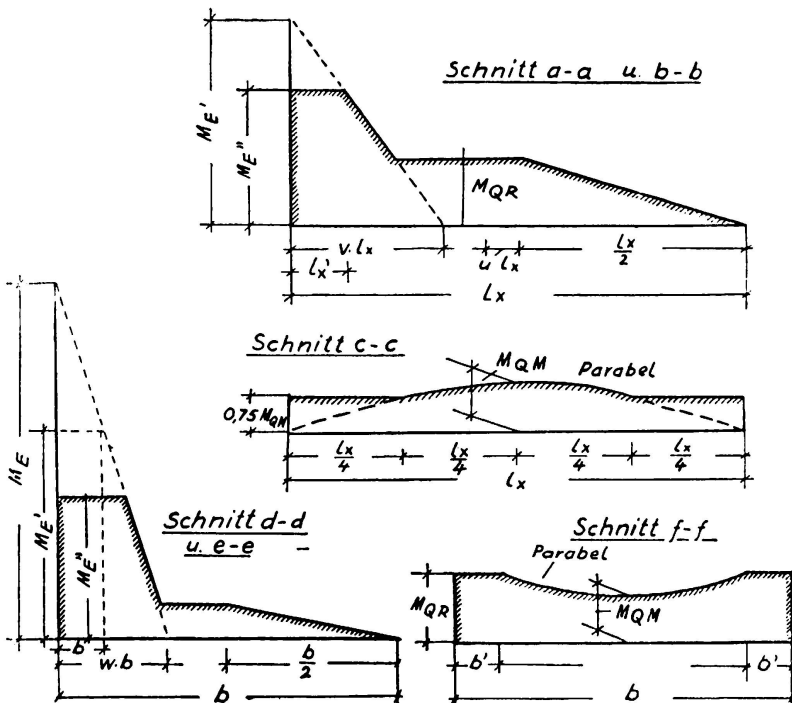


BILD. 4. Grösse und Verteilung der Momente quer zur Tragrichtung



Bei schiefen Plattenstreifen über mehrere Felder werden die auftretenden Fragen natürlich bedeutend schwieriger. Auch hier konnten

jedoch eine Reihe wichtiger Erkenntnisse gesammelt werden. Leider sind die Unterlagen noch zu lückenhaft, um ebenso wie bei schiefen Einfeldplatten ein Berechnungsschema anzugeben. Bei schiefen Platten über mehreren Feldern sind daher Modellversuche erforderlich, wenn nicht Modellversuche von Brücken mit ähnlicher Schiefe und ähnlichen Stützweitenverhältnissen vorliegen, die ein Interpolieren gestatten.

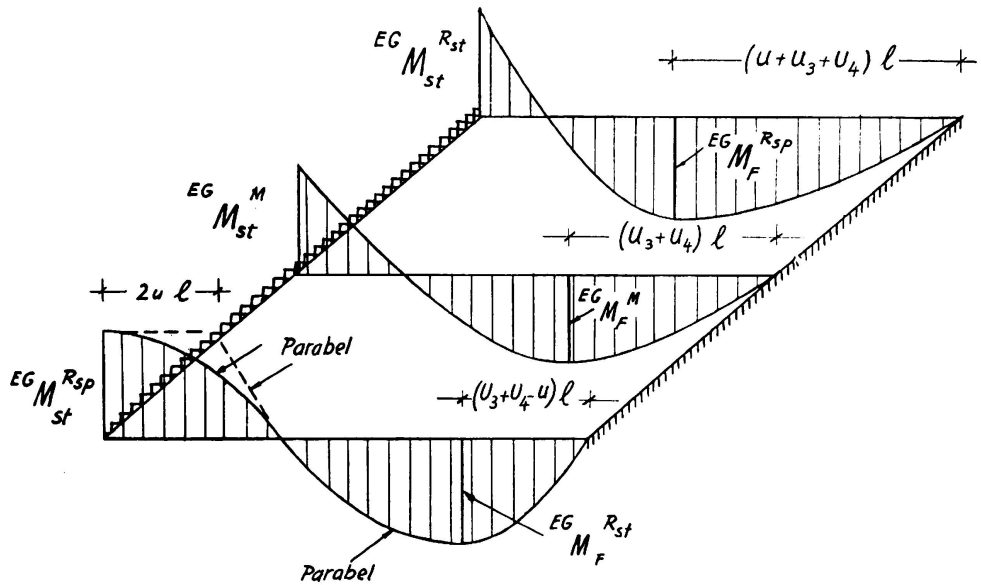


BILD. 5. Momente in Tragrichtung durch ständige Lasten

Als wichtigste Erkenntnis ergab sich, dass das Problem der Durchlaufwirkung und das Problem der Schiefwinkligkeit nicht getrennt behandelt werden können. Die Durchlaufwirkung ist von der Grösse der Schiefwinkligkeit abhängig. Bei schiefwinkligen Systemen geht je nach

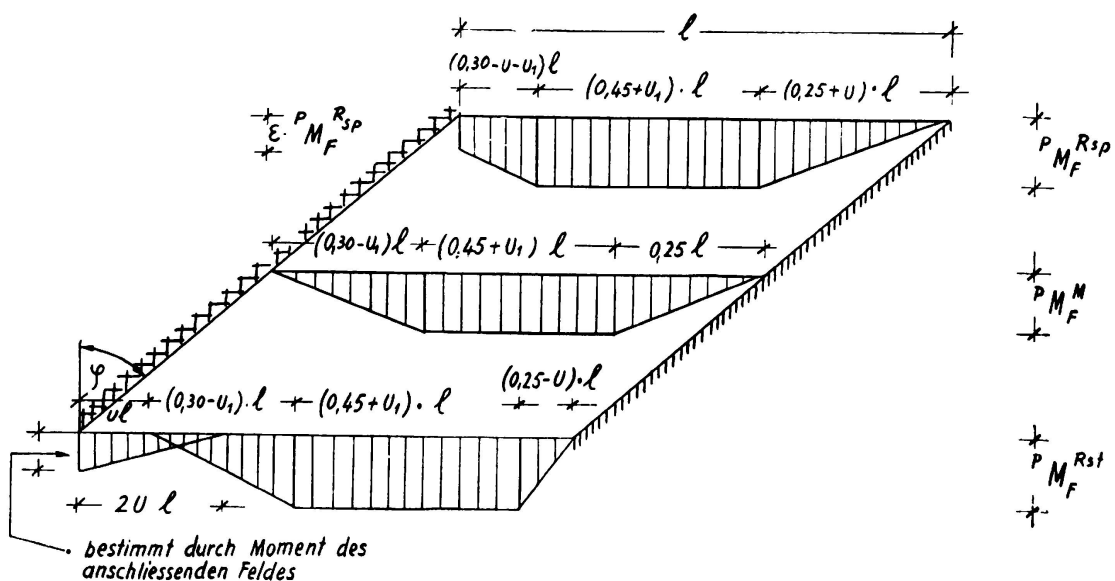


BILD. 6. Positive Momente in Tragrichtung durch Verkehrslast

dem Grad der Schiefe ein Teil der Durchlaufwirkung verloren. Das bedeutet insbesondere für den Fall Eigengewicht, dass die Stützmente kleiner und die Feldmente grösser werden.

Für Verkehrslast sind die Verhältnisse noch etwas undurchsichtiger. Man hat aus den bisher vorliegenden Ergebnissen den Eindruck, dass das Verhältnis der extremen Stütz- und Feldmente vom Winkel unabhängig ist, dagegen jedoch vom Stützweitenverhältnis abhängig ist. Der Winkel macht sich in der Grösse der Momente bemerkbar. Bei den Feldmomenten macht sich mit zunehmender Schiefe der Verlust an Durch-

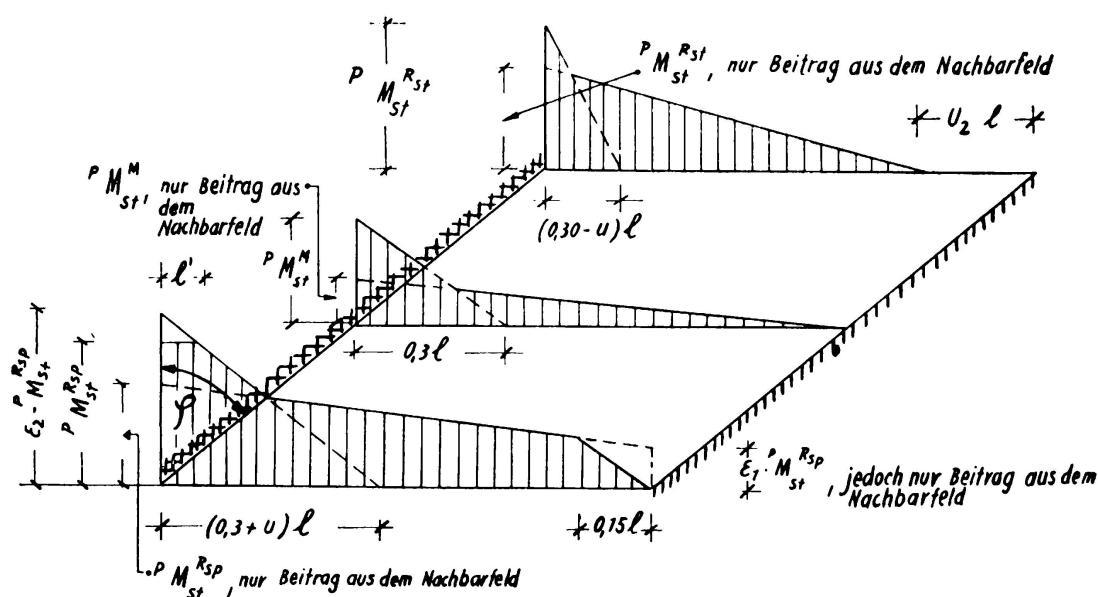


BILD. 7. Negative Momente in Tragrichtung durch Verkehrslast

laufwirkung bemerkbar. Die extremen Feldmomente werden daher grösser als erwartet. Bei den Stützmomenten macht sich die grössere Quersteifigkeit bemerkbar, so dass auch die Stützmente grösser werden als erwartet.

Auch die Form der Momentenlinien zeigen erhebliche Abweichungen gegenüber den bekannten Formen bei rechtwinkligen Systemen. Als Beispiel sollen hier 3 typische Momentenbilder für ein Endfeld gezeigt werden. (Bild 5, 6, 7).

Die negativen Quermomente am Rande bei durchlaufenden schiefen Platten sind nicht wie bei Einfeldplatten vom positiven Feldmoment abhängig, sondern von der absoluten Summe des Stütz- und Feldmomentes in der Tragrichtung.

#### LITERATUR

1. VOGT — *Die statische Behandlung schiefwinkliger Brücken*. Der Ingenieur 1955, H. 8.
2. VOGT — *Das statische Verhalten von zweiseitig aufgelagerten schiefwinkligen Einfeldplatten*. Beton- und Stahlbetonbau 1955, H. 11.

**ZUSAMMENFASSUNG**

Es wird über Erfahrungen bei der statischen Behandlung der für den Brückenbau wichtigen schiefen Platten mitgeteilt. Zweckmäßige Untersuchungsmethoden werden genannt. Für den Fall der zweiseitig aufgelagerten schiefen Platten werden Grenzlinien für die Momente in und quer zur Tragrichtung angegeben. Auf typische Besonderheiten des Tragverhaltens durchlaufender Plattenstreifen mit zwei freien Rändern wird hingewiesen.

**RESUMO**

Descrevem-se ensaios estáticos de placas oblíquas aplicadas na construção de pontes. Indicam-se as envolventes dos momentos, transversal e paralelamente à portada, para o caso de placas oblíquas apoiadas em dois lados. Descrevem-se ainda particularidades típicas de comportamento das placas contínuas com dois lados livres.

**RÉSUMÉ**

L'auteur décrit des essais statiques de plaques obliques appliquées à la construction de ponts. Il donne les enveloppes des moments parallèlement et transversalement à la portée dans le cas de plaques obliques appuyées sur deux côtés. Il décrit également, des particularités typiques de comportement de plaques continues à deux bords libres.

**SUMMARY**

Statical tests of skew plates for bridge structures are described. Enveloping curves are given for the bending moments parallel and tranverse to the span, for skew plates supported along two edges. Typical cases of behaviour of continuous plates with two free edges are also described

## **II a 4**

### **Der Einfluss von biege- und torsionssteifen Randträgern bei Plattenbrücken**

### **Influência dos reforços laterais de torção e flexão nas pontes-laje**

### **Influence des raidisseurs latéraux de torsion et flexion dans les ponts-dalle**

### **Influence of flexural and torsional edge stiffeners in plate bridges**

DR. ING. B. GILG

*Elektro-Watt*

Zürich

Eine Rechteckplatte von der Dicke  $h$  sei längs zwei gegenüberliegenden Rändern im Abstand  $l$  frei drehbar gelagert und längs den beiden andern Rändern, deren Abstand  $b$  beträgt, durch Träger verstärkt. Die Randträgerachsen liegen im Abstand  $s$  unter der Plattenmittelfläche. Sämtliche äusseren Lasten greifen an der Platte an, welche einem kombinierten Biege- und Membranspannungszustand unterliegt, während die Verstärkungsträger nur durch die an den entsprechenden Rändern auftretenden Plattenschnittkräfte beansprucht werden. Nach der Elastizitätstheorie gehorcht die Platte den beiden als Platten- und Scheibengleichung bekannten partiellen Differentialgleichungen 4. Ordnung <sup>(1)</sup>. Für den Fall einer gleichmässig belasteten Platte mit gleichartigen Randträgern an den beiden verstärkten Rändern wurden die Schnittkräfte in Funktion der folgenden Parameter zusammengestellt:

$\lambda$  = Verhältnis der Plattenspannweite zur Plattenbreite.

$\epsilon$  = Verhältnis des Axabstandes der Träger von der Plattenmittelfläche zur Plattendicke.

$\varphi$  = Verhältnis der Plattenquerschnittsfläche zu derjenigen des Trägers.

---

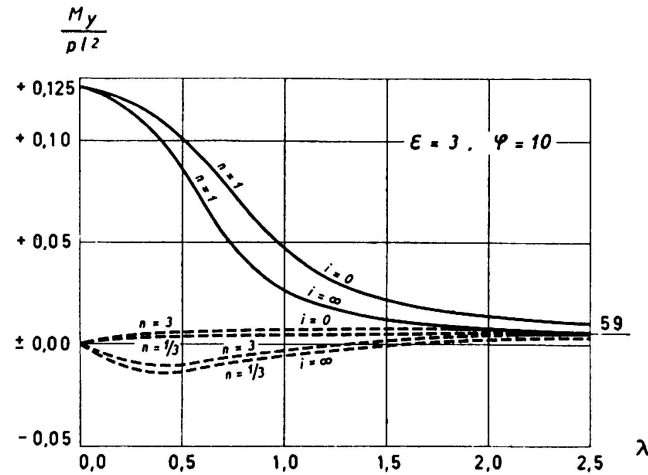
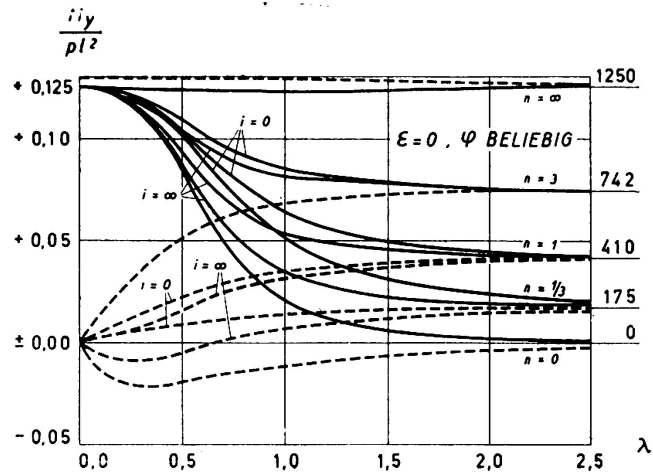
<sup>(1)</sup> vgl. Sch. Bauzeitg., 1953, S. 704 ff

$n$  = Verhältnis der Plattenbiegesteifigkeit zur vertikalen Trägerbiegesteifigkeit.

$i$  = Verhältnis der Trägertorsionsteifigkeit zur vertikalen Trägerbiegesteifigkeit.

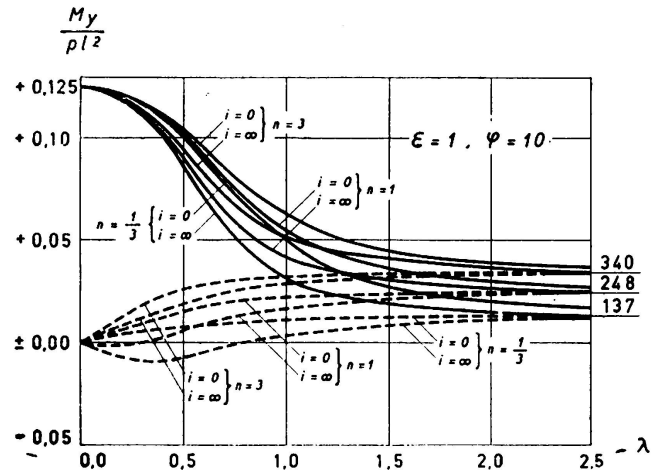
Der Einfluss der horizontalen Biegesteifigkeit des Trägers ist vernachlässigbar klein. Es werden nur die Werte für  $i = 0$  und  $\infty$  wiedergegeben, wobei aber die folgende Zahlentabelle erlaubt, bei gegebenem  $n$  und  $\lambda$  diejenige Zahl für  $i$  zu ermitteln, bei welcher die Schnittkraft den Mittelwert zwischen den beiden oben erwähnten Extremen annimmt:

|     |                 |      |     |
|-----|-----------------|------|-----|
| $n$ | $\lambda = 0,5$ | 1,0  | 2,0 |
| 1/3 | $i = 0,10$      | 0,18 | 0,4 |
| 1   | 0,30            | 0,54 | 1,2 |
| 3   | 0,9             | 1,6  | 3,4 |



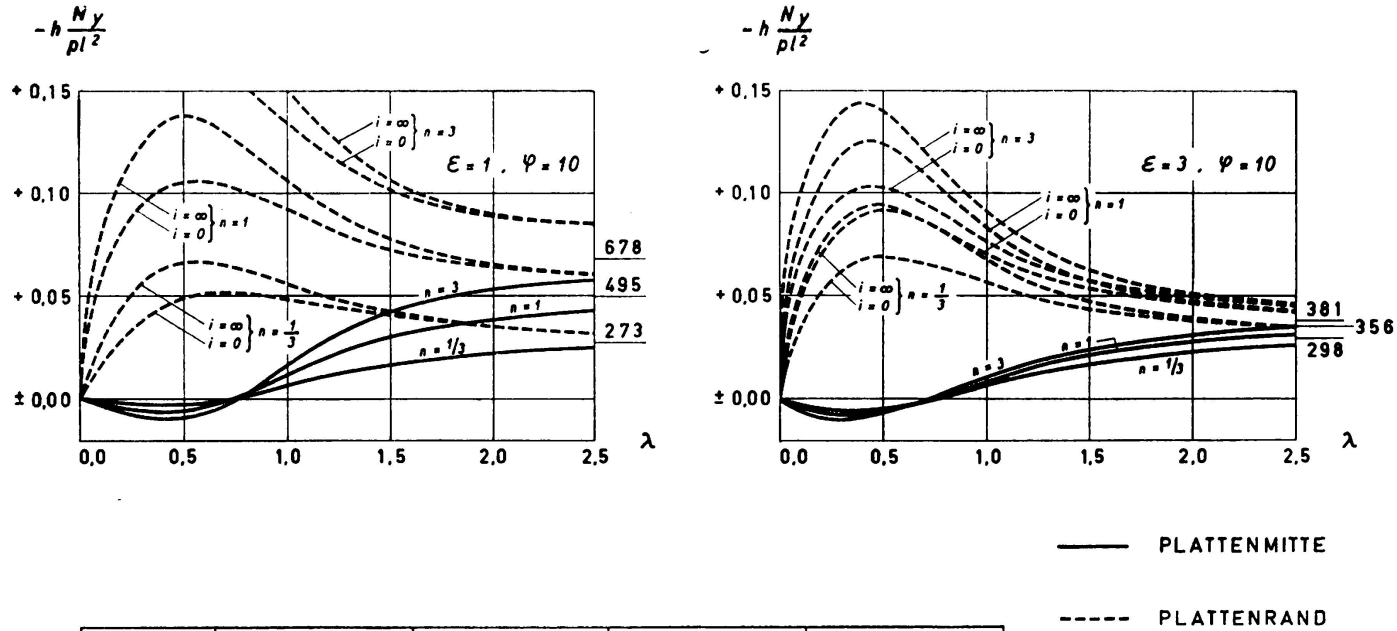
— PLATTENMITTE  
 - - - PLATTENRAND

$\lambda = \frac{l}{b}$   
 $E = \frac{s}{h}$   
 $\varphi = \frac{(EF)_{Pl}}{(EF)_R}$   
 $n = \frac{b \cdot D}{(EJ_x)}$   
 $i = \frac{(GJ_p)}{(EJ_x)}$



| $\lambda$   | 0.5  |      |      |      | 1.0 |     |     |     | 2.0 |     |     |     | $\infty$ |     |    |     |  |
|---|------|------|------|------|-----|-----|-----|-----|-----|-----|-----|-----|----------|-----|----|-----|--|
|   | 1    |      | 3    |      | 1   |     | 3   |     | 1   |     | 3   |     | 1        |     | 3  |     |  |
| $\varphi$   | 3    | 30   | 3    | 30   | 3   | 30  | 3   | 30  | 3   | 30  | 3   | 30  | 3        | 30  | 3  | 30  |  |
| $n = \frac{1}{3} \begin{cases} i=0 \\ i=\infty \end{cases}$ | 1005 | 1007 | 998  | 1002 | 488 | 506 | 446 | 473 | 179 | 221 | 106 | 161 | 104      | 158 | 25 | 90  |  |
| $n = 1 \begin{cases} i=0 \\ i=\infty \end{cases}$           | 1019 | 1027 | 999  | 1006 | 533 | 599 | 448 | 494 | 234 | 374 | 109 | 195 | 159      | 329 | 26 | 128 |  |
| $n = 3 \begin{cases} i=0 \\ i=\infty \end{cases}$           | 1032 | 1056 | 999  | 1010 | 566 | 711 | 449 | 506 | 270 | 543 | 110 | 214 | 193      | 514 | 26 | 148 |  |
| $n = \frac{1}{3} \begin{cases} i=0 \\ i=\infty \end{cases}$ | 76   | 80   | 27   | 48   | 99  | 128 | 29  | 74  | 106 | 153 | 27  | 87  | 104      | 158 | 25 | 90  |  |
| $n = 1 \begin{cases} i=0 \\ i=\infty \end{cases}$           | -78  | -63  | -146 | -113 | 18  | 56  | -73 | -14 | 82  | 132 | -4  | 61  |          |     |    |     |  |
| $n = 1 \begin{cases} i=0 \\ i=\infty \end{cases}$           | 150  | 186  | 34   | 75   | 171 | 280 | 33  | 109 | 167 | 321 | 12  | 126 | 159      | 329 | 26 | 128 |  |
| $n = 3 \begin{cases} i=0 \\ i=\infty \end{cases}$           | 39   | 96   | -136 | -71  | 108 | 241 | -68 | 31  | 148 | 311 | -2  | 101 |          |     |    |     |  |
| $n = 3 \begin{cases} i=0 \\ i=\infty \end{cases}$           | 216  | 338  | 37   | 91   | 224 | 460 | 34  | 128 | 206 | 507 | 30  | 146 | 193      | 514 | 26 | 148 |  |
|   | 142  | 202  | -131 | -46  | 174 | 451 | -66 | 56  | 189 | 506 | -1  | 174 |          |     |    |     |  |

FIG. 1. Zeigt die Längsmomente pro Breitereinheit im Plattenmittelpunkt und im Mittelpunkt des Plattenrandes

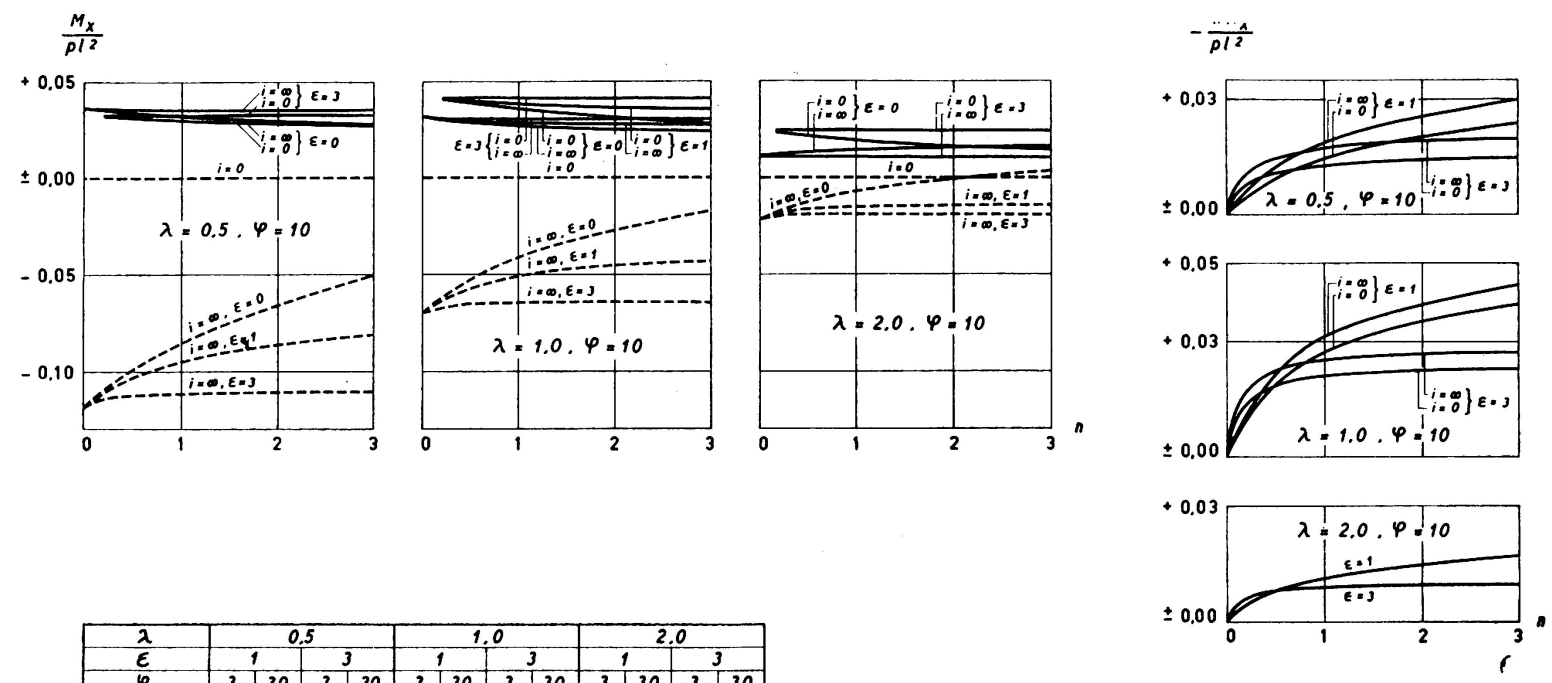


| λ       | 0,5   |      |      |      | 1,0  |      |     |     | 2,0 |      |     |     | ∞   |     |     |     |     |                 |
|---------|-------|------|------|------|------|------|-----|-----|-----|------|-----|-----|-----|-----|-----|-----|-----|-----------------|
|         | 1     |      | 3    |      | 1    |      | 3   |     | 1   |      | 3   |     | 1   |     | 3   |     |     |                 |
| ε       | 3     | 30   | 3    | 30   | 3    | 30   | 3   | 30  | 3   | 30   | 3   | 30  | 3   | 30  | 3   | 30  |     |                 |
| n = 1/3 | i = 0 | -33  | -14  | -39  | -25  | 87   | 26  | 78  | 47  | 357  | 91  | 273 | 156 | 502 | 119 | 358 | 202 | IN DER<br>MITTE |
|         | i = ∞ | -45  | -19  | -54  | -34  | 103  | 32  | 94  | 55  | 372  | 93  | 286 | 165 | 502 | 119 | 358 | 202 |                 |
| n = 1   | i = 0 | -67  | -32  | -49  | -39  | 147  | 58  | 90  | 68  | 565  | 192 | 302 | 224 | 764 | 247 | 390 | 287 | AM<br>RAND      |
|         | i = ∞ | -88  | -42  | -67  | -52  | 175  | 66  | 107 | 80  | 587  | 197 | 316 | 233 | 764 | 247 | 390 | 287 |                 |
| n = 3   | i = 0 | -101 | -59  | -54  | -47  | 199  | 96  | 94  | 81  | 700  | 304 | 312 | 261 | 926 | 385 | 401 | 334 | AM<br>RAND      |
|         | i = ∞ | -130 | -72  | -73  | -64  | 229  | 106 | 113 | 95  | 724  | 307 | 327 | 271 | 926 | 385 | 401 | 334 |                 |
| n = 1/3 | i = 0 | 650  | 276  | 790  | 504  | 759  | 229 | 674 | 399 | 613  | 154 | 462 | 263 | 502 | 119 | 358 | 202 | IN DER<br>MITTE |
|         | i = ∞ | 674  | 372  | 1083 | 687  | 892  | 267 | 802 | 470 | 632  | 157 | 477 | 271 | 502 | 119 | 358 | 202 |                 |
| n = 1   | i = 0 | 1348 | 644  | 984  | 775  | 1304 | 497 | 766 | 581 | 962  | 322 | 507 | 376 | 764 | 247 | 390 | 287 | AM<br>RAND      |
|         | i = ∞ | 1694 | 835  | 1348 | 1045 | 1508 | 562 | 910 | 679 | 986  | 326 | 524 | 385 | 764 | 247 | 390 | 287 |                 |
| n = 3   | i = 0 | 1955 | 1165 | 1065 | 942  | 1708 | 817 | 802 | 685 | 1184 | 508 | 524 | 438 | 926 | 385 | 401 | 334 | AM<br>RAND      |
|         | i = ∞ | 2444 | 1434 | 1458 | 1263 | 1954 | 891 | 952 | 797 | 1212 | 508 | 540 | 448 | 926 | 385 | 401 | 334 |                 |

— PLATTENMITTE  
 - - - PLATTENRAND

λ = l / b  
 ε = s / h  
 φ = (EF)<sub>pl</sub> / (EF)<sub>R</sub>  
 n = (b · D) / (EJ<sub>x</sub>)  
 i = (GJ<sub>p</sub>) / (EJ<sub>x</sub>)

FIG. 2. Zeigt die mit der Plattendicke multiplizierten Längsnormalkräfte pro Breitereinheit in analoger Lage wie Fig. 1 (N+ = Zug)

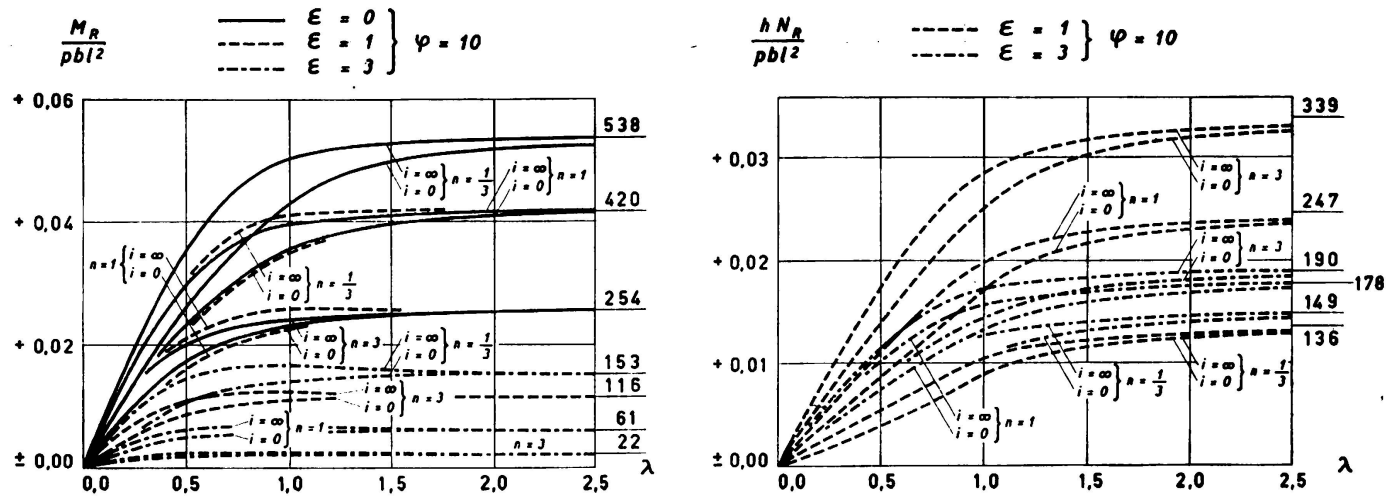


| $\lambda$   | 0.5   |       |       |       | 1.0  |      |      |      | 2.0  |      |      |      | $\frac{M_x}{pl^2} \cdot 10^4$ |
|---|-------|-------|-------|-------|------|------|------|------|------|------|------|------|-------------------------------|
|   | 1     |       | 3     |       | 1    |      | 3    |      | 1    |      | 3    |      |                               |
| $\epsilon$  | 3     | 30    | 3     | 30    | 3    | 30   | 3    | 30   | 3    | 30   | 3    | 30   |                               |
| $n = \frac{1}{3} \begin{cases} i=0 \\ i=\infty \end{cases}$ | 322   | 321   | 326   | 324   | 406  | 400  | 421  | 411  | 233  | 227  | 244  | 236  | IN DER MITTE                  |
| $n = 1 \begin{cases} i=0 \\ i=\infty \end{cases}$           | 315   | 310   | 325   | 321   | 396  | 368  | 420  | 404  | 225  | 203  | 244  | 231  |                               |
| $n = 3 \begin{cases} i=0 \\ i=\infty \end{cases}$           | 308   | 295   | 325   | 319   | 380  | 330  | 420  | 400  | 219  | 177  | 244  | 228  | AN RAND                       |
| $n = \frac{1}{3}, i=\infty$                                 | -1080 | -1068 | -1149 | -1115 | -612 | -587 | -673 | -632 | -174 | -158 | -202 | -181 |                               |
| $n = 1, i=\infty$   | -979  | -916  | -1139 | -1076 | -552 | -463 | -669 | -604 | -153 | -100 | -201 | -167 |                               |
| $n = 3, i=\infty$   | -870  | -718  | -1134 | -1052 | -507 | -325 | -667 | -588 | -141 | -38  | -201 | -160 |                               |
| $n = \frac{1}{3} \begin{cases} i=0 \\ i=\infty \end{cases}$ | 92    | 38    | 109   | 70    | 222  | 68   | 199  | 118  | 118  | 24   | 89   | 51   | IN DER MITTE                  |
| $n = 1 \begin{cases} i=0 \\ i=\infty \end{cases}$           | 186   | 89    | 136   | 108   | 383  | 148  | 227  | 173  | 185  | 62   | 97   | 72   |                               |
| $n = 3 \begin{cases} i=0 \\ i=\infty \end{cases}$           | 280   | 162   | 148   | 131   | 505  | 244  | 238  | 204  | 227  | 97   | 100  | 84   |                               |
|   | 361   | 200   | 203   | 178   | 580  | 267  | 284  | 239  | 232  | 97   | 103  | 89   |                               |

$\lambda = \frac{l}{b}$   
 $\epsilon = \frac{s}{h}$   
 $\varphi = \frac{(EF)_{Pl}}{(EF)_R}$   
 $n = \frac{b \cdot D}{(EJ_x)}$   
 $i = \frac{(\theta J_p)}{(EJ_x)}$

— PLATTENMITTE  
 - - - PLATTENRAND

FIG. 3. Zeigt die Quermomente und -Normalkräfte pro Breitereinheit in den analogen Punkten wie Fig. 1 und 2



| λ                     | 0,5 |     |     |     | 1,0 |     |     |     | 2,0 |     |     |     | ∞   |     |     |     | IM TRÄGER                               |
|-----------------------|-----|-----|-----|-----|-----|-----|-----|-----|-----|-----|-----|-----|-----|-----|-----|-----|---|
|                       | ε   |     | φ   |     | ε   |     | φ   |     | ε   |     | φ   |     | ε   |     | φ   |     |   |
| n = 1/3 { i=0 / i=∞ } | 3   | 30  | 3   | 30  | 3   | 30  | 3   | 30  | 3   | 30  | 3   | 30  | 3   | 30  | 3   | 30  | MR · 10 <sup>4</sup> / pbl <sup>2</sup> |
|                       | 216 | 245 | 84  | 151 | 304 | 394 | 90  | 229 | 328 | 469 | 82  | 269 | 322 | 487 | 76  | 277 |   |
| n = 1 { i=0 / i=∞ }   | 153 | 191 | 35  | 77  | 175 | 287 | 34  | 111 | 172 | 329 | 30  | 128 | 163 | 337 | 28  | 131 |   |
|                       | 201 | 249 | 48  | 103 | 202 | 325 | 40  | 131 | 176 | 337 | 31  | 133 | 163 | 337 | 28  | 131 |   |
| n = 3 { i=0 / i=∞ }   | 74  | 115 | 13  | 31  | 77  | 158 | 12  | 44  | 71  | 174 | 10  | 50  | 66  | 176 | 10  | 51  |   |
|                       | 96  | 142 | 17  | 42  | 88  | 173 | 14  | 51  | 70  | 175 | 10  | 51  | 66  | 176 | 10  | 51  |   |
| n = 1/3 { i=0 / i=∞ } | 53  | 23  | 65  | 42  | 143 | 43  | 128 | 76  | 221 | 56  | 168 | 96  | 251 | 60  | 179 | 101 |   |
|                       | 68  | 31  | 89  | 57  | 169 | 51  | 153 | 90  | 229 | 58  | 175 | 100 | 251 | 60  | 179 | 101 |   |
| n = 1 { i=0 / i=∞ }   | 106 | 53  | 81  | 64  | 247 | 95  | 146 | 111 | 349 | 118 | 186 | 137 | 382 | 124 | 195 | 143 |   |
|                       | 136 | 69  | 111 | 86  | 286 | 107 | 175 | 131 | 360 | 120 | 193 | 142 | 382 | 124 | 195 | 143 |   |
| n = 3 { i=0 / i=∞ }   | 165 | 96  | 88  | 78  | 325 | 157 | 153 | 131 | 431 | 187 | 192 | 160 | 463 | 192 | 201 | 167 |   |
|                       | 210 | 119 | 121 | 106 | 374 | 171 | 183 | 153 | 444 | 188 | 199 | 166 | 463 | 192 | 201 | 167 |   |

$$\lambda = \frac{l}{b}$$

$$\epsilon = \frac{s}{h}$$

$$\varphi = \frac{(EF)_{Pl}}{(EF)_R}$$

$$n = \frac{b \cdot D}{(EJ_x)}$$

$$i = \frac{(GJ_p)}{(EJ_x)}$$

FIG. 4. Zeigt die im Randträgermittelpunkt auftretenden Trägermomente und- Normalkräfte

## ZUSAMMENFASSUNG

Die Schnittkräfte in den Hauptpunkten einer durch Randträger versteiften zweiseitig gelagerten Rechteckplatte sowie in den Trägern werden in Abhängigkeit verschiedener geometrischer und elastischer Parameter in Diagrammen und Tabellen zusammengestellt.

## RESUMO

O autor apresenta sob forma de diagramas e tabelas, em função de vários parâmetros geométricos e elásticos, os esforços interiores nos pontos principais de uma placa rectangular apoiada em dois lados e reforçada ao longo dos bordos; também indica os esforços interiores nas vigas de reforço.

## RÉSUMÉ

L'auteur présente sous forme de diagrammes et de tables, en fonction de plusieurs paramètres géométriques et élastiques, les efforts intérieurs aux points principaux d'une plaque rectangulaire appuyée aux deux extrémités et raidie le long des bords; il présente également les efforts intérieurs dans les poutres de raidissement.

## SUMMARY

The author classifies in diagrams and tables, according to different geometric and elastic quantities, the internal forces at the principal points of an edge-stiffened rectangular plate supported at both ends; internal forces in the stiffening beams are also indicated.

Leere Seite  
Blank page  
Page vide

## **II b 1**

### **Spannungsverteilung in orthotropen Scheiben**

### **Distribuição das tensões em paredes delgadas reforçadas ortogonalmente**

### **Distribution des contraintes dans les parois minces orthotropes**

### **Stress distribution in orthogonally stiffened thin slabs**

PROF. DR. H. BEER

DR. F. RESINGER

Graz

Die Verfasser behandeln das Problem der Krafteinleitung in rechtwinklig ausgesteifte, dünne Scheiben, wie sie z. B. im Stahlbau als hohe Stege oder sehr breite Gurtplatten von Flächentragwerken vorkommen. Die Forderung, ein Berechnungsverfahren zu entwickeln, welches es gestattet, auch eine Veränderung der Blechstärke und des Querschnittes der orthogonalen Aussteifungsrippen zu berücksichtigen, hat die Verfasser veranlasst, von einer elastizitätstheoretischen Betrachtung des Problems abzusehen und ein baustatisches Verfahren als Lösung zu wählen. Sie bauen hierbei auf einer Arbeit aus der Flugzeugstatik <sup>(1)</sup> auf, welche die orthogonal ausgesteifte Scheibe der Tragflügel von Flugzeugen behandelt. Während jedoch dort die Unbekantengruppen als Kraftgrößen mit Hilfe von Elastizitätsgleichungen ermittelt wurden -wobei selbst bei Entkoppelung in einer Richtung noch eine, im allgemeinen grosse Zahl von Gleichungen aufzulösen ist- wenden die Verfasser ein Ausgleichsverfahren <sup>(2)</sup> mit ausgezeichneter Konvergenz zur Berechnung der unbekanntenen Kraftgrößen an. Letztere haben denselben Aufbau wie die Wölbkraftgruppen in Kastenträgern. Ferner erweitern die Verfasser den auf dem Schubfeldschema aufgebauten Berechnungsgang von Ebner und Köller auf die exaktere Erfassung der Blechmitwirkung zur Aufnahme von Normalkräften in Richtung beider Steifenscharen und berücksichtigen den Poissoneffekt.

---

<sup>(1)</sup> H. Ebner u. H. Köller, Luftfahrtforschung 1938, S. 527.

<sup>(2)</sup> F. Resinger, Dissertation T. H. Graz, 1956.

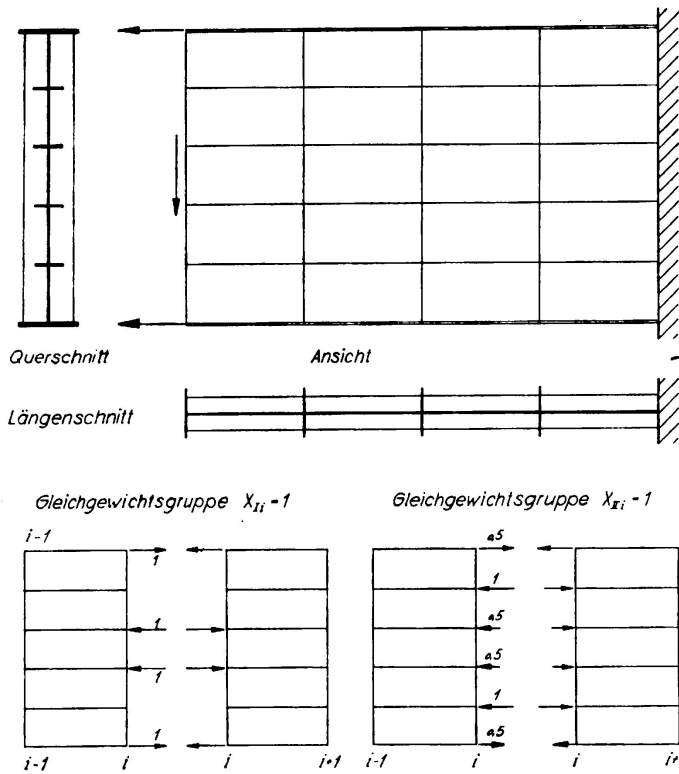


FIG. 1

In Fig. 1 ist ein einfaches Krafteinleitungsproblem dargestellt und die Wahl des statisch bestimmten Grundsystems so getroffen, dass an jeder Querrippe eine Längsbewegung der Längsrippen mit Normalkraft aufnehmendem Blech möglich ist. Die Schubkraftaufnahme des Bleches soll dadurch nicht beeinträchtigt werden. Die unbekannten Kraftgruppen wählen wir so, dass sie ein örtliches Gleichgewichtssystem bilden und am gegebenen Tragwerk die Eigenschaft des raschen Abklingens besitzen. Ferner wird noch darauf zu achten sein, dass die gegenseitige Beeinflussung (Koppelung) der an einer Querrippe angebrach-

ten Unbekantengruppen möglichst gering ist. Wir erhalten somit ein System von «Wölbkraftgruppen» (Fig. 1) als Unbekannte.

Für die Belastung der Scheibe machen wir eine plausible Annahme der Krafteinleitung, die zwar an jeder Querrippe im Gleichgewicht ist, aber noch nicht die Formänderungsbedingungen erfüllt. Letzteres geschieht durch die statisch unbestimmte Rechnung, die -wenn die Annahme gut war- nur den Charakter einer Korrektur hat (Fig. 2).

Wir berechnen zunächst die Kräfte in den einzelnen Scheibenfeldern am Grundsystem aus den Gleichgewichtsbedingungen, wobei wir für das Einzelfeld linear abklingende Längskraft und damit konstante Schubverteilung annehmen (Fig. 3).

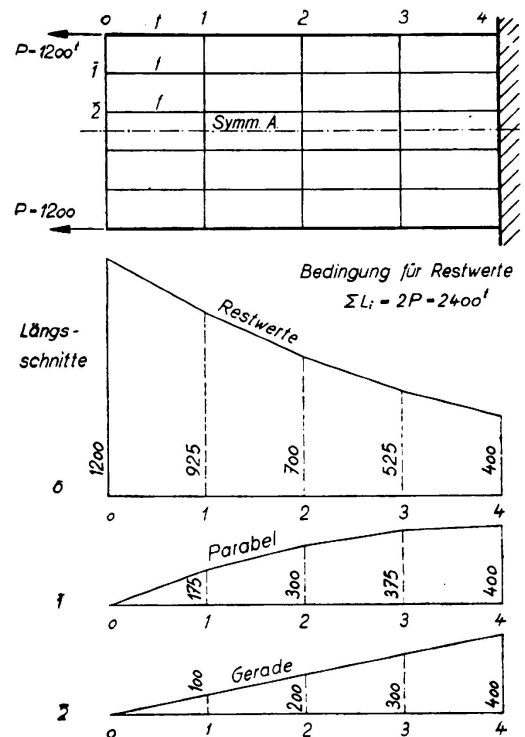


FIG. 2

Wir erhalten die Querkräfte:

$$Q_{il} = L_{il} - L_{i-1,l} \qquad Q_{in} = 0 \text{ (Symmetrie)}$$

$$Q_{im} = L_{il} + L_{im} - L_{i-1,l} + L_{i-1,m} = -L_{in} + L_{i-1,n}$$

und die Querrippenkräfte:

$$V_{il} = 0 \text{ (Rand)}, \quad V_{im} = (L_{i-1,l} - L_{il}) \frac{b}{a_i} - (L_{il} - L_{i+1,l}) \frac{b}{a_{i+1}},$$

$$V_{in} = (L_{i-1,l} - L_{il}) \frac{2b}{a_i} - (L_{il} - L_{i+1,l}) \frac{2b}{a_{i+1}} +$$

$$+ (L_{i+1,m} - L_{im}) \frac{b}{a_i} - (L_{im} - L_{i+1,m}) \frac{b}{a_{i+1}}.$$

Die Relativverwölbung für den Zustand  $X_{ii} = 1$ .  $\delta_{ii,0}$  setzen wir zusammen aus dem Anteil der Längenänderung der Gurte  $\delta_{ii,L}$ , der Schubverformung der Blechfelder  $\delta_{ii,Q}$ , der Längenänderung der Querrippen  $\delta_{ii,V}$ , und des Poissoneffektes  $\delta_{ii,P}$ .

Es wird:

$$E \delta_{ii,L} = \sum_{i-1}^{i+1} \int L^{(0)} L^{(1)} \frac{1}{f} dx, \qquad E \delta_{ii,Q} = \frac{E}{G} \sum_{i-1}^{i+1} Q^{(0)} Q^{(1)} \frac{b}{a d},$$

$$E \delta_{ii,V} = \sum_{i-1}^{i+1} \int V^{(0)} V^{(1)} \frac{1}{f_V} dy,$$

$$E \delta_{ii,P} = -\mu \sum_{i-1}^{i+1} \left\{ \iint \sigma_y^{(0)} \sigma_x^{(1)} dx dy + \iint \sigma_x^{(0)} \sigma_y^{(1)} dx dy \right\}.$$

Zur Vorbereitung des Ausgleiches berechnen wir mit Hilfe der Relativverwölbungen die Volleinspannwerte  $\bar{X}_i = -\Delta \delta_{i0} : \bar{\delta}_{ii}$  der unbekanntenen Wölbkraftgruppen und stellen sie im Schema der Fig. 4 zusammen. Hierbei lassen wir vorläufig den Anteil der Querrippen  $\delta$

und des Poissoneffektes  $\delta_{\nu}$  unberücksichtigt. Eine wesentliche Vereinfachung bietet hier die Möglichkeit, die Verwölbungen so aufzuteilen, dass in jedem Feld symmetrische, bzw. antimetrische Stützbedingungen

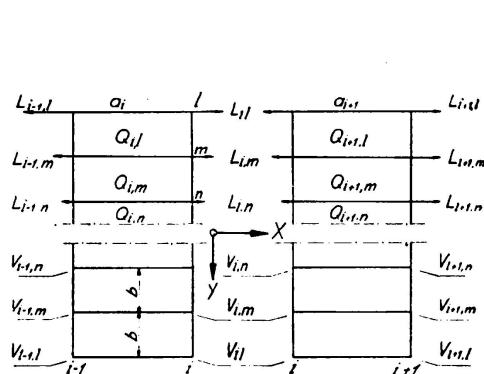


FIG. 3

Aufteilung der Verwölbungen

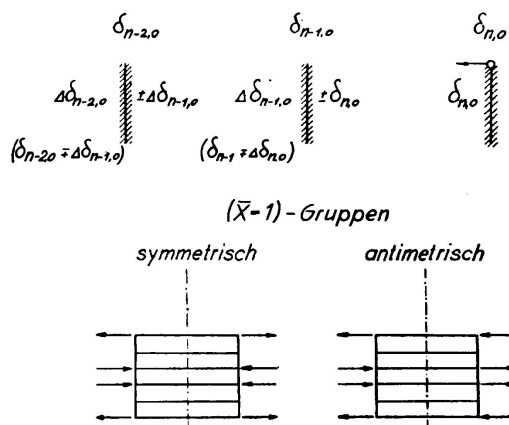


FIG. 4

und somit Einspannwerte entstehen. In Analogie zum Momentenausgleich nach Cross erhalten wir nun die Wölbsteifigkeitszahl  $\mu_i$  und den Fortleitungsfaktor  $\gamma_i$  zu:

$$\mu_i = \frac{a_c}{z E f_c} \cdot \frac{1}{\partial_{ii}}, \quad \gamma_i = \frac{\partial_{i-1,i}}{\partial_{ii}};$$

$a_c, f_c$  sind Festwerte.

Für das vorliegende Beispiel (Fig. 5) ist für den Zustand  $X_I$   $z = 2$  und für  $X_{II}$   $z = \frac{8}{3}$ . Es ergibt sich

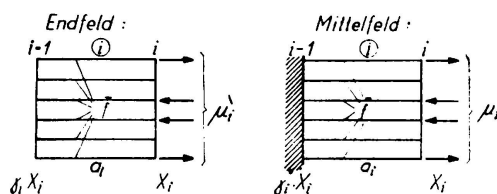


FIG. 5

sodann im Endfeld:  $\mu_i = \frac{a_c}{a_i} \frac{\bar{f}_i}{f_c} \frac{3}{2(2 + \rho_i)}, \gamma_i = 0$  und

im Mittelfeld:  $\mu_i = \frac{a_c}{a_i} \frac{\bar{f}_i}{f_c} \frac{2 + \rho_i}{2(1 + 2\rho_i)}, \gamma_i = \frac{1 - \rho_i}{2 + \rho_i}$ .

$\rho_i$  bedeutet in den Formeln den (verzerrten) Schubanteil. Entsprechend Fig. 5 ist mit  $\lambda = \frac{E}{G}$ :

$$\rho_{II} = \frac{6\lambda \bar{f}_i b}{a_i^2 d_i}, \quad \rho_{III} = \frac{2\lambda \bar{f}_i b}{a_i^2 d_i} - \frac{\rho_{II}}{3}.$$

Um für den beabsichtigten Iterationsschritt mit einem einzigen Ausgleich auszukommen, berechnen wir die gebundenen Fortleitungsfaktoren  $\bar{\gamma}_i$  und Steifigkeitszahlen  $\bar{\mu}_i$  am kontinuierlichen System nach den Rekursionsformeln:

$$\bar{\gamma}_i = \frac{\gamma_i}{1 + \frac{\mu_i \gamma_i}{\mu_{i+1}}}, \quad \bar{\mu}_i = \frac{\mu_i}{1 - \gamma_i \gamma_i} \quad \text{und}$$

leiten nach dem Schema der Fig. 6 fort.

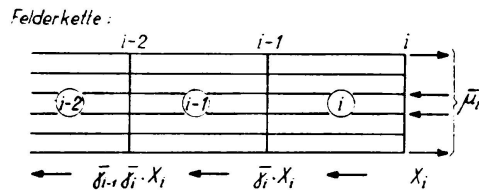


FIG. 6

Der erste Ausgleich erfüllt jedoch noch nicht die Formänderungsbedingungen, da die Eigenkraftgruppen  $X_{II}$  und  $X_{III}$  gekoppelt sind und die Nachgiebigkeit der Querrippen und der Poissoneffekt im Ausgleich selbst nicht berücksichtigt wurden. Daher müssen wir einen zweiten Rechnungsgang anfügen und zu diesem Zwecke die Relativverwölbungen für die mit Hilfe des ersten Ausgleiches erhaltenen Gesamtschnittkräfte am Grundsystem berechnen. Der Ausgleich wird sodann nochmals durchgeführt. Das Verfahren ist stark konvergent, so dass dieser zweite Rechnungsgang schon eine ausreichende Genauigkeit ergibt und ein eventuell durchgeführter dritter Rechnungsgang nur mehr der Kontrolle dient. Beim letzten Rechnungsgang wird zweckmässig -auf Grund der vorher erhaltenen Normalkraftverteilung- eine Korrektur der mitwirkenden Blechstreifen vorgenommen.

In Fig. 7 sind die Normalspannungen  $\sigma_x$ , welche infolge der Einleitung zweier symmetrischer Randkräfte in die orthotrope Scheibe entstehen, für eine Scheibenhälfte dargestellt. Man kann an diesem Spannungskörper auch die Einflüsse der elastisch nachgiebigen Querrippen und des Poissoneffektes erkennen.

Die Berechnung wurde hier an Hand des Beispiels mit sechs Längsrippen durchgeführt. Sind mehr solche Rippen vorhanden, so kann man mit für die Praxis ausreichender Genauigkeit ihren Querschnitt auf 6 ideale Rippen aufteilen. Die Verfasser sehen als Vorteil des von ihnen entwickelten Verfahrens seine weitgehende Anpassungsfähigkeit

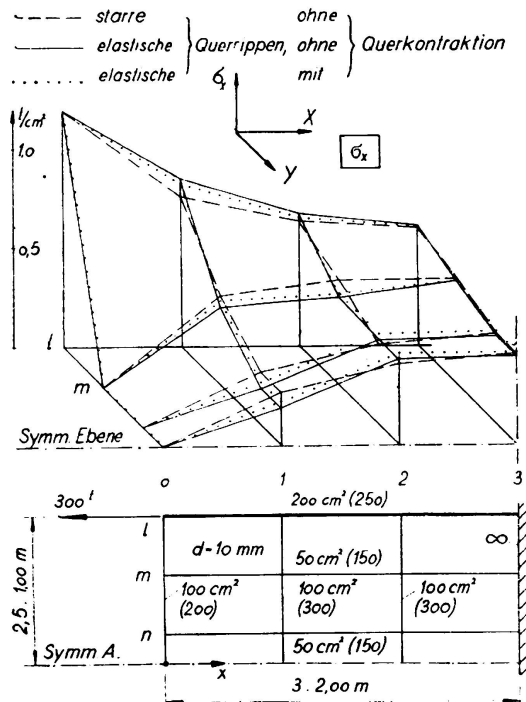


FIG. 7

an die Bedürfnisse der Praxis und seinen relativ geringen Rechenaufwand an. Vom Ingenieur werden bei der Anwendung nur die Kenntnisse der Baustatik vorausgesetzt.

ZUSAMMENFASSUNG

Es wird die Krafteinleitung in ein rechtwinklig ausgesteiftes Stahlblech mit Hilfe einer baustatischen Lösungsmethode und unter Anwendung eines hierbei entwickelten Wölbkräfteausgleichsverfahrens behandelt. Man kann hierbei auch veränderliche Blechdicken und verschiedene Steifenquerschnitte berücksichtigen.

RESUMO

Os autores resolvem o problema da distribuição das tensões em paredes metálicas delgadas reforçadas ortogonalmente, por meio de um método de cálculo estático utilizando um processo de compensação para os grupos de forças desconhecidas. Este método permite também considerar paredes de espessura variável e reforços de secções diferentes.

## R É S U M É

Les auteurs traitent le problème des contraintes dans une paroi mince métallique raidie orthogonalement, au moyen d'une méthode de calcul statique, et en appliquant un procédé de compensation pour les groupes de forces inconnues. Cette méthode permet de considérer aussi des parois d'épaisseur variable et des nervures de sections différentes.

## S U M M A R Y

The authors deal with the problem of stress-distribution in orthogonally stiffened, thin steel-slabs by a method of static computation, using a process of compensation for the unknown groups of forces. With this method, slabs of variable thickness and stiffeners of different cross-sections can also be considered.

Leere Seite  
Blank page  
Page vide

## **II b 2**

**Folded slabs in latticed steel construction**

**Faltwerke in aufgelöster Stahlkonstruktion**

**Lajes dobradas trianguladas de aço**

**Dalles pliées en treillis d'acier**

FELIX J. SAMUELY

London

Latticed steelwork to form a «shell» construction was well-known a long time before reinforced concrete shell construction was invented. After its initial appearance, however, no further development took place until recently. Generally speaking, the theory of latticed work is somewhat simpler than that of solid slabs, requiring less mathematical knowledge for the analysis. However, this is correct only if all deformations remain small compared with the differential dimensions of the construction.

Just as a latticed girder can always replace a plate girder, a latticed construction can always be substituted for any portion of a shell or folded slab. This allows the employment of any prefabricated material such as steel, timber, precast concrete, used in conjunction with lightweight roof covering.

With steelwork, as much as possible should be assembled in the workshop to reduce the number of site connections. In the following examples, it may be noted that each latticed girder has tubular chords which lend themselves particularly well to this application because of the connections being in a different plane from that of the actual girder. Plates are welded to each of these chords, and when two lattices are fitted together the corresponding plates are connected by bolts to take the required shear. In analysing the stresses in such a lattice the procedure is similar to that for concrete. Forces acting at the cranks, i. e. the intersections of two consecutive girders, are resolved into the planes of these lattices, and each latticed girder has to transmit two sets of loads which may add to or subtract from each other.

The two chord members which adjoin each other cannot elongate separately, and it is therefore correct to assume that both together take

the sum of the calculated forces. For instance, if one of the members has to take 20 tons in compression, and the other 40 tons, they will in fact each have to take 30 tons in compression.

Unfortunately, with this type of construction it is impossible to keep the two members on the actual centre line, and in the transmission of shear from one to the other certain local bending moments will be introduced. However, as the shear is just near the supports where the members are usually not otherwise fully stressed, if the distance between



FIG. 1

the two members is kept to a minimum, little material is needed to take these additional stresses. As the connection between two lattices is tantamount to a hinge, the first calculation can be taken as correct if, as mentioned before, the deformations are not too large.

The shape given in Fig. 1 approximates more to that of a shell, and is the roof of a factory of three aisles 50'0", 110'0" and 50'0" wide respectively. Here, the outward appearance is that of a continuous curve, apart, of course, from the north light, and curved cement asbestos was used as roof covering. There are six latticed girders, and the angle

between any two adjoining ones is very obtuse. If the deflection is obtained as described in the paper on folded slabs, it will be found that this is relatively large with such obtuse angles, and in fact, so large that the whole transmission of forces is altered. There are two ways of dealing with this problem - (a) by calculating these deflections, re-calculating the forces and obtaining a progression similar to that described for reinforced concrete, and (b) by introducing a special degree of stiffness between the various latticed girders strong enough to reduce deformations to a reasonable amount. In the example shown in fig. 1 a certain amount of rigidity has been produced by welding two consecutive latticed girders

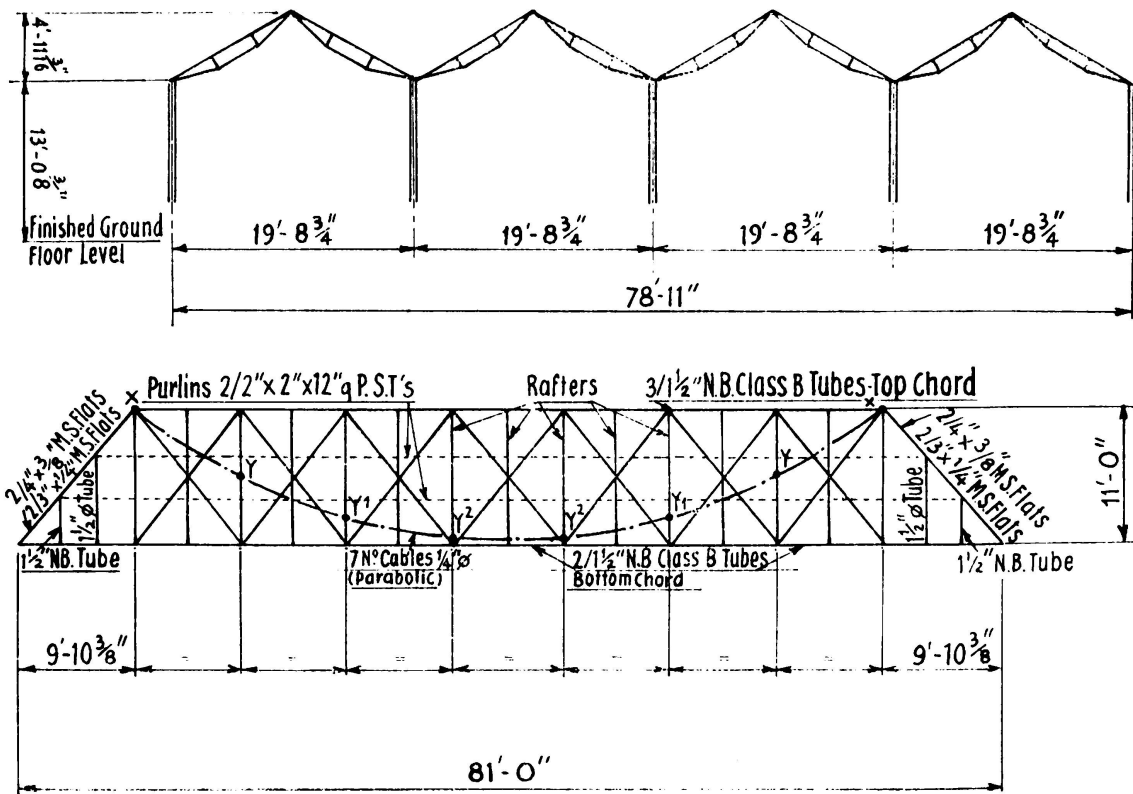


FIG. 2

together instead of bolting them, and even this small amount of rigidity was sufficient to stabilise the latticed construction. More stringent measures may have to be taken, as for instance, the introduction of a rib or of local stiffening plates, as shown in fig. 5. Method (a) is, of course, suitable only where deformations are appreciable, but not so large that they could in themselves prove a danger to stability. For steelwork it is usually more advantageous to have a smaller number of facets, with more acute angles between them. This is particularly so because very frequently the roof covering becomes simpler the smaller the number of cranks.

In fig. 2 a construction is shown which has been used for two workshops respectively 90'0" x 90'0" and 80'0" x 80'0". In this case the latticed girders are placed in the inclined planes of the roof. The trussed beams shown in the cross section serve to distribute the loads to the eaves and ridges, and the whole girder is in fact post-tensioned by means of a number of jacks at the points  $Y, Y_1, Y_2$ , which transfer a large part of the load to the cable  $XX$ . The economy effected by this cable would have been even larger if the roof had not been hipped for architectural requirements, and if the cable could have been carried

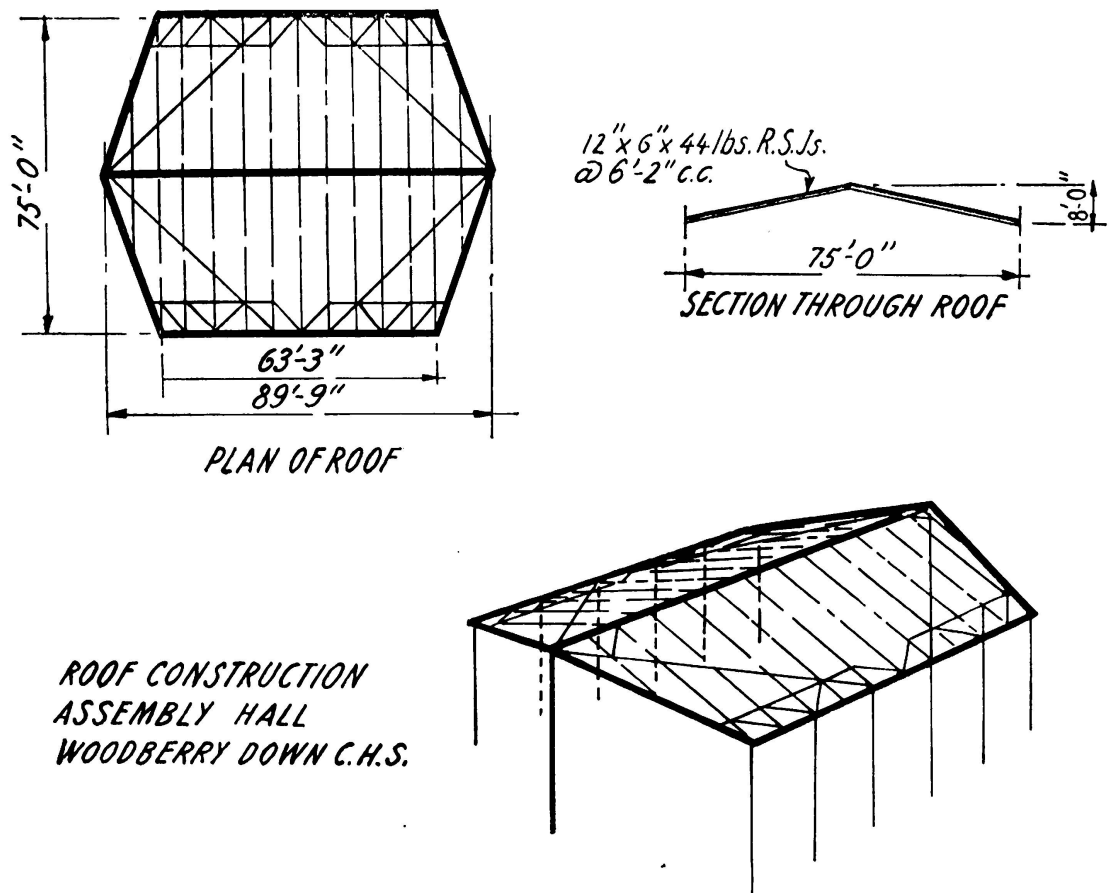


FIG. 3

from support to support. It was possible in this case to erect each strip of roof 90'0" x 22'6" in one operation with temporary struts between the eaves.

Fig. 3 shows a similar roof construction for an Assembly Hall. This was flatter than would have been desirable from an engineering point of view. Note that where large areas are concerned it is not possible to have a parallel girder over the whole area, as all connections would have to be done at the site, but part only of any one plane can be latticed, or, as in this example, have a three-pin frame in each, which is more easily produced than a deep latticed construction.

In fig. 4 many of the members are from timber, particularly the compression boom along the ridge. The distribution from eaves to ridge is made by prestressed trussed beams, with the main boom from timber.

Finally, in fig. 5 a shell roof over a gymnasium is shown, which consists of a series of rectangular standard timber frames laid side by

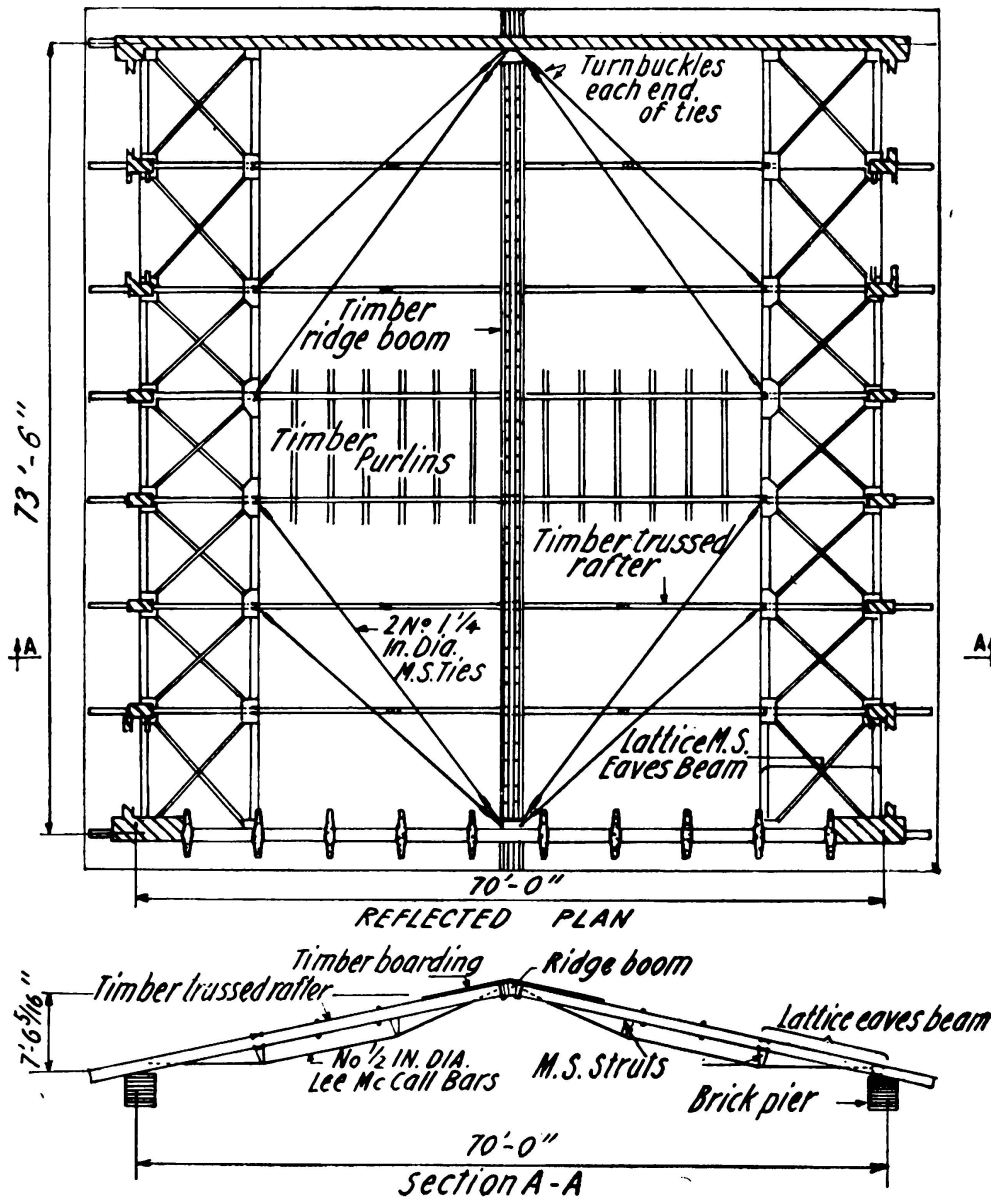


FIG. 4

side. Each frame has two stressed bars crossing each other which hold the frame rigid, and each two consecutive frames are bolted together. The main longitudinal tension occurs along the eaves, and is taken by post-tensioning all the frames together by the Lee McCall method. As the

radius is rather large it was found necessary to stiffen some of the joints by a steel plate acting in a cross plane, which is capable of transmitting a certain amount of bending from frame to frame and thus prevents any deformations, which would in their turn have given rise to increased stresses.

Because of the reduced weight, a steel shell construction can very well hold its own economically in a comparison with reinforced concrete.

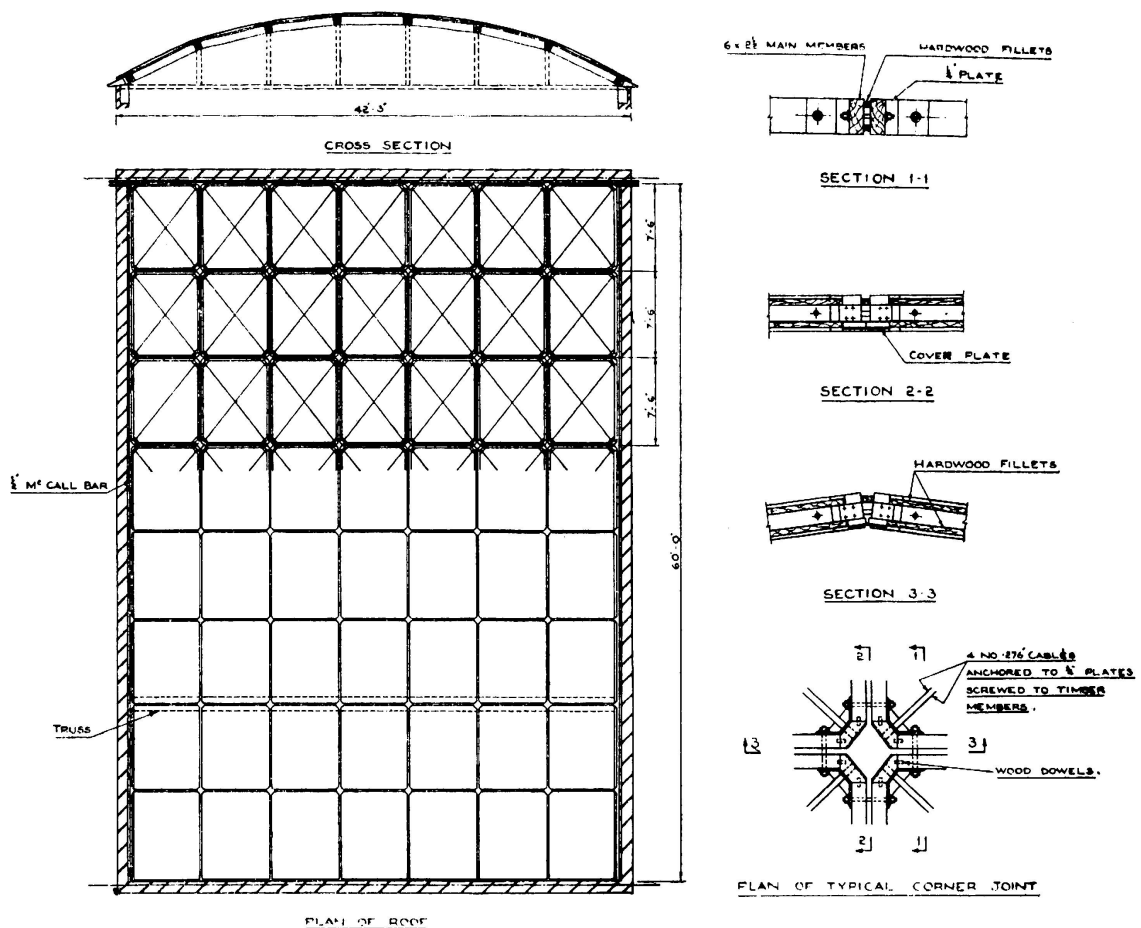


FIG. 5

In some instances it was found that the weight of steel in a steel shell construction was in fact smaller than the amount of reinforcement required in a comparable reinforced concrete shell.

#### SUMMARY

This is in principle similar to the contribution under II (c), but deals with steelwork in place of reinforced concrete.

In these cases latticed steel construction is arranged in the planes of the roof so that steelwork similar to a shell is achieved. Two structures are mentioned where timber has been used in the same way.

## ZUSAMMENFASSUNG

Diese Tragwerke sind im Prinzip ähnlich denen des Beitrages unter II (c); es handelt sich jedoch um Stahlkonstruktionen an Stelle von Eisenbetonbauwerken.

Es wird eine Stahlgitterkonstruktion in den Dachflächen angeordnet, so dass eine Stahlkonstruktion ähnlich einer Schale entsteht. Zwei Bauten werden erwähnt, wo Holz an Stelle von Stahl in der gleichen Weise verwendet wurde.

## RESUMO

Estas estruturas são, em princípio, semelhantes às descritas em II c, sendo aqui o betão armado substituído pelo aço.

A estrutura triangulada é, neste caso disposta nos planos da cobertura, de modo a formar um conjunto semelhante a uma parede delgada. Indica-se duas estruturas onde se empregou madeira de maneira semelhante.

## RÉSUMÉ

Ces charpentes sont, en principe, semblables à celles décrites en II c, le béton armé étant ici remplacé par de l'acier.

La charpente en treillis est, dans ce cas, disposée dans les plans de la couverture de manière à former un ensemble semblable à un voile mince. L'auteur mentionne encore deux charpentes où l'on a utilisé du bois de la même manière.

Leere Seite  
Blank page  
Page vide

## **II c 1**

**Poutres de grande hauteur supportées le long de leurs  
bords verticaux**

Dans le cas de portées et de charges modérées, la solution classique n'offre pas d'inconvénients. Au contraire, les essais de pièces de béton armé démontrent qu'il s'agit d'une structure extrêmement résistante.

Cependant, on ne pourrait arriver à une épaisseur aussi réduite que celle indiquée dans la fig. 1 (25 cms.) car dans ce cas la contrainte moyenne serait de:

$$\text{Contrainte moyenne} = \frac{1260000}{100 \times 25} = 500 \text{ kgs/cm}^2$$

Cette impossibilité d'envisager la structure en accord avec la distribution d'efforts comme dans le cas classique, conduit à la concevoir en partant d'un point de vue différent. On devait éviter la formation des

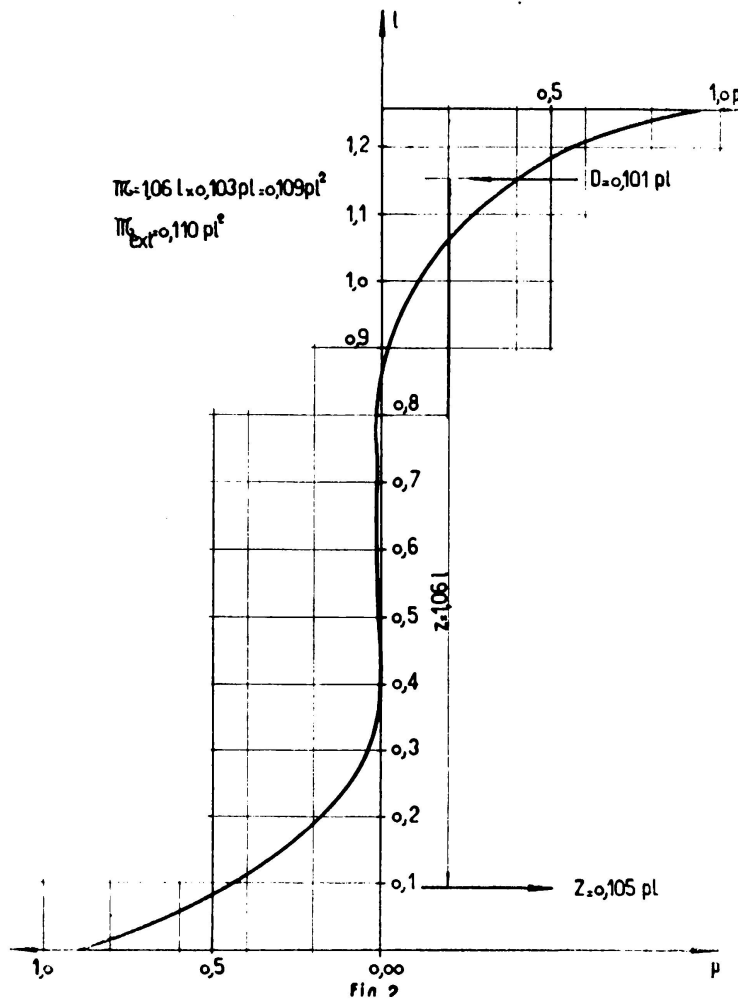


FIG. 2. Poutre simplement appuyée. Contraintes principales  $\sigma_1$  dans la section centrale ( $x = 0,5$ )

arcs de décharge afin d'empêcher la concentration d'efforts sur les appuis, en déviant la marche de ceux-ci, de manière à ce que leur entrée dans la colonne soit progressive.

Cette modification de contours se manifeste aussi dans la section centrale, par une modification de la distribution des efforts normaux de

flexion, avec un grand accroissement du bras de levier et, en conséquence, une notable diminution de l'effort de traction interne. Toute la hauteur de la poutre se convertit en hauteur utile, et la zone active ne se limite pas à une portion qui est fonction exclusive de la portée, comme l'établit le principe de Saint-Venant.

L'effet de bord rigide s'obtient dans la pratique en insérant chaque bord de la paroi tout le long d'une colonne de dimensions appropriées, comme on le voit schématiquement dans la fig. 1.

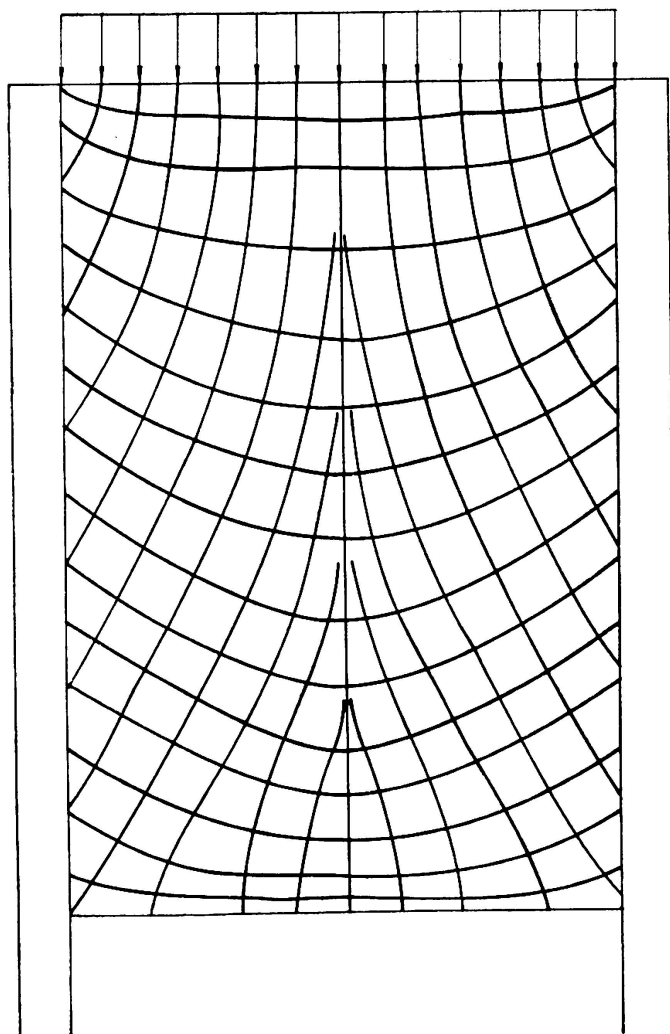


FIG. 3. Isostatiques de la poutre simplement appuyée

Pour constater rigoureusement les résultats prévus d'après ce que l'on vient d'exposer, une étude expérimentale photo-élastique, fut réalisée en appliquant la méthode de H. Fabre, comme on le décrit ci-dessous.

## 2) Investigation photo-élastique Résultats

Les études furent réalisées sur deux modèles construits en «Perspex», l'un d'eux d'une poutre simplement appuyée et l'autre d'une poutre continue à deux portées égales, toutes deux soumises à une charge uniforme sur le bord supérieur.

### 2.1) Poutre simplement appuyée

Dans la fig. 2 on a représenté les valeurs des contraintes normales de flexion dans la section centrale. Dans la fig. 3 on a représenté les isostatiques.

### 2.2) Poutre continue

On détermina les valeurs des contraintes  $\tau_{xy}$ , avec les-

quelles, par intégration au long de chaque section, on construisit le diagramme des efforts tranchants.

En se fondant sur ce diagramme on a pu résoudre l'indétermination du système hyperstatique, et tracer ainsi le diagramme des moments fléchissants qui sollicitaient la poutre. Dans la fig. 4 on donne les isostatiques et dans la figure 5 on a représenté les contraintes normales de flexion dans la section de moment maximum.

3) *Commentaires sur les résultats obtenus:*

De l'observation des différents diagrammes on peut conclure que la coincidence entre les résultats prévus et ceux obtenus expérimentalement est très satisfaisante.

La valeur moyenne des contraintes  $\sigma_1$  de traction sur les bords des colonnes est différente, inférieure, selon les valeurs mesurées, que celle

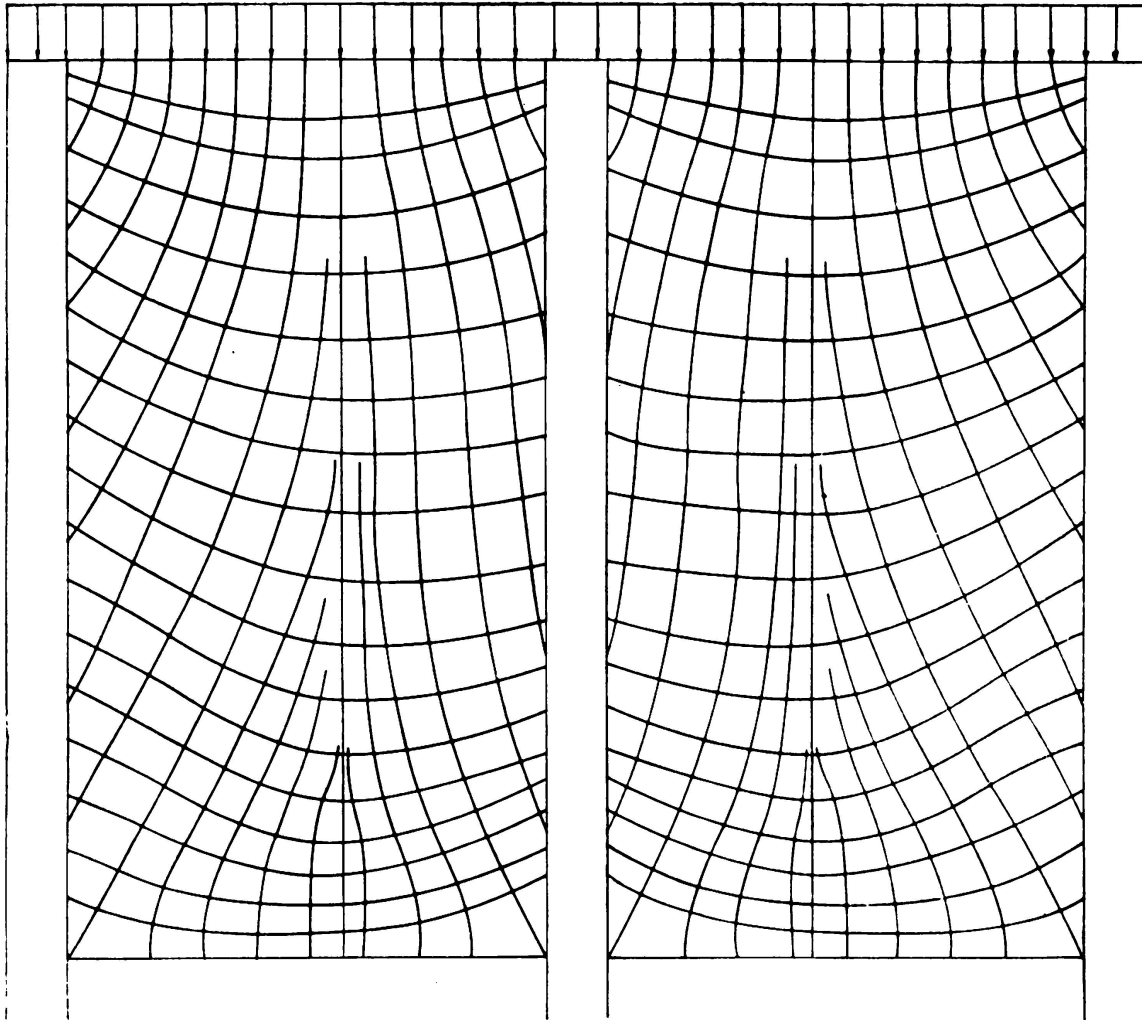


FIG. 4. Poutre continue. Isostatiques

qui correspond au  $\tau_{xy}$  moyen, c'est-à-dire qu'il ne s'agit pas d'un glissement pur.

La section centrale présente des zones de traction et compression presque symétriques, et le bras de levier s'est accru très considérablement, si nous le comparons à la valeur qu'il aurait dans le cas commun.

Comme on peut s'en rendre compte, le résultat de l'essai a été pleinement satisfaisant et offre un panorama de contraintes extrêmement régulier, sans concentrations d'efforts. Les contraintes principales de

traction sur le bord des colonnes sont modérées, ce qui permet d'affirmer que la stabilité de la paroi serait pleinement assurée avec une armature réduite, disposée en forme de carré composé de fers verticaux et horizontaux, non supérieure au minimum nécessaire imposé par des raisons constructives.

Il est intéressant de remarquer que le modèle de poutre continue a été construit avec la même rigidité dans les trois colonnes. Il en résulte

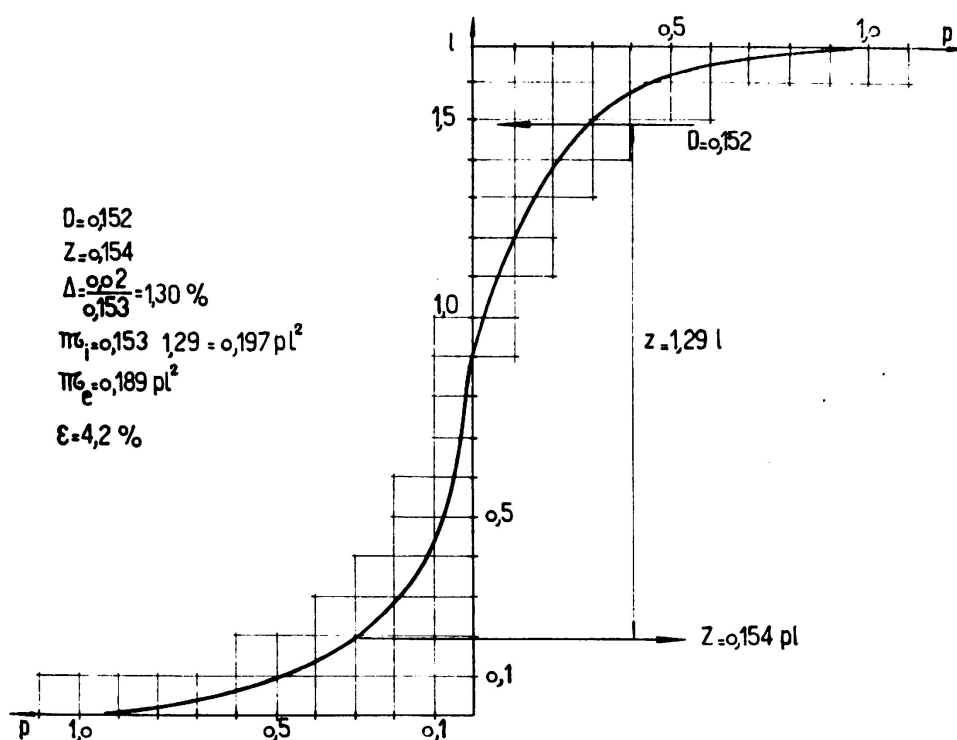


FIG. 5. Poutre continue, contraintes principales  $\sigma_1$  dans la section de moment maximum

que la charge prise par la colonne centrale est presque égale à la charge des colonnes latérales (seulement 15 % de différence). Ceci, à son tour, se manifeste sur le système, comme si, pratiquement, il n'avait pas de continuité.

Pour éclairer ce point, nous sommes en train de considérer la réalisation d'essais complémentaires avec une colonne centrale de rigidité double, et des essais de modèles en ciment armé, chargés le long du bord inférieur de la poutre.

Ceci fera l'objet d'une autre communication.

#### RÉSUMÉ

Pour le nouvel entrepôt frigorifique du «Mercado de Abasto Proveedor de la Ciudad de Buenos Aires», on a adopté, pour des raisons économiques et constructives, une structure formée par des parois porteuses s'appuyant sur des colonnes, tirant ainsi parti des cloisons qui

doivent exister entre les différentes chambres frigorifiques. Pour éviter une forte concentration de contraintes aux appuis, les colonnes ont été prolongées le long des faces verticales des parois, auxquelles elles ont été liées par des armatures. La répartition ainsi obtenue est entièrement satisfaisante, les contraintes de cisaillement ne dépassant pas  $15 \text{ kg/cm}^2$ .

Les résultats ont été vérifiés d'une manière rigoureuse par des essais effectués par la méthode photo-élastique de H. Fabre.

Un programme d'essais complémentaires est en cours dont les résultats seront communiqués plus tard.

#### S U M M A R Y

For the new refrigerated warehouse of the «Mercado de Abasto Proveedor de la Ciudad de Buenos Aires», a structure incorporating load-bearing walls supported by columns was adopted for economical, as well as constructive, reasons, thus taking advantage of the partitions between each chamber. To avoid the heavy stress concentration in the vicinity of the supports, the columns were continued upward along the vertical faces of the walls, to which they are connected by reinforcing bars. The repartition thus attained is entirely satisfactory, the shearing stresses remaining smaller than  $15 \text{ kg/cm}^2$ .

These results were accurately checked through tests carried out by the photoelastic method of H. Favre.

A series of complementary tests are under way, the results of which will be published at a later date.

#### ZUSAMMENFASSUNG

Für das neue Kühlhaus des «Mercado de Abasto Proveedor de la Ciudad de Buenos Aires» wurde aus wirtschaftlichen und konstruktiven Gründen ein System von tragenden Wänden gewählt. Diese werden von Stützen getragen und bestehen aus den ohnehin notwendigen Trennwänden der Kühlräume. Um grosse Spannungskonzentrationen im Bereich der Stützen zu vermeiden, wurden diese längs der Wände hochgezogen und mit ihnen durch Armierungseisen verbunden. Die so erhaltene Spannungsverteilung befriedigt vollkommen, die Schubspannungen überschreiten den Wert von  $15 \text{ kg/cm}^2$  nirgends.

Mit der Methode der Photo-Elastizität nach H. Favre wurden die Ergebnisse sehr genau überprüft.

Zusätzliche Versuche sind gegenwärtig im Gang; ihre Ergebnisse sollen später veröffentlicht werden.

#### R E S U M O

Para o novo armazém frigorífico do «Mercado de Abasto Proveedor de la Ciudad de Buenos Aires», optou-se, por razões económicas e construtivas, por uma estrutura formada por vigas-paredes apoiadas em colunas, tirando assim proveito das divisórias que têm de existir entre as diversas câmaras frigoríficas. Para combater a forte concentração

de tensões nos apoios, prolongaram-se as colunas ao longo das faces verticais das paredes ligando ambas por meio de armaduras. A repartição obtida é inteiramente satisfatória ficando as tensões de corte sempre inferiores a 15 kg/cm<sup>2</sup>.

Estes resultados foram verificados rigorosamente por meio de ensaios efectuados pelo método foto-elástico de H. Favre.

Está em curso um programa de ensaios complementares cujos resultados serão comunicados posteriormente.

## II c 2

Some folded slab constructions carried out recently

Über einige neuere Faltwerkkonstruktionen

Algumas lages dobradas construídas recentemente

Quelques dalles pliées construites récemment

FELIX J. SAMUELY

London

Folded slab construction has been found to be an economical substitute where the very convenient «shell» type of roof was required but was too expensive. With the series of straight planes in folded slabs, local bending has to be taken into account, a disadvantage offset by the simpler formwork. In most cases precast concrete units, forming part of the finished structure, can be used as permanent formwork. Also, the variety of shapes available in folded slabs is sufficient to satisfy most aesthetic requirements. The author has carried out a number of buildings where the roofs have been designed as folded slabs in a composite construction of precast and insitu concrete, and also some from precast units only. In the latter cases, the precast members were unified by means of post-tensioning.

Exact methods of calculation of such folded slabs have been admirably described in a number of books, and it will be assumed that they are generally well-known, but as such structures are invariably highly statically indeterminate, a method of consecutive approximations following the actual behaviour of reinforced concrete has much to commend it, and will lead to any desirable degree of accuracy.

For example, fig. 1 shows a cross section of a School Assembly Hall at Wigan. At each intersection or «crank», the loads can be resolved into two components in the direction of the slabs which, acting as very deep beams, can transmit loads to supports. Therefore, in the first approximation, each crank is assumed to be a support, and in this example a slab over four spans results, acting as shown in fig. 1a. The bending moment and reactions can be determined, and the reactions are resolved in the components along the outline of the roof, as shown in fig. 1. Each slab, which acts as a deep beam in the longitudinal direction of the build-

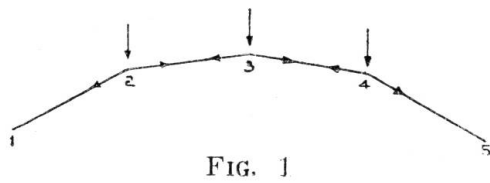


FIG. 1

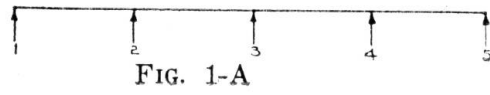


FIG. 1-A

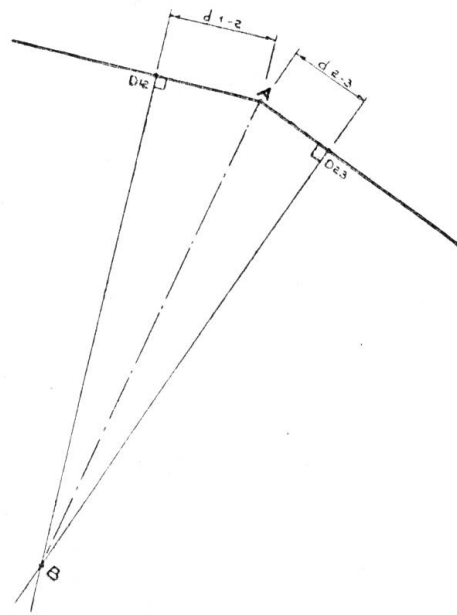


FIG. 1-B



FIG. 2

ding, has to take two of these components, which may either add to or subtract from each other. With reasonably acute angles this may be the final stress distribution. However, with obtuse angles at the cranks, there may be considerable deformation. If deformation is appreciable,

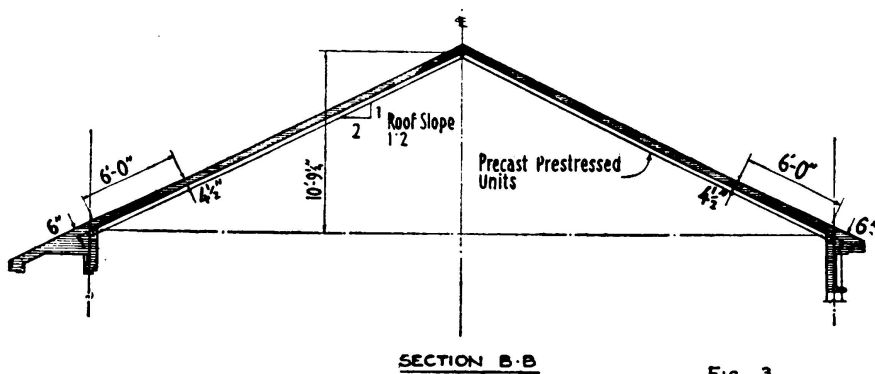
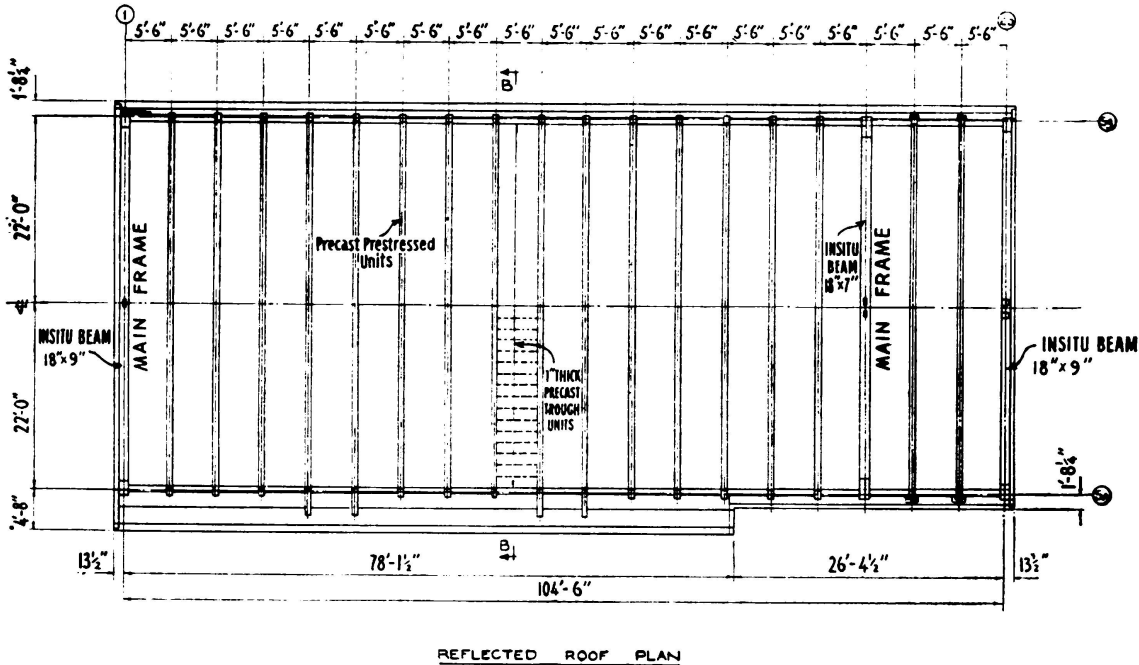


FIG. 3

FIG. 3.

the stress distribution will be altered. Taking point 2 (fig. 1b), the deformation in the centre of the slab 1,2 may be marked as  $d_{1-2}$  and of slabs 2,3 as  $d_{2-3}$ . Assuming the slabs can have unlimited deflection on their weakest axis, the final deflection can be to a point anywhere on lines drawn at 90° at points  $D_{12}$  and  $D_{23}$  and as their point of intersection is at B, AB is the deflection. If similar deflections are calculated for all cranks, and the beams shown in fig. 1a recalculated with supports having the given deflections, a new bending moment diagram and reactions will result, which resolve differently in the planes 1-2, 2-3, 3-4, etc.

This new stress distribution will be nearer the truth than the original one. If there is considerable difference between these and the original deflections, the method must be repeated sufficiently to make sure that the progression of deflections converges. Non-convergence of the progres-

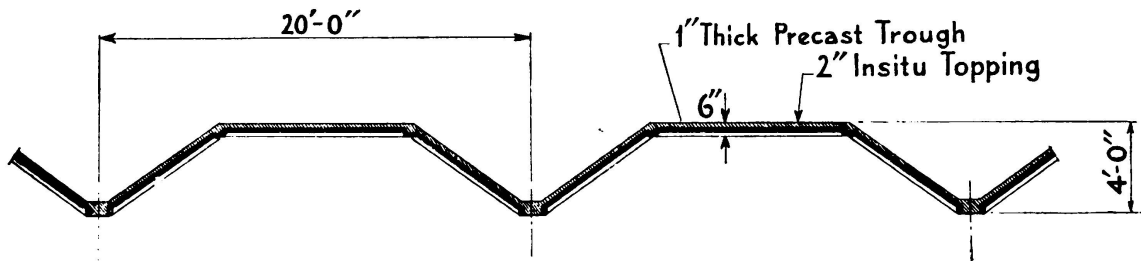


FIG. 4

sion, with too obtuse angles, would indicate that the construction is unsuitable. This particular roof, which is 75'0"  $\times$  45'0", consists of precast concrete troughs, temporarily supported along the horizontal intersections. Steel reinforcement above the troughs takes the tension stresses

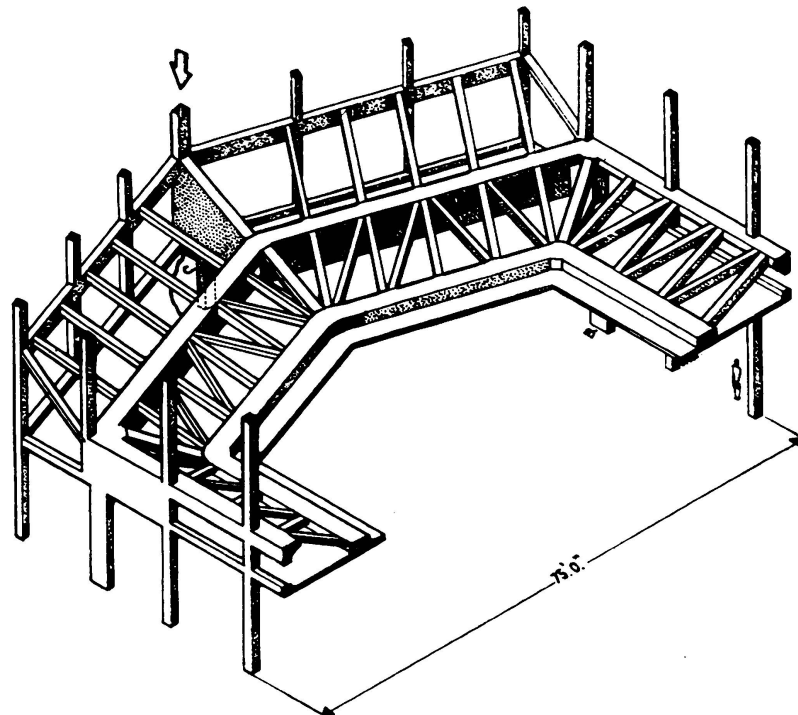


FIG. 5

at eaves, and the roof is finished with 1 1/2" of insitu concrete. Advantageously, the weight is that of the thickness of the troughs and topping (2 1/2"), but the stiffness, that of the 6" depth. Fig. 2 shows the finished Assembly Hall.

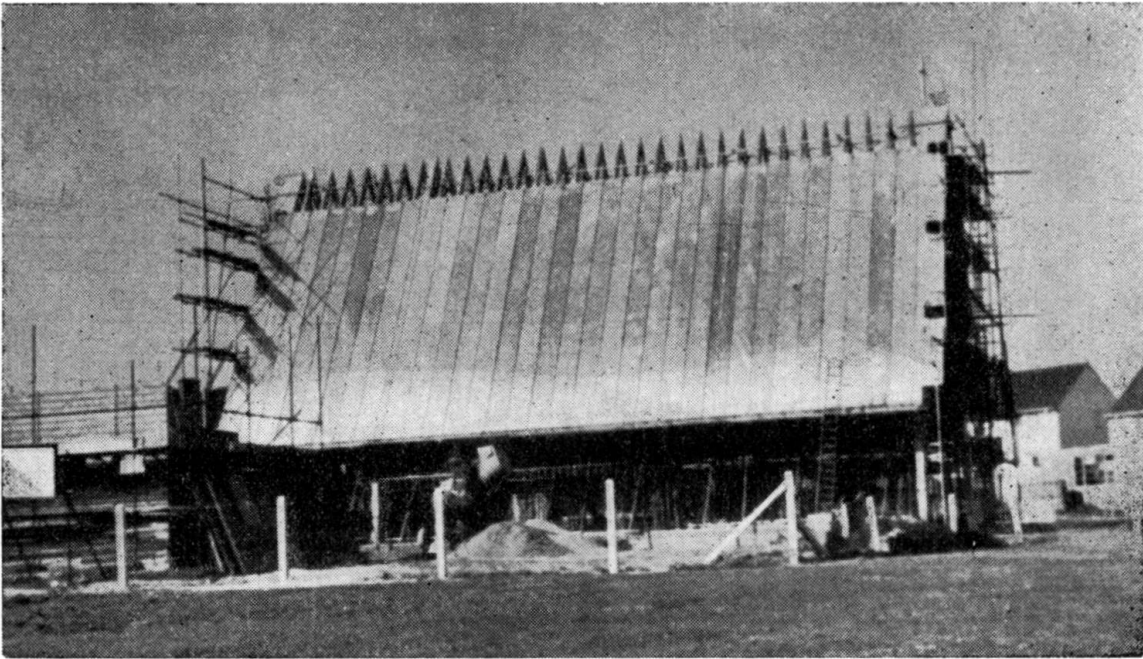
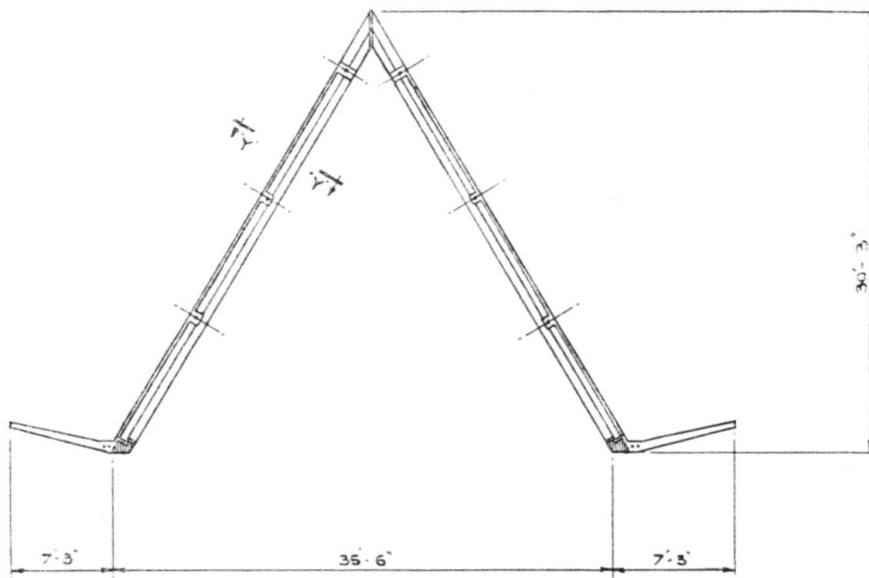
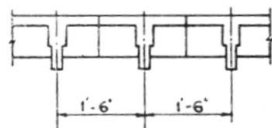


FIG. 6



SECTION A-A



SECTION Y-Y

FIG. 7

Fig. 3 and 3a shows another Assembly Hall, at Hatfield, 44'0" × 88'0", with a 16'6" cantilever. Here the inclined roof slabs consist of prestressed planks, with precast troughs between, the whole covered with insitu concrete. Prestressed units were also used as tie members at either end of the building.

Fig. 4 shows the cross section of a similar roof used for laboratories in East Anglia.

Apart from roofs this construction can be used wherever slabs meet an angle. Fig. 5 shows it used for a gallery in an Assembly Hall.

Care must be taken where a slab is steeper than 1:2, as then expensive top formwork is required for the insitu concrete. To avoid this, use only precast units and post-tension them, as described before.

Figs 6 and show a small church constructed in this way. Each slab consists of a series of prestressed tee units, with flanges uppermost, as shown in section Y-Y. The tees were grouted together and then post-tensioned through the flanges to produce compression over the whole area and make it possible for the whole plane AB to act as a beam. The two planes AB and A'B' do not actually touch, but loads can be resolved into their direction at C, which is rigidly connected to both planes.

#### S U M M A R Y

The contribution refers to folded slab construction which covers areas in a manner similar to shell construction. The general calculation is explained, and, in particular, how it is possible to deal with highly statically indeterminate constructions of this type in stages, so that any degree of approximation can be achieved.

#### ZUSAMMENFASSUNG

Der Aufsatz behandelt Faltwerke, die Räume in ähnlicher Weise wie Schalenkonstruktionen überdecken. Es wird die allgemeine Rechenmethode erklärt und besonders erläutert, wie es möglich ist, hochgradig statisch unbestimmte Konstruktionen dieser Art in stufenweiser Näherung zu behandeln, so dass jeder gewünschte Näherungswert erreicht werden kann.

#### R E S U M O

O autor descreve lajes dobradas utilizadas em coberturas. Explica-se o cálculo geral e como é possível calcular estruturas estáticamente indeterminadas deste tipo por aproximações sucessivas de forma a conseguir um dado grau de precisão.

#### R É S U M É

L'auteur décrit des dalles pliées utilisées comme voiles de couverture. Il rend compte de la méthode générale de calcul et explique comment il est possible de traiter par approximations successives les structures statiquement indéterminées de ce genre, de façon à obtenir un degré de précision donné.

## **II c 3**

### **Essais de chargement d'un plancher dalle en béton précontraint**

#### **Loading tests of a prestressed concrete slab**

#### **Lastversuche an einer vorgespannten unterzugslosen Decke**

#### **Ensaio de carga de uma laje de betão presforçado**

P. LEBELLE

*Directeur de l'Institut Technique du Bâtiment et des Travaux Publics*

Paris

L'auteur a eu l'occasion de dresser les projets de différentes constructions mixtes dans lesquelles sont utilisées conjointement la technique des précontraintes et celle du béton armé classique. Ces constructions se comportent bien en service.

Cette constatation l'a amené à appliquer le même procédé aux planchers dalles sans champignons, dont l'emploi se développe rapidement. Or, à l'heure actuelle, le seul moyen pratiquement utilisable pour créer des précontraintes dans un plancher dalle consiste à placer dans celui-ci deux nappes orthogonales superposées de câbles rectilignes tendus par appui sur le béton durci. Dans un panneau intérieur, les précontraintes ainsi obtenues seront pratiquement uniformes dans toute l'épaisseur de la dalle et dans toute l'étendue du panneau. Si l'intensité de ces précontraintes devait être telle que les contraintes totales en service soient toujours des compressions en tout point du plancher supposé en régime élastique, la quantité d'acier nécessaire rendrait prohibitif le prix du plancher.

L'auteur décrit les essais effectués sur un élément de plancher dalle pour lequel la résistance était obtenue par emploi simultané des câbles tendus et d'armatures ordinaires non mises en tension.

Les résultats des essais montrent que la théorie des lignes de rupture de K. W. JOHANSEN est applicable aux planchers de ce type. En prenant

pour base des calculs un coefficient de sécurité de 2,5 rapporté à la surcharge seule, on obtient un plancher présentant une excellente tenue en service dans les cas courants où la surcharge n'est pas susceptible de varier très rapidement et où les chocs ou vibrations ne sont pas à craindre.

#### R É S U M É

L'auteur décrit des essais effectués sur une dalle, simplement appuyée, en béton partiellement précontraint et montre que la théorie des lignes de rupture de K. W. JOHANSEN est applicable dans ce cas.

#### S U M M A R Y

The author describes tests carried out on a simply supported slab of partly prestressed concrete and shows that the theory of the rupture lines of K. W. JOHANSEN is applicable to this case.

#### ZUSAMMENFASSUNG

Der Verfasser beschreibt Versuche, die an teilweise vorgespannten, unterzugslosen Decken mit Einzelabstützung durchgeführt wurden und zeigt, dass die Bruchlinientheorie von K. W. JOHANSEN auf diese Decken anwendbar ist.

#### R E S U M O

O autor descreve ensaios realizados com uma lage, simplesmente apoiada, de betão parcialmente preesforçado e mostra que a teoria das linhas de rotura de K. W. JOHANSEN pode ser aplicada neste caso.

**Discussão livre**

**Discussion libre**

**Free Discussion**

**Freie Diskussion**

Leere Seite  
Blank page  
Page vide

## II 1

### Slabs and curved structures — Experimental methods

*Discussion*

### Flächentragwerke — Experimentelle methoden

*Diskussion*

### Placas, lajes e paredes delgadas — Métodos experimentais

*Discussão*

### Voiles minces, dalles, parois minces — Methodes expérimentales

*Discussion*

PROF. DR. A. M. HAAS

Gravenhage

As Prof. Lardy has pointed out in his General Report, experimental methods are valuable contributions to our general calculations. The papers presented show that there is a tendency to use materials which enable us to investigate the behaviour in the elastic range. If this is done in the analysis of models we should be very careful to interpret the results in relation to the real reinforced concrete structure. The latter consists of a non-homogeneous material and may be defined to behave elastically and plastically as well.

There are two problems to be solved; that of strength and that of stability. The strength problem may only be solved correctly if we pass in our tests through the stage of elasticity into plastic deformations to the final rupture.

A research which confines itself to elasticity will be of great value in order to know the qualitative behaviour (f. i. elastic stability) and also to check on elasticity-theories. To that end a material as proposed by Prof. Benito which has been called «litargel» may successfully be applied. As has been stated by him it has a low modulus of elasticity and the deadweight already creates large deformations. As a rule reinforcement is not put into the material. If this is done it should be such a kind of steel that its modulus of elasticity is related to that of the material of which the model is made and which enables the steel to have proportionally large deformations.

To me it appears to be essential to raise this point. If we should try and extend by extrapolation the test results found in the elastic stage to the strength at failure we may be seriously wrong and mistakes might be the result.

#### SUMMARY

Research on models made of materials with a low modulus of elasticity will enable to know the elastic behaviour of real structures. One should be very cautious when extrapolating the test-results.

#### RÉSUMÉ

Les essais sur des modèles construits avec des matériaux à faible module d'élasticité pourront permettre de connaître le comportement élastique des structures réelles. Il faut être prudent lors de l'extrapolation des résultats d'essais.

#### RESUMO

Os ensaios efectuados em modelos construídos com materiais de módulo de elasticidade fraco, poderão permitir conhecer o comportamento elástico das estruturas reais. Convém ter muito cuidado quando se extrapolam os resultados de ensaios.

#### ZUSAMMENFASSUNG

Untersuchungen an Modellen, die aus einem Material mit niedrigem Elastizitätsmodul bestehen, dienen der Erforschung des elastischen Bereiches der wirklichen Konstruktionen. Bei der Übertragung der Versuchsergebnisse auf die Wirklichkeit sollte sehr vorsichtig vorgegangen werden.